THE PROCEEDINGS OF
THE PHYSICAL SOCIETY

VOL. 61, PART 5 1 November 1948 No. 347

Sur les Conditions d'Auto-Oscillation des Systèmes Vibrants

PAR YVES ROCARD
École Normale Supérieure, Paris

A Discourse delivered 5 *May* 1948, *on the occasion of the presentation of the Third Holweck Prize and Medal to Professor Y. Rocard*

MS. received 5 *July* 1948

RÉSUMÉ. Le professeur Rocard a rassemblé en une doctrine plus compréhensible les conditions dans lesquelles les systèmes vibrants peuvent devenir auto-oscillants. On a depuis longtemps des moyens mathématiques très bien adaptés pour déterminer ces conditions. Il restait à les analyser et à en comprendre la nature. On peut sur quelques exemples voir la complexité du sujet ; l'auteur cite le roulement des bogies, des locomotives (la conicité des roues engendre l'auto-oscillation sous forme de " lacet "), des auto-oscillations du genre des coups de bélier entretenus dans les conduites, enfin les vibrations d'ailes d'avion, ou " wing flutter ".

Il faut distinguer dans ces systèmes ceux qui résultent du couplage d'un certain nombre de circuits oscillants ou pendulaires ayant chacun leur période propre (le " wing flutter " est de cette sorte) et ceux qui résultent du couplage d'éléments n'ayant pas de période propre, mais seulement des constantes de temps : les télécommandes sont de cette sorte, et aussi les systèmes d'équations un peu arbitraires que l'on peut construire dans les théories économétriques. On peut établir alors les résultats suivants :

1. Si un système n'a qu'une fréquence propre, les forces qui peuvent le rendre auto-oscillant ont forcément le caractère d'une résistance *négative*.

2. Si un système résulte du couplage de plusieurs " degrés de liberté " ayant chacun leur fréquence propre, tout couplage passif (par self, capacité, inertie, etc.) *écarte* les fréquences propres composantes les unes des autres pour donner les fréquences propres du système, mais il existe des couplages *réactifs* qui peuvent rapprocher les dites fréquences propres, sans l'introduction d'aucune résistance positive ou négative. On démontre alors qu'un tel système devient auto-oscillant au moment où deux fréquences propres se confondent.

On peut imaginer dans les problèmes de " wing flutter " des cas très simples qui illustrent ce théorème, et on peut en donner des modèles électriques également très simples.

3. Dans un système tel que ci-dessus (§ 2) mettons maintenant des forces de résistance (proportionnelles aux vitesses) dans l'espoir d'amortir les auto-oscillations. On démontre ce résultat surprenant que, tant que les fréquences propres ne sont pas profondément modifiées, ces résistances ne font que faciliter l'auto-oscillation, qui prend naissance alors que deux fréquences propres se rapprochent mais ne sont pas encore confondues.

Ces résultats font d'ailleurs perdre à la théorie des oscillations de relaxation beaucoup de son importance philosophique, le mécanisme de la résistance négative n'apparaissant plus comme obligatoire dans l'auto-oscillation.

4. Dans le cas de systèmes tout à fait généraux, où on ne peut distinguer des fréquences propres composantes, il n'est naturellement pas possible de se livrer à une analyse aussi pénétrante, mais on démontre encore que si l'on attaque le système par une petite perturbation sinusoïdale dont on fait croître la fréquence, toutes les conditions de stabilité connues (Routh, Leonhard, Nyquist) expriment une vérité très simple : quand, à impédance croissante avec la fréquence, on passe par une résonance (la réactance s'annulant) le terme de résistance trouvé doit être positif.

Je dois tout d'abord exprimer mes remerciements à la Physical Society de Londres pour la haute distinction dont elle m'honore aujourd'hui. J'ai eu la rare chance, pendant la dernière guerre de pouvoir utiliser pour la défense de la Liberté mes propres possibilités scientifiques. Cette action comportait en elle-même sa récompense, et pour celle qui vient s'y ajouter aujourd'hui, je ne puis qu'en reporter le mérite sur ceux de nos collègues qui ont perdu la vie du fait de l'ennemi. Outre notre grand Holweck, je citerai spécialement MM. H. Abraham, E. Bloch, G. Bruhat. Tous trois ont dirigé le laboratoire de Physique de l'École Normale Supérieure, dont je suis maintenant chargé, et cette École s'honore aussi d'avoir vu beaucoup de ses élèves combattre pour la Liberté, aux côtés de ses meilleurs défenseurs, les Anglais. Elle sait de quelles traditions elle est la gardienne, et elle ne faillirait pas devant des tâches nouvelles qui se présenteraient.

Pendant la guerre, l'activité scientifique dans les pays occupés était profondément affectée par des circonstances en général fâcheuses, notamment une certaine asphyxie intellectuelle qui venait du manque de bibliographie en langue anglaise. Cependant certains savants, dont l'existence antérieure n'était peut-être pas assez repliée dans la méditation, ont trouvé dans les loisirs forcés de l'Europe Nouvelle l'occasion de mener à bien certaines tâches de longue haleine. Ainsi, plusieurs de mes illustres maîtres ont séjourné quelque trois semaines dans la prison de Fresnes. Ils ont assuré en être sorti les uns et les autres avec la solution enfin trouvée de problèmes mathématiques qui leur avaient paru jusque-là insolubles . . .

Bien que n'ayant pas été soumis à un traitement aussi efficace, c'est un peu de cette manière que mes propres travaux ont évolué, ce qui me fournit tout naturellement le sujet de cette "Address".

Dès 1934 ,j'ai eu à m'occuper de questions concernant la stabilité des systèmes mécaniques, et des conditions dans lesquelles ils deviennent auto-oscillants. Nous conviendrons donc aujourd'hui de rassembler sous le même vocable d'"oscillateur" des objets aussi différents que

— une locomotive qui a du lacet
— une lampe triode qui oscille
— une flute ou un tuyau d'orgue mis en mouvement par un jet d'air
— le wing-flutter des avions

etc... et nous chercherons ensemble quelles sont les causes qui provoquent l'auto-oscillation.

La locomotive est l'engin le plus difficile : on ne comprend même pas comment elle roule. Le Professeur Andrade est, je crois, l'auteur d'un petit livre sur les locomotives, il saura me redresser si mon exposé contient des erreurs :—Les roues des locomotives sont coniques, le rayon de roulement varie donc avec l'écart latéral de l'essieu sur la voie. Posons donc sur une voie un essieu avec ses deux roues, un peu de travers (figure 1), et poussons en avant, on voit sans trop de peine que l'essieu roule en avançant d'un mouvement sinusoïdal entretenu pur : l'oscillation est pendulaire, mais sa cause est purement cinématique. Si cependant l'on pose sur une voie un bogie avec ses deux essieux et ses quatre roues, les deux sinusoïdes qu'ont envie de décrire en roulant les deux essieux sont incompatibles avec les liaisons (les deux essieux doivent rester parallèles, etc...).

Un simple bogie ne peut donc même pas "rouler". Et cependant, il a bien l'air de rouler. Quel est donc son mouvement ? — On sait depuis Reynolds que des déformations des rails et des roues autour de l'aire de contact finissent par rendre le mouvement possible moyennant l'intervention de certaines forces proportionnelles aux dites déformations. Ces forces ne dérivent pas d'un potentiel, elles peuvent soit amortir les oscillations latérales propres, soit les auto-entretenir: c'est généralement ce qui se passe au-dessus d'une certaine vitesse critique, et j'ai autrefois rempli deux petits volumes de calculs de telles vitesses critiques de locomotives. Je calculais très bien mais je comprenais très mal, lorsque les malheurs de la guerre obligèrent la généralité des Français à s'intéresser aux bicyclettes.

Or, on y trouve l'exemple le plus simple possible d'un oscillateur où la cause de l'auto-oscillation réside dans les liaisons non holonômes du roulement. Soit en effet le petit chariot représenté sur la figure 2, et largement simplifié : il est articulé en O, et toute la masse m est rassemblée en O. Un système de ressorts tend à mettre le bras l_1 dans la direction du bras l_2. La masse m tend alors à osciller, en déplacement latéral, comme un pendule. Cette oscillation fait changer l'orientation des roues. Si alors on suppose que la machine se meut en avant ($V>0$) ou en arrière, les liaisons du roulement réagissent sur le mouvement latéral de m, lequel est régi finalement par l'équation :

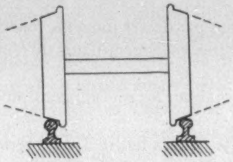

Figure 1.

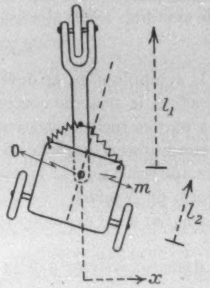

Figure 2.

$$\left[\frac{d^2}{dt^2}+\left(\frac{1}{l_2}-\frac{1}{l_1}\right)V\frac{d}{dt}+\frac{K}{m}\left(\frac{1}{l_1}+\frac{1}{l_2}\right)-\frac{V^2}{l_1 l_2}\right]\frac{d^2x}{dt^2}=0, \qquad \ldots\ldots(1)$$

x étant l'abscisse latérale de m ; K est le coefficient du couple $K\psi$ exercé par le ressort lorsque les bras l_1, l_2 font entre eux un angle ψ.

Cette équation est très instructive : (i) Pour $V=0$ elle donne un mouvement pendulaire simple, sans amortissement. (ii) Si l'engin roule ($V\neq 0$) on a un terme d'*amortissement*, si le centre de gravité est en arrière du milieu quand on se tourne vers l'avant (donc, $l_2<l_1$ si $V>0$ et inversement $l_2>l_1$ si $V<0$). (iii) Dans le cas inverse, mettons $l_2<l_1$ et $V<0$ par exemple, on a un frottement négatif procurant un auto-entretien. (iv) Si la vitesse grandit encore on a, lorsque $V^2/l_1 l_2$ l'emporte sur $(K/m)(1/l_1+1/l_2)$ un *nouveau type* d'instabilité, avec écart exponentiel sans auto-oscillation. Si en particulier $l_1=l_2$, l'amortissement positif ou négatif disparaît, et c'est seulement ce type d'instabilité qui intervient. Nous le retrouverons dans d'autres problèmes.

On voit donc que la locomotive était un exemple inutilement compliqué, et que des liaisons de roulement pur suffisent pour nous donner de beaux exemples d'oscillateurs.

Je ne m'étendrais pas davantage sur les oscillateurs à un seul degré de liberté, dont l'exemple le plus connu est celui de la triode oscillatrice, car en en étudiant d'autres, (une aile d'avion vibrant en torsion seulement, une anche dans un tuyau d'orgue) nous retrouverions toujours ce résultat.

Un système à un degré de liberté devient auto-oscillant par une résistance négative.

Si l'on aborde maintenant les oscillateurs à plusieurs degrés de liberté les conclusions deviennent toutes différentes, et nous découvrons de nouvelles causes d'auto-oscillation. Quoique la théorie soit très générale, nous parlerons seulement pour deux degrés de liberté. Commençons par examiner les moyens mathématiques à notre disposition. En mettant en équation ces problèmes, nous trouverons généralement une équation différentielle portant sur une des variables, y, il sera suffisant de la considérer comme linéaire au moment où l'on sera à la limite de stabilité. Elle s'écrira donc symboliquement

$$a_0p^n + a_1p^{n-1} + \dots a_n = 0, \qquad \dots\dots(2)$$

p étant le symbole d/dt, et devenant aussi un paramètre algébrique lorsque l'on pose $y = e^{pt}$, et le système correspondant sera stable si l'équation (2) n'a que des racines à parties réelles négatives.

Les conditions d'une telle stabilité s'expriment par divers moyens, très connus, et en principe équivalents : le critérium de *Routh* (ou les déterminants de *Hurwitz*) ; le critérium de *Nyquist*.

Mais on fait ainsi des calculs aveugles, sans analyser les mécanismes physiques à la base.

Soit donc un système à deux degrés de liberté : sur la figure 3, on a représenté

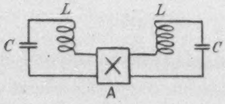

Figure 3.

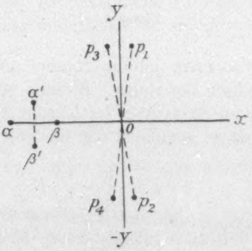

Figure 4.

deux circuits L, C et un organe de couplage A. L'étude de ce système nous mène à une équation $a_0p^4 + a_1p^3 + a_2p^2 + a_3p + a_4 = 0$, et les conditions de stabilité sont, d'après Routh, les suivantes :

$$\left.\begin{aligned} &(a_2/a_0) - (a_3/a_1) > 0 \text{ et en outre, } a_0,\ a_2,\ a_4 > 0, \\ &(a_3/a_1) - \frac{a_4/a_0}{a_2/a_0 - a_3/a_1} > 0 \text{ ainsi que } a_1,\ a_3 > 0. \end{aligned}\right\} \qquad \dots\dots(3)$$

Elles sont bien classiques, mais on les écrit rarement sous cette forme. Nous avons voulu au contraire dans les équations (3) mettre en évidence que les termes *impairs* a_3, a_1 n'intervenaient que par leur *rapport*. Or ces termes impairs viennent *uniquement* des *résistances* qui peuvent figurer dans les circuits, et si l'on convient de faire tendre les résistances vers zéro en leur gardant leurs valeurs relatives, les équations (3) montrent que les conditions de stabilité ne changent pas.

D'où la question suivante : *un système totalement denué de résistances, positives ou négatives, peut-il être auto-oscillant ?*

Cela revient à étudier les racines de l'équation :

$$a_0p^4 + a_2p^2 + a_4 = 0. \qquad \ldots\ldots(4)$$

Sur la figure 4, nous avons représenté à la fois le plan complexe de la variable p^2, et le plan complexe de la variable p.

α et β sont les deux racines en p^2 (deux nombres réels négatifs) lorsque $a_2{}^2 - 4a_0a_4 > 0$. Mais ces deux racines passent en α', β' lorsque $a_2{}^2 - 4a_0a_4 < 0$. Elles sont alors imaginaires conjuguées. Extrayant leurs racines carrées pour obtenir p_1, p_2, p_3, p_4, les quatre racines de l'équation (4) on en trouve deux (p_1, p_2) à partie réelle positive, en divisant par deux l'angle argument de α' par exemple. Dans ce cas, l'équation (4) décrit un mouvement instable.

Or, le cas limite étant obtenu pour $a_2{}^2 - 4a_0a_4 = 0$, lorsque l'équation (4) avait ses deux périodes propres *confondues*. Nous avons donc obtenu la proposition suivante :

La propriété est visiblement générale, on peut la démontrer pour un nombre quelconque de degrés de liberté, et même pour une infinité (oscillations avec propagation, lignes électriques, tuyaux sonores...) et énoncer :

Dans un système à nombre quelconque de degrés de liberté, dépourvu de résistances positives ou négatives, l'instabilité naît avec la confusion de deux fréquences propres.

Si l'on cherche des exemples de tels systèmes, on trouve que tous les couplages *passifs* écartent les fréquences propres, donc ne peuvent donner naissance à l'instabilité. C'était bien nécessaire pour la conservation de l'énergie.

Ainsi, sur la figure 5, les deux pulsations propres sont (dans le cas simple où $L_1 = L_2$, $C_1 = C_2$) sans couplage ($M = 0$) $\omega_1 = \omega_2 = 1/\sqrt{(LC)}$, avec couplage ($M \neq 0$) $\omega_1 = 1/\sqrt{\{(L+M)C\}}$; $\omega_2 = 1/\sqrt{\{(L-M)C\}}$. Ces couplages passifs sont d'ailleurs caractérisés par la *symétrie* des coefficients dans les deux équations.

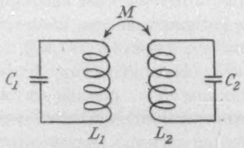

Figure 5.

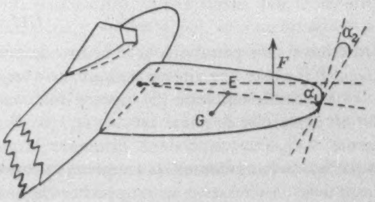

Figure 6.

Un système mécanique équivalent au schéma de la figure 5 est fourni par *une aile d'avion* qui vibre en flexion-torsion (figure 6).

L'axe élastique E est le lieu des points où l'on peut mettre des poids sur l'aile sans la tordre. L'angle α_1 décrit la flexion de l'aile. L'angle α_2 décrit la torsion.

Si le centre de gravité G n'est pas sur l'axe élastique on conçoit sans peine qu'en empoignant l'aile en A et en la levant brusquement, la force d'inertie appliquée en G va l'obliger à se tordre d'un certain angle α_2: flexion et torsion sont donc *couplées* et, avec les variables choisies, le couplage est *par inertie*. On obtiendra donc finalement deux équations du type:

$$\left.\begin{aligned} \left(I_1\frac{d^2}{dt^2}+K_1\right)\alpha_1+I_{12}\frac{d^2\alpha_2}{dt^2}&=0,\\ I_{12}\frac{d^2\alpha_1}{dt^2}+\left(I_2\frac{d^2}{dt^2}+K_2\right)\alpha_2&=0.\end{aligned}\right\} \qquad \ldots\ldots(5)$$

Par exemple, pour un avion de chasse, on peut avoir:

	Sans couplage ($I_{12}=0$)	Après couplage ($I_{12}\neq 0$)
Fréquence propre de flexion	13 cycles/seconde	10 cycles/seconde
Fréquence propre de torsion	24 cycles/seconde	30 cycles/seconde

Faisons maintenant voler l'avion qui possède cette aile, à une certaine vitesse V, elle va devenir un oscillateur, et d'ailleurs, cesser presque immédiatement: c'est là le "wing flutter", et voici comment on l'explique.

En vol, des forces aérodynamiques s'exercent, ces forces sont modifiées par la flexion et la torsion. Les nouvelles forces issues de la flexion sont négligeables (et ont d'ailleurs le caractère d'un amortissement), celles issues de la torsion sont proportionnelles à α_2 (angle qui vient augmenter l'incidence) et au carré de la vitesse. Elles peuvent être appliquées au voisinage de l'axe élastique, auquel cas elles ne réagissent pas sur la torsion elle-même, mais, en tout cas, elles exercent un moment de flexion considérable (force F sur la figure 6) de sorte que la première des équations (5) se récrit ainsi (β, coefficient)

$$\left(I_1\frac{d^2}{dt^2}+K_1\right)\alpha_1+I_{12}\frac{d^2\alpha^2}{dt^2}=\beta V^2\alpha_2, \qquad \ldots\ldots(6)$$

donnant naissance au déterminant en p:

$$\begin{vmatrix} I_1p^2+K_1 & I_{12}p^2-\beta V^2\\ I_{12}p^2 & I_2p^2+K_2\end{vmatrix}=0.$$

On trouve sans peine que si le centre de gravité est en *arrière* de l'axe élastique ($I_{12}<0$) il existe une vitesse critique, on s'en explique l'origine ainsi:

La seconde équation (5) montre que, aux fréquences ω basses ($K_2>I_2\omega^2$), α_1 est en *opposition de phase* avec α_2($I_{12}<0$, $d^2/dt^2=-\omega^2$). Dans l'équation (6), le terme $-I_{12}\omega^2\alpha_2$ vient donc diminuer le rappel élastique $K_1\alpha_1$ mais le terme $-\beta V^2\alpha_2$ va l'augmenter, la fréquence propre de flexion va donc *augmenter* sans cesse avec la vitesse et se rapprocher de la fréquence de torsion: l'*avion meurt quand elles se confondent*.

On trouve facilement l'*équivalent électrique* d'un tel système: les équations (5) conviennent à la figure 5 si α_1 et α_2 représentent les *charges* des condensateurs C_1, C_2. On réalise le cas de l'équation (6) par le schéma de la figure 7, où un amplificateur A attaqué par une tension en α_2 la transforme en une force électromotrice réinjectée dans le circuit de gauche (sous la forme d'un très fort courant passant dans une très petite résistance). Le gain de A est ici l'analogue du paramètre V^2 pour l'avion.

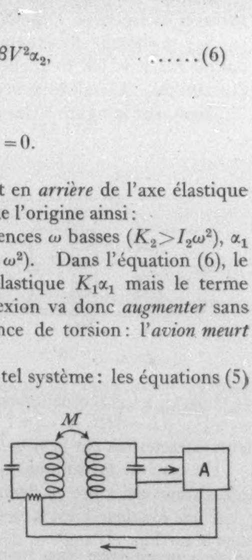

Figure 7.

La question de l'auto-oscillation par confusion des fréquences propres est donc bien claire, elle exige d'ailleurs des forces qui ne dépendent pas d'un potentiel, mais qui n'ont pas à être en phase avec des vitesses, la résistance négative n'est pas le seul mécanisme qui amène à l'auto-oscillation, comme on avait tendance à le croire après les beaux travaux de M. van der Pol, continuant Sir Edward Appleton, sur les oscillations de relaxation.

Mais les systèmes réels sont beaucoup plus compliqués que ceux que nous venons de décrire, et il est nécessaire d'examiner l'effet des résistances sur la stabilité.

Introduisant alors des résistances dans un schéma tel que figure 7 nous trouvons ce très curieux théorème : à fréquences propres constantes, l' *introduction de résistances positives ou négatives ne fait qu'augmenter la tendance à l'auto-oscillation :*

S'il s'agit des circuits de la figure 7, l'amplificateur accrochera pour une valeur plus faible du gain ; s'il s'agit de l'aile de la figure 6 elle cassera pour une vitesse plus faible si sa structure est amortie.

Pour le voir, reprenons l'équation du quatrième degré, en p, et les conditions (3).

Posons $a_3/a_1 = \mu a_2/a_0$, une première condition de stabilité est $0 < \mu < 1$, quant à la seconde, elle s'écrit

$$\mu \frac{a_2}{a_0} - \frac{a_4/a_0}{(a_2/a_0)(1-\mu)} > 0 \quad \text{ou} \quad \frac{a_2^2}{a_0^2} > \frac{1}{\mu(1-\mu)} \frac{a_4}{a_0}. \qquad \ldots\ldots(7)$$

Or $1/\mu(1-\mu)$ est constamment supérieur à 4 quand μ varie de 0 à 1, donc la limite d'instabilité $a_2^2 = 4a_0a_4/\mu(1-\mu)$ est atteinte pour des valeurs des paramètres telles que $a_2^2 > 4a_0a_4$, c'est-à-dire *avant* que les deux fréquences propres, en train de se rapprocher, ne soient confondues.

On trouve sans grande peine des démonstrations tout à fait générales de cette propriété, pour un nombre quelconque de degrés de liberté. Cela revient à énoncer le théorème suivant :

Si un polynôme en x^2, *à coefficients tous positifs, a une racine double négative* (donc quatre racines imaginaires pures pour x, valant $\pm j\omega$), *et si on lui ajoute un polynôme quelconque ne contenant que des termes de degre impairs en* x, *le polynôme résultant aura au moins une racine à partie réelle positive.*

On trouve aussi un théorème semblable pour les équations fonctionnelles (et non plus algébriques) auxquelles donne lieu l'étude de la stabilité des systèmes à propagation. Il y aurait beaucoup d'exemples à développer où l'on verrait comment la théorie précédente éclaire les conditions qui règnent à l'auto-oscillation, mais le cadre de cette conférence générale ne nous permet guère de nous étendre.

Consacrons plutôt les instants qui nous restent à déduire encore quelques conséquences nouvelles concernant le sens des conditions qui expriment la stabilité des systèmes.

Soit $H_{(p)}$ l'équation différentielle ou fonctionnelle qui exprime l'évolution de la variable y caractéristique du système $H_{(p)} . y = 0$. Si l'on pose $y = e^{j\omega t}$, on obtient

$$R + jX = 0, \qquad \ldots\ldots(8)$$

R et X devenant deux fonctions de ω ; l'équation (8) en général *n'est pas* satisfaite, mais si exceptionnellement on peut trouver une valeur de ω telle que $R(\omega) = X(\omega) = 0$ c'est que les conditions concernant la limite de stabilité sont juste satisfaites.

Soit en particulier *un pendule amorti*

$$m(d^2y/dt^2)+f(dy/dt)+Ky=0,$$

$$R=K-m\omega^2, \qquad X=f\omega,$$

la limite de stabilité exigerait $f=0$, et si f était fonction de la fréquence, il faudrait plus particulièrement $f=0$ pour $\omega=\omega_1$ tel que $K-m{\omega_1}^2=0$. On remarque aussi que en faisant varier ω, lorsqu'on passe la *résonance* $K-m\omega^2=0$, on trouve une *résistance* $f\omega$ *positive*.

Il est à remarquer que l'expression $R/j\omega$, ici $K/j\omega+jm\omega$, est la *réactance* du système, et qu'elle est une *fonction croissante de la fréquence*. (Il y a un théorème qui l'exige.)

Or, il y a de fortes raisons de penser qu'un système quelconque, pour les fréquences voisines de sa fréquence de résonance est assimilable à un pendule avec une certaine masse, une certaine élasticité et un certain frottement (positif ou négatif):

En effet, au lieu de laisser le système au repos, attaquons-le par un signal $ae^{j\omega t}$, mesurons y en amplitude et en phase, de cette mesure résultent $R(\omega)$ et $X(\omega)$. Attachons-nous à une valeur ω_1 de ω telle que $R(\omega)_1=0$, qui donne $X(\omega_1)=X_1=f_1\omega$, essayons les fréquences voisines $\omega_1-\Delta\omega$ donne $R(\omega_1-\Delta\omega)=-\Delta\omega(dR/d\omega)$ (mesuré). Essayons de poser $R=K_1-m_1\omega^2$ pour ω voisin de ω_1 on aura

$$(1) \quad K_1=m_1{\omega_1}^2,$$

$$(2) \quad -2m_1\omega_1\Delta\omega=-\Delta\omega(dR/d\omega)_1 \text{ (connu)},$$

d'où

$$m_1\omega_1=-\tfrac{1}{2}(dR/d\omega)_1 \text{ et } K_1=-\tfrac{1}{2}\omega_1(dR/d\omega)_1.$$

On trouve donc K_1 et m_1. Si ces deux termes ont des valeurs *positives*, il est clair que, physiquement, si le système est stable, c'est que le frottement f_1 doit être positif, donc X_1 doit être trouvé positif. Or K_1 et m_1 sont positifs si $(dR/d\omega)_1$ est négatif, donc la condition de stabilité que nous trouvons est la suivante:

L'expression $X(dR/d\omega)$ doit être négative pour toute valeur $\omega_1, \omega_2, \ldots$ de ω qui annule R comme R ne dépend que de ω^2, on peut, plus simplement encore dire:

$$X(dR/d\omega^2)<0. \qquad \ldots\ldots(9)$$

En termes physiques, on dirait plutôt: la condition de stabilité est qu'on trouve un frottement X positif à toute résonance de réactance $R=0$ *parcouru dans le sens des impédances croissantes* (sinon, on trouve une masse négative, une élasticité négative, et la stabilité veut alors un frottement négatif, tous les signes de l'équation étant alors changés).

Les remarques qui précèdent, *extrêmement simples*, nous donnent alors la clé des conditions mathématiques déjà connues, mais dont on comprend mieux maintenant la nature.

Ces conditions connues, pour la stabilité, sont (i) le critérium de Nyquist, (ii) l'entrelacement des racines de R et de X. Il a déjà été démontré que ces conditions sont équivalentes. Or notre condition (9) est équivalente à l'entrelacement: En effet à chaque racine successive ω_1, ω_2 de R, $dR/d\omega^2$ change de signe, donc, dans le cas de la stabilité, $X(\omega_1)$, $X(\omega_2)$ etc. . . . sont alternativement de signes contraires, donc les racines de X et de R sont entrelacées.

Comme exemple de problèmes de stabilité traités suivant ces méthodes, nous pourrions citer beaucoup de problèmes de télécommande, mais sans doute la plupart des personnes qui m'écoutent prendront-elles plus d'intérêt à la solution de quelques problèmes concernant la stabilité des automobiles.

J'en citerai rapidement deux:

1. ***Stabilité de route d'une voiture qui roule, direction bloquée.***

La figure 8 représente l'avant de cette voiture, vu de dessus, roulant normalement. Les aires de contact des bandages avec le sol sont hachurées. La figure 9 représente ce qui se passe si une force latérale agit sur la voiture, les roues se déforment, sans que l'aire de contact change de place, mais elles vont du fait de leur déformation rouler dans une direction oblique. L'angle ϵ est proportionnel à la force F.

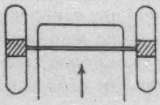

Figure 8.

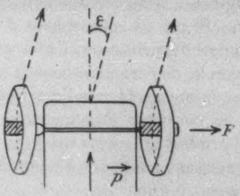

Figure 9.

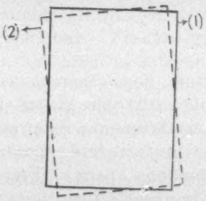

Figure 10.

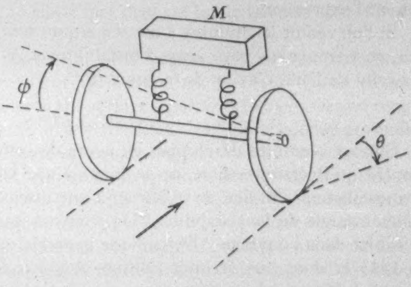

Figure 11.

La prise en considération de cet effet permet la mise en équation du "roulement" compte tenu des oscillations du rectangle (1) représentant la voiture par rapport au rectangle (2) des aires de contact, ce rectangle (2) étant lui-même susceptible de "rouler" dans une direction oblique suivant les forces qui tirent sur lui, et qui viennent du déplacement relatif du rectangle (1) (figure 10).

La résolution de ce problème m'a conduit aux résultats suivants

(*a*) Si les quatre pneus sont également gonflés, la voiture ne présente pas de "vitesse critique d'instabilité" si le centre de gravité tombe entre le milieu et un certain point un peu sur l'avant.

(*b*) Si le centre de gravité est, pour simplifier, pris au milieu de la voiture, celle-ci ne présente pas de vitesse critique d'instabilité si les pneus avant sont un peu moins gonflés que les pneus arrière, dans une proportion d'ailleurs limitée.

Telles sont les meilleures conditions de stabilité d'une automobile. J'espère que la prospérité bientôt retrouvée dans nos deux pays nous permettra à tous de les expérimenter....

2. *Le Shimmy des voitures comportant un essieu avant.*

Ce vieux phénomène, qu'on tend à oublier, était bien gênant en 1928 environ. En 1948, il reste intéressant, parce que c'est un cas pur d'oscillateur selon nos idées, avec l'auto-oscillation par confusion de deux fréquences propres. Le figure 11 montre un essieu avant, avec deux roues, suspendu sous une voiture. Les masses et les ressorts de la suspension, des pneus, donnent une période propre d'oscillation pour l'angle ϕ. Mais les roues roulent vers l'avant, et vont créer un effet gyroscopique. Si par un mouvement ϕ, la roue de gauche s'élève, le plan des deux roues change d'orientation, l'effet gyroscopique le fait tourner de θ, la voiture roule en cercle, de *part les liaisons du roulement*. Il naît alors une *force centrifuge* F qui pousse la masse M vers l'extérieur et tend à donner une variation contraire à ϕ; voilà le couplage dissymétrique qui rend le système auto-oscillant: Une *rotation* θ produit un *couple* sur ϕ (en plus de l'effet gyroscopique avec son *couple* en $d\theta/dt$ agissant aussi sur ϕ), tandis qu'une rotation ϕ ne produit sur ϕ que le couple gyroscopique.

Le nouveau couple introduit est proportionnel à V^2, on voit sans peine qu'il confond les fréquences propres en θ, ϕ à une certaine vitesse critique V_c, dont on obtient l'expression.

Si l'on réduit le Shimmy à ces remarques très simples en le schématisant un peu, on y trouve *une seule cause* d'instabilité, et on a un schéma tout à fait calqué sur celui de l'aile d'avion de la figure 6.

CONCLUSION

Sur les exemples développés au cours de cette lecture, nous espérons avoir montré qu'il était possible de se livrer à une véritable analyse des causes des auto-oscillations, au lieu de se borner à une discussion mathématique rigoureuse moins aveugle de leur stabilité. On trouvera une doctrine complète exposée à ce subjet dans l'ouvrage "Dynamique générale des vibrations" paru en France en 1943 et dont une seconde édition plus étendue s'imprime en ce moment. Une traduction anglaise est en cours, sans qu'on puisse encore préciser sa date de parution.

Je tiens en terminant à adresser un vif remerciement à la Physical Society de Londres pour m'avoir donné cette occasion très flatteuse pour moi d'exposer ces quelques travaux.

The Growth of Crystals

By G. P. THOMSON
Imperial College, South Kensington, London

Thirty-second Guthrie Lecture, delivered on 4 *June* 1948

In choosing a subject for the Guthrie Lecture it seems important to consider the use to which such a lecture can be put. There is so much published now on physics that any addition to the literature needs justification. I have no great discovery to report, but there is a field in which considerable work has been done at Imperial College both in the Physics Department and in that of our President[*], and which I think it may be profitable to bring to your notice because it seems very promising, and it is one which has not perhaps received due attention in this country—the growth of crystals.

While the last thirty years have seen an enormous increase in knowledge of how the atoms are arranged inside crystals, there has not been a corresponding advance in understanding of the kinetics of the process of growth, or of the causes which determine outward form.

Certain thermodynamical arguments have long—perhaps too long—dominated this study, and though I hope to show that they are liable to misuse, it is best to start from them.

In general a crystal must start from small beginnings, and the same sort of argument which governs the growth of water drops in a mist or a Wilson chamber applies here. Free energy resides in the surface separating two phases and retards the formation of a second phase inside the first. On dimensional grounds a surface effect must be more and more important compared with a volume effect the smaller the volume. Hence for very small drops the effect of surface tension is greatly to increase the vapour pressure with which the drop is in equilibrium, according to the well known formula $\ln p_r/p_\infty = 2v\sigma/r\mathbf{k}T = \delta$, where σ is the surface tension, r the radius of the drop, v the volume occupied per molecule of the liquid, and δ is the supersaturation measured as the logarithm of the ratio of the vapour pressure in equilibrium with the drop to that in equilibrium with a flat surface. The drop is of course unstable. Increase of radius makes the vapour oversaturated with respect to it so that it grows more.

If a crystal is started without a previous nucleus we should expect a similar expression to apply. It is true that Gibbs (1906)[†] pointed out—"..... We cannot imagine a body of the internal structure and external form of a crystal to grow or dissolve by an entirely continuous process, or by a process in the same sense continuous as condensation or evaporation between a fluid and a gas, or corresponding process between an amorphous solid and a fluid. The process is rather to be regarded as periodic." Kossel (1934) has raised a similar objection. Yet by considering the growth of a complete layer over the surface of a small crystal we can derive an expression similar in form to the above with the modification that the linear parameter corresponding to r can only increase by discrete steps corresponding to the addition of layers one cell thick all over the crystal, while the quantity corresponding to σ may have to be averaged for different faces if the crystal includes more than one "form".

---

[*] Professor G. I. Finch.

[†] I am indebted to Mr. Humphreys-Owen for calling my attention to this and the following quotation.

Stranski (1928) has shown that for a cube of side $2r$,

$$\ln\frac{p_r}{p_\infty}=\frac{2v}{kT}\left(\frac{\sigma}{r}+\frac{K}{2r^2}\right),$$

where the second term is due to edge energy.

We may digress here to note how, from the thermodynamic point of view, the equilibrium shape is determined. As P. Curie long ago pointed out, the crystal truly in equilibrium with solution or vapour will take a shape such that the free energy is a minimum for a given volume. Take some point P, inside the crystal. Let p_1 etc. be the perpendiculars from P on the faces of the crystal of area F_1 etc. Then the volume V is the sum of the pyramids with P as vertex and the faces as bases : $V=\frac{1}{3}\sum_1^n p_1F_1$, but the free energy $A=\sum_1^n\sigma_1F_1$, where σ_1 etc. are the surface tensions. Now let one set of faces grow at the expense of another. The change in volume can be written either as $\sum_1^n F\,dp$ or $\frac{1}{3}\sum_1^n(F\,dp+p\,dF)$. If we keep the volume constant both are zero, and hence $\sum_1^n p\,dF=0$. But the condition that A is constant gives $\sum_1^n\sigma\,dF=0$ (neglecting any variation of σ with F), so that faces for which it is possible to vary F independently must be so situated that $p\propto\sigma$. This implies that the point is taken midway between each pair of faces with equal σ, and when so taken p/σ is constant for all possible forms. This result is due to Wulff (1901).

But all this has its limitations. When we consider quantities, we find that for a crystal of a few cubic centimetres the difference in the equilibrium concentration between one form and another, e.g. (100) and (110) for rocksalt (Brandes 1927) is only of the order of 1 in 10^6. (Notice that, like all surface energy effects, it vanishes as the crystal grows indefinitely). This is too small to make any appreciable difference except perhaps for the slowest possible growth such as might occur in geological time. In any laboratory process small fluctuations of temperature or of concentration due to diffusion will far outweigh this.

What matters is the *rate* of growth, and this may well be governed by some initial step. Gibbs (1906) early recognized this : "Since the difficulty in the formation of a new layer is at or near the commencement of the formation, the necessary value of the Potential may be independent of the area of the side except when the side is very small. The value which is necessary for the growth of a crystal will however be different for different kinds of surfaces, and will probably generally be greatest for the surfaces for which the Surface Tension is least.... As a final result, a large crystal will generally be bounded by those surfaces on which the deposit of new matter takes place least readily. If one kind of surface cannot form a closed figure, a crystal will be bounded by two or three kinds of surfaces determined by the same condition. The kinds of surfaces thus determined will probably be generally those for which the Surface Tension has the least values. But the relative development of different kinds of sides will not be such as to make the sum of the Surface Energies a minimum." Gibbs's conception has been developed by Kossel (1928) and Stranski (1943) and their pupils in the following way. Consider a simple cube lattice built up of cubes of matter and suppose for simplicity that the only forces are those between the faces of the little cubes that come into actual contact.

Suppose the crystal has grown till its side is n units and that it is a cube. Then of the $6n^3$ faces all will be in contact except the $6n^2$ on the surface. If ϕ is the binding energy for each pair of faces, the average binding energy per unit is $(3n^3-3n^2)\phi/n^3=3\phi(1-1/n)$. When the crystal is infinite this is 3ϕ, and a unit which requires this work to detach it will just be in equilibrium with a solution or vapour saturated for a large crystal.

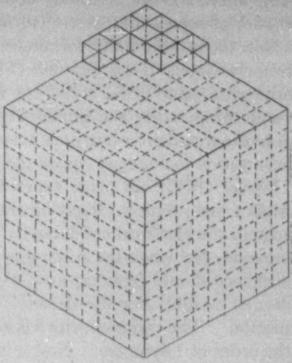

Figure 1.

Now build a new layer on one face. The first unit, say at a corner, only has one face in contact with the crystal—work ϕ. The next along an edge has work 2ϕ, there are $2(n-1)$ of these or $2(m-1)$ if the layer only covers m^2 of the units, $m<n$. The remainder all have the full work 3ϕ. This corresponds to what Kossel calls the "repeatable step". Once we have got over the initial difficulty, the crystal will grow or diminish according as the solution is under- or over-saturated for this "repeatable step". But what is the measure of the initial difficulty? The total separation energy for the whole plane is $\phi+4(m-1)\phi+(m-1)^2 3\phi=3\phi m^2-2\phi m$. For a line added to an incomplete plane the separation energy is $3\phi m-\phi$. The defect is due to the fact that we have extended two faces of the cube by an amount r^2m each, where r is the side of a unit cube, and added two new steps of equal area, and so produced surface energy $4mr^2\sigma$; so $4mr^2\sigma=2m\phi$ or $2\sigma=\phi/r^2$, as is otherwise obvious.

The defect in separation energy requires an extra concentration of energy in the form of a probability fluctuation. The amount required is $2m\phi=4mr^2\sigma$, and increases in proportion to the side of the embryo produced. Small fluctuations are frequent, but unless the embryo produced is large enough to be in equilibrium with the degree of supersaturation present, it will relapse back into its elements and come to nothing. The production of an embryo thus becomes more likely the greater the supersaturation, because the greater this is the smaller the embryo needs to be.

While the work for the "repeatable step" is the same for a small or large embryo the small embryo is unlikely to survive. It is, indeed, equally likely to gain or lose at each step, but its chance of growing really large is small, for it will probably be extinguished by chance fluctuations. The case is rather analogous to a man gambling at Monte Carlo. If he goes on he is pretty sure to lose all his capital, even apart from the zero in favour of the bank, just because of probability fluctuations. The smaller energy of attachment of the first few pieces acts against the crystal something like the zero against the gambler. The crystal can only be saved by the solution being supersaturated. There appears to be no way of supersaturating Monte Carlo!

A similar explanation may apply to the growth of large crystals at the expense of small, as in the process of annealing.

In calculating the energy fluctuation necessary to produce an embryo which will be in equilibrium with a particular degree of supersaturation account has to be taken of the work done by the gaseous (or osmotic) pressure, and this reduces the fluctuation required from $F\sigma$ to $F\sigma/3$ in the case of three dimensions (Volmer 1921) and from $u\rho$ to $u\rho/2$ in the case of two dimensions (Volmer and Adhirkari 1925, 1926), where u is the perimeter in equilibrium with the supersaturation and ρ is the work of separation per cm^2 surface.

Now the trouble is that for moderate supersaturations the energy fluctuation is extremely large. Thus Brandes (1927) calculates for rocksalt with 1% supersaturation a value of $2{\cdot}3\times10^{-9}$ erg for the surface embryo. This is $6\times10^4\,\boldsymbol{k}T$ at room temperature and growth should be negligible, while in fact a crystal of visible size would grow fairly fast at such a supersaturation. The chance of energy concentration includes of course the Boltzmann factor, $\exp(-W/\boldsymbol{k}T)$.

Amsler (1942) has made experiments on the delay times for the growth of crystals from solution, detecting the onset of crystallization by measuring the change in the electrical conductivity. The delay time is subject to a probability fluctuation, but when the stirring is good the results are surprisingly consistent. The chance should go as $\exp(-C/\delta^2)$ where $C=16\pi M^2N\sigma^3/3\rho^2R^2T^3$, where M is molecular weight, ρ is the density, N is Avogadro's constant and δ the supersaturation. The variation with δ is as expected, but the constant gives a value of σ of the order of 1 dyne/cm. Now σ is the difference of the surface tensions of the solid and liquid if the contact angle is zero. The calculated value for rocksalt is 107·5 dyne/cm. for a large crystal and that for the solution is 78·8 dyne/cm. giving a difference of about 30 dynes which is cubed in the exponential so that the factor here is of the order 30^3. Amsler thinks that the change in surface tension of the solid with size may account for the difference but it seems unlikely that it would so closely approach that of the liquid, especially as results with NaCl and KCl are closely similar.

In any case, the difficulty remains in the two-dimensional case which Amsler's work merely confirms.

The way out seems to lie in an early suggestion of Volmer (1921), to whom indeed much of the above theory is due. He supposed that the surface of a growing crystal is covered with a mobile supersaturated layer. He and Estermann (1921) brought forward evidence for the motion of mercury atoms over the surface of a growing crystal, showing that the material reaching a face directly from the vapour might be many times less than that which actually formed on it. He also (Volmer and Weber 1926) found that crystals of benzophenone appeared to lose and gain matter by flow over the surface, and measured the diffusion of a very thin film of benzophenone over a glass plate. It should be mentioned perhaps that the transference by vapour pressure was appreciable in these latter experiments. Other instances of atoms migrating over surfaces are the effects observed by Stern, Estermann and Cockcroft with molecular beams, and the technically important effects studied by Langmuir and others in which alkali atoms migrate over tungsten.

If now we suppose that a layer exists on a growing crystal which can diffuse rapidly over the surface, but which is much more concentrated than the vapour or solution round the crystal, we can explain the rapid formation of embryos in such a case. The fluctuations of energy needed to form an embryo of given size, and the size of the embryo needed to produce growth, are now quite different from what we have calculated above. The equilibrium condition is enormously hastened, as by a catalyst. There is strong evidence for the existence of such a layer, not only in the work of Volmer, but in a line of experiments started by Berg (1938) and recently developed at Imperial College by Humphreys-Owen, to whom I am indebted for allowing me to give some of his results. The experiments consist in illuminating a crystal growing from solution between optical flats in such a way as to produce interference fringes. From these the variation of concentration from point to point of the solution can be determined, lines of equal concentration can be drawn and the flow normal to the force of the crystal determined, since this by the law of diffusion is proportional to the normal concentration gradient. Berg and Humphreys-Owen agree in finding that the surface of the growing crystal is far from being a surface of constant concentration (see figure 2), and also that the normal flow is not constant along a growing face, being most at the centre and least at the corners. Since the face in fact grows flat, there must be a flow of material from the centre outwards in a layer too thin to be observable, which means less than about 0·01 mm. The distribution of flow is sufficiently often symmetrical about the middle point for one to regard this as the normal case, but there are frequent cases of exception due presumably to greater ease of growth at one side or the other (figure 3). Humphreys-Owen finds that the maximum flow in the layer is proportional to the inflow in the normal case, and is about 7% of it.

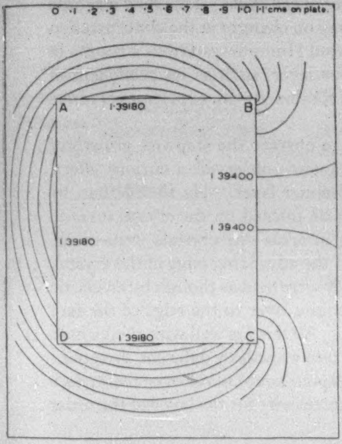

Figure 2. The lines show surfaces of equal concentration. The face at the right has stopped growing, others are growing normally. The concentration at the corners is greater than that in the middle of the face.

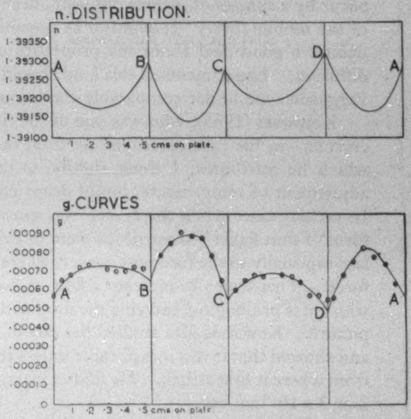

Figure 3. The top half shows the distribution of concentration over the four faces AB—BC—CD—DA. The lower half shows the normal flow at various points on these faces. The crystal to which this figure refers, unlike that in figure 2, is growing normally on all faces.

At this point I should like to show you a film kindly lent me by Mr. Ferguson of Imperial Chemical Industries which shows some experiments on crystal growth : the film has been shown before but the results have not yet been published. You will notice that the growing face increases in thickness discontinuously. Steps are formed, often at a corner, which sweep across the crystal. Marcellin (1918) seems to have been the first to observe this phenomenon. Sometimes one step will catch up on another and the whole move forward together. I suggest that we see here the absorption of the mobile layer at the step, and that the speed with which the step advances is governed at least in part by the mobility of the layer. Thus in figure 4 material from the old face of the crystal will be flowing towards the advancing step to build it up, while a new layer will be reforming on top of the step and flowing in the opposite direction. Both these layers will flow in a way determined by some law of diffusion, though it seems reasonable to suppose that their thickness is limited to some saturation value. If the step is shallow it will be able to advance more rapidly than if it is deep, for it will not have to wait for so much material to flow in from parts of the mobile layer ahead of it. This flow can only occur by a species of surface diffusion, depending on changes in the concentration of the mobile layer. It ought to be possible from Humphreys-Owen's results to deduce a good deal about the properties of the layer, such as its coefficient of diffusion. Experiments of this kind should be combined with experiments of the Ferguson type under comparable conditions.

Kowarski (1935), who was one of the first to observe the stepwise growth of crystals—in his case paratolindine from the vapour—observed a curious effect, which he attributes, I think rightly, to the Volmer layer. He found that, by adjustment of temperature, liquid drops could be formed on the crystal surface. In certain cases when the crystal was growing in area—the crystals were in the form of thin flakes—these drops were drawn to the advancing edge of the crystal, and especially to the foremost corner, where they were held as though by an elastic force. This seems to indicate a flow of the mobile layer to the edge of the face which it is prolonging, carrying the drop with it. All this fits well with the Volmer picture. Kowarski also studied the rate of surface growth in different directions and showed that it was inexplicable unless the vapour could move over the surface from where it first struck. He finds a maximum velocity for the layer of the order 2 or 3×10^{-2} cm/sec.

In considering crystal growth one's interest naturally centres on the atomic processes, but there are other factors which may be more important in practical cases—for example diffusion. If a crystal is growing fast it will exhaust the material in its immediate neighbourhood, and any protrusion will be more favourably situated than the rest. We have now seen how up to a point a crystal can continue to grow flat faces though different parts of them are at different concentrations, but there must be a limit to this, and when it comes the crystal grows out to unexploited regions. This leads to dendritic growth. Even for a crystal of compact shape the effect is important and may govern the rate of growth. We can make a crude model (Valeton 1923, 1924) which brings out the main points, by supposing that there is a discontinuity of concentration $C_s' - C_s$ at the surface of the crystal, supposed a sphere of radius a, and that the flow of material into the crystal is $k(C_s' - C_s)$ per cm². Then if D be the coefficient of diffusion (taking 1 cm³ of solid crystallite as unit of material) it is easy to show that

$$\frac{da}{dt} = \frac{C_\infty - C_s}{a/D + 1/k},$$

where C_∞ is the concentration of the distant solution. The two terms in the denominator can be regarded as series resistances, one due to diffusion in the bulk of the liquid and the other due to the surface layer. If the resistance due to diffusion is the important one, da^2/dt is constant, but if that due to the surface layer is predominant, then da/dt is constant.

Humphreys-Owen finds that for his crystals the first was the case (his crystals were in two dimensions which gives a somewhat different law, but the difference is slight). It should be noticed, however, that the relative importance of the terms depends on a, but his crystals were fairly small, approximately 2 mm., and the law should hold *a fortiori* for larger ones.

It is well known that the habit of crystals is influenced by the presence of colloids in the solution, which favour dendritic growth. They probably act by reducing the coefficient of diffusion of the salt and so increasing the difficulty of supply of the material, making this relatively more important than the resistance to embryo formation.

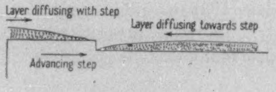

Figure 4.

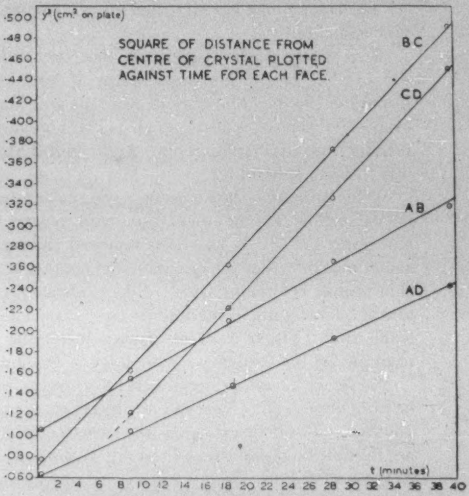

Figure 5. Showing normal growth of a crystal for which the square of the characteristic dimension increases linearly with time. The zero of time is the moment when observation started, not that when the crystal started growth.

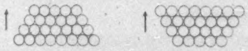

Figure 6.

(*a*) (*b*)

(*a*) Quick-growing face is extinguished.
(*b*) Quick-growing face increases.

There may, however, sometimes be another effect which, indeed, almost certainly occurs when some dyes are present in solution. These are preferentially absorbed on certain faces, and so inhibit their rate of growth. It is usually supposed that the faces finally produced are those which grow most slowly, the more quickly growing faces extinguishing themselves. This is not self evident, as is seen by a comparison of figure 6 (*a*) and (*b*). It is conceivable that in certain circumstances a face might extend as it grows as in (*b*). This may occur in certain cases of very rapid growth where the supply of material is the determining factor to the exclusion of considerations of energy.

Another way in which non-atomic considerations may modify crystal growth is the purely geometrical effect of surroundings. Thus crystals which tend to form flat plates and are grown from vapour on a solid substratum tend to be orientated with the plates parallel to the substrate (Thomson and Cochrane 1938). If the vapour is directed as a molecular jet they tend to be orientated normal to the jet, and when both causes are present a compromise is reached. These effects may be explained by the greater ease of growth afforded to a plate which happens to start parallel to the solid surface, or in the second case by the greater mass intercepted by the face normal to the stream. In both cases we must suppose that the molecules that strike the surface form a mobile layer over it which moves so as to build up the edge of the discs, as in Volmer and Estermann's experiment.

Professor Finch has informed me of a similar effect when crystals are grown in fine scratches.

It is pretty general experience that very thin films formed by spluttering or evaporation are, if not amorphous, at least micro-crystalline (Thomson and Cochrane 1938). The work of Andrade and Martindale (1935) on gold is a good example of this, as is also Lotmer's (1945) on antimony. Increased deposition or heating leads to crystallization. Andrade and Martindale found that the first stage was to form spherulites.

When growth occurs it seems to do so over the surface of the substrate, and the crystals show strong orientation with regard to this surface (Thomson and Cochrane 1938). It has been reported (Kowarski 1935) that one crystal can sometimes influence the orientation of another at a distance, which suggests a very thin mobile crystalline layer. The evidence for this is not yet conclusive, but it would be intriguing if the Volmer layer turned out to have an ordered structure of some kind. Other cases of crystals increasing in size with time are probably examples of the tendency for the large to swallow up the small.

So far we have considered a crystal growing from a seed of its own composition, or from none at all. Very interesting effects occur when one crystal is grown upon another. The classical case is the growth of sodium nitrate on calcite. The two are isomorphous and the sodium nitrate grows from solution with its axes parallel to those of calcite. Many other cases are known, for growth both from solution and from melts, for electrolytically deposited crystals and for crystals grown from vapour.

Isomorphism is not essential. Sodium nitrate will form orientated crystals from the melt on mica (Lassen 1934), and very large crystals can be grown in this way, but though mica is monoclinic, the top layer of atoms is pseudo-hexagonal and similar to the (111) face of soldium nitrate.

The view is often expressed that orientated growth of this kind, or epitaxis as it is called, depends essentially on a near equality of spacing between atoms in the top layer of the substrate and those in the layer of the crystal that grows to join it. Certainly such an agreement exists in many of the most striking cases, but I would like to suggest that the importance of this has been exaggerated and that other considerations are equally important. In particular I think that the existence of steps and cracks in the mother crystal are often the determining factor. Atoms align themselves along these steps, which become a zone axis of the daughter crystal, some prominent face grows out over the surface of the mother crystal, and thus orientation is established. Certainly this is more easily done if there is a similarity in the atomic patterns of the two layers, but even this is not essential.

Andrade and Martindale have shown the importance of cracks in determining the siting of crystals of silver and gold grown on glass and diamonds. Strictly, this is not quite the same thing, since they were concerned with the way in which minute crystals scattered over a substrate surface grouped themselves while we are interested in the direction of the axes of the individual crystals. Still, the attraction of the cracks for the atoms that are trying to form up as a crystal is strikingly shown in their work.

I should like to call your attention to three or four examples in which epitaxis has been observed for groups of crystals.

Let us take first the classical work of Royer (1928) on the growth of alkali halides on mica. He found that among 25 alkali halides, both of the face- and body-centred types, 11 showed good orientation on mica. In all cases the (111) face of the halide coincided with the cleavage of the mica. The pattern on this face is of course one of equilateral triangles, and in all cases but one these were so turned as to fit the corresponding pattern of the mica. If the difference in the dimensions of the pattern was less than 12% orientation occurred, if more it did not. In one case, KCl, orientation sometimes occurred with a 14·5% discrepancy. But there is another type of orientation in which the triangles are set at right angles. The fit here is much better for KCl—almost perfect—but it applies only to $\frac{1}{4}$ of the atoms. It is the less common form of orientation of the two. Four other of the halides could adopt this form of orientation with less percentage discrepancy than in the one they actually chose, but this is not observed. This goes to show that the specific nature of the planes and lines on which the fit occurs is more important than the actual numerical closeness of agreement.

Another example is given by metals deposited by spluttering on rocksalt. They have been studied by Lassen and Brück (Brück and Lassen 1935, Brück 1936) using the method of electron diffraction. They find many examples where the orientation actually chosen is not that which gives the closest fit, as can be seen from table 1. Brück interpreted his results in terms of the mean distance of atom in the mother and daughter crystals averaged over a cell, which he found tended to be a minimum, but in view of the different electrical character of the Na and Cl atoms in the surface it seems doubtful if much weight can be attached to this.

In all Brück's cases important lines of atoms coincided in the two crystals, and this appears also from the experiments of Rüdiger (1937), who studied the deposit of Au, Ag, Pt on calcite, mica and fluorite.

It should however be pointed out that in Brück's case, at least, there is no single direction on the mother crystal, which is always a zone axis for the daughter.

When metals are deposited on metals there is a strong tendency to follow completely the structure of the underlying metal as shown in the work of Cochrane (1936) and Finch and Sun (1936), who in both cases deposited the metal electrolytically and tested the result by electron diffraction. Many suitable metals have nearly the same structure and spacing, so on almost any theory one would expect them to fit in this way. Interesting exceptions are iron on palladium and gold, where Finch and Sun found cube planes in contact, but the face diagonal of the iron parallel to the cube edge of the substrate. This gives a good fit. The same authors found a peculiar effect of nickel on gold in which the same arrangement as that for iron occurs, though complete parallelism would actually give a *better* fit.

Cochrane found that a substrate of copper forces nickel to adopt the copper spacing, which is 2·5% different, for very thin deposits. The strain causes

Table 1. Metal films evaporated on to rocksalt. Brück (1936)

Metal	Plane ‖ (100) NaCl	Orientation	% errors w.r.t. NaCl	Any better fit	Plane ‖ (100) NaCl	Orientation	% errors w.r.t. NaCl	Remarks
Ni	(100)	Cube edges ‖	+25 0%	Yes ?	(210)	Ni edge ‖ NaCl face diag.	− 0·8% −11·2%	Only good fit in one direction. Symmetry relation lost
Cu	(100)	Cube edges ‖	+28·0%	Yes ?	(210)	Cu edge ‖ NaCl face diag.	+ 1·1% − 9·5%	Ditto.
Fe at two diff. temps.	(110)	Cube edges ‖	−28·1% + 1·4%	Yes	(100)	Cube edges ‖	+ 1·4%	Apparently a much better fit with no loss of symmetry relation
	(100)	NaCl edge ‖ Fe face diag.	−28·1%	Yes				
Cr at two diff. temps.	(110)	Cube edges ‖	−27·9% + 1·5%	Yes	(100)	Cube edges ‖	+ 1·5%	Ditto
	(100)	NaCl edge ‖ Fe face diag.	−27·9%	Yes				
Al at two diff. temps.	(111)	A pair of face diags. ‖	+24·0% −28·4%	Yes	(100)	Al edge ‖ NaCl face diag.	+ 1·2%	Ditto
	(100)	Cube edges ‖	−28·4%	Yes				
Ag	(100)	Cube edges ‖	−27·6%	Yes	(100).	Ditto.	+ 2·4%	Ditto
Av at two diff. temps.	(111)	A pair of face diags. ‖	+24·8% −28·0%	Yes	(100)	Au edge ‖ NaCl face diag.	+ 2·1%	Ditto
	(100)	Cube edges ‖	−28·0%	Yes				

Table 2. Metals deposited on beaten foils. Finch and Sun (1936)

Substrate	Deposit	Substrate orientation	Deposit plane ‖ surface	Other planes ‖		% error w.r.t. substrate	Any better fit ?	Deposit plane ‖ surface	Other planes ‖		% error w.r.t. substrate	Remarks
				Sub.	Dep.				Sub.	Dep.		
Pt	Cu	(110)	(110)	$(1\bar{1}0)$	$(1\bar{1}0)$	− 7·6%	No	—	—	—	—	Symmetrical orientation
Pt	Ni	(110)	(110)	$(1\bar{1}0)$	$(1\bar{1}0)$	− 9·9%	No	—	—	—	—	Ditto
Pt	Co	(110)	(110)	$(1\bar{1}0)$	$(1\bar{1}0)$	− 9·1%	No	—	—	—	—	Ditto
Pd	Cu	(100)	(100)	$(1\bar{1}0)$	$(1\bar{1}0)$	− 6·7%	No	—	—	—	—	Ditto
Pd	Fe	(100)	(100)	(110)	(100)	+ 4·8%	No	—	—	—	—	Change of orientation due to body-centred deposit.
Au	Fe	(100)	(100)	(011)	(001)	− 0·6%	No	—	—	—	—	Ditto
Au	Co	(100)	(100)	(001)	(001)	− 12·8%	No	—	—	—	—	Symmetrical orientation
Au	Ni	(100)	(100)	(011)	(001)	+ 22·3%	Yes	(100)	(100)	(100)	− 13·5%	Unusual since only face-centred metal showing this orientation

frequent twinning of the nickel when the deposit grows thicker. Chromium on copper showed two orientations in both of which important zone axes are parallel in the two crystals.

An example of the influence of faults on crystal growth is shown in a paper by Willems (1943) which studies the growth of urotropine on gypsum. The small parallelograms of the urotropine appear lined up with their sides parallel to steps in the gypsum.

While mere agreement in spacing is not conclusive, even when accompanied, as it must be, by similarity in arrangement of the atoms, there is no doubt from Royer's work that it plays an important part. If we take a figure of 12% as giving the maximum permissible disagreement for halides of mica, we can estimate the size of the embryo crystal which is sufficient to ensure indefinite growth under the conditions of the experiment. If the spacings of halide and mica are 1 and $1+\alpha$, then after n steps the atoms will be αn apart. We may suppose that while this is less than $\frac{1}{2}$, the forces on the whole tend to favour growth compared with a random position, but when it exceeds this value then they are unfavourable. Hence $\alpha n=\frac{1}{2}$, which for $\alpha=0{\cdot}12$ gives $n=4$. The spacing in question being 5·15 A., we get 20 A. as the size of the embryo.

Table 3. Metallic deposits on copper. Cochrane (1936)

Metal	Orientation	% error w.r.t. Cu	Any better fit?	Orientation	% error w.r.t. Cu	Remarks
Ni	Completely ∥	− 2·4%	No	—	—	Takes Cu lattice constants for thin layer
Cu	Ditto	Nil	No	—	—	—
Zn	Does not orientate	—	—	—	—	—
Cd	Ditto	—	—	—	—	—
Ag	Completely ∥	+13·2%	Yes	(111)'s ∥. Rotated 30° w.r.t. one another.	−2·0%	Not complete symmetry
Cr	(110) Cr ∥ (111) Cu. Cube edge of Cr ∥ face diag. of Cu.	+12·7% − 8·1%	No	—	—	Two possibilities of orientation
Co	Completely ∥	− 1·6%	No	—	—	—

One might expect the necessary size of the embryo would decrease with increasing supersaturation, and it would be interesting to try if any effect of this kind can be observed.

Another kind of orientated growth is that which sometimes occurs when a crystal takes part in a chemical reaction. Many years ago I was able to show (Thomson 1930) that a single crystal of copper could oxidize to Cu_2O in such a way that the axes of the two crystals, both of which are cubic, were parallel. Since then a number of other examples have been found. In studying these we must remember that only certain faces of the original crystal will be exposed, and that, except in the case of cleavage faces, these are not necessarily the apparent faces, since, for example, etching may produce pits covering the whole or almost the whole of the apparent surface. It is only on exposed faces that orientated growth can occur.

An examination of the observed instances allows certain general conclusions to be drawn. In general we have to do with a reaction in which new atoms are introduced, as when metals are oxidized, or in which some new atoms are substituted for old ones, as in the growth of one halide of silver on another, or silver bromide on thallous bromide, recently studied by Schwab (1947).

In most cases the atoms that remain keep their relative positions, though the distances between them necessarily often change. In some cases, e.g. growth of cuprous bromide and iodide on the (111) face of copper (Usmani 1941), the arrangement of atoms is similar in the two crystals but of different orientation. Here the copper atoms in both the metal and the halide form a lattice of equilateral triangles, but the two are turned with respect to one another through a right angle. The two planes appear always to have the same symmetry and general arrangement of atoms.

There is a preference for a fit in actual spacing where this is possible. Thus the rotation of the planes of the copper halides just mentioned greatly improves the fit, which is about 3% for the iodide and still better for the bromide, though it necessarily implies that not every atom has a partner in the new crystal.

The requirements of fit are not too exacting. Thus Schwab (1947) found hexagonal AgI can grow on the (111) face of AgBr with a difference of 13%, and some of the oxides show even larger differences, 18% for copper and 28% for barium (Burgers and Van Amstel 1936). Schwab has pointed out that the growth of AgBr on TlBr is probably helped by the fit normal to the plane of contact, which is (110) in both crystals, the large bromine atoms filling spaces left by the smaller metal atoms in the layer. The discrepancy in dimensions in this case is 2·5%.

There is much yet to be found out in the study of orientated growth. It is probable that different considerations are dominant in different cases. Equality of spacing is important but is not the only thing that matters. Crystal growth, and especially the part played in it by the Volmer layer, is a fascinating subject, which may be expected to increase greatly our knowledge of the other surface phenomena. The study of orientated crystals produced by chemical action is one of the most promising ways of finding out more about the mechanism of chemical change on which, after centuries of chemical study, science is still grossly ignorant.

REFERENCES

AMSLER, J., 1942, *Helv. Phys. Acta*, **15**, 699.
ANDRADE, E. N. DA C., and MARTINDALE, J. G., 1935, *Phil. Trans. Roy. Soc.* A, **235**, 69.
BERG, W. F., 1938, *Proc. Roy. Soc.* A, **164**, 79.
BRANDES, H., 1927, *Z. phys. Chem.*, **126**, 196.
BRÜCK, L., 1936, *Ann. Phys., Lpz.*, **26**, 233.
BRÜCK, L., and LASSEN, H., 1935, *Ann. Phys., Lpz.*, **22**, 65.
BURGERS, W. G., and VAN AMSTEL, J. J. A. P., 1936, *Physica*, **3**, 1037.
COCHRANE, W., 1936, *Proc. Phys. Soc.*, **48**, 723.
COCKCROFT, J. D., 1928, *Proc. Roy. Soc.* A, **119**, 293.
FINCH, G. I., and SUN, C. H., 1936, *Trans. Faraday Soc.*, **32**, 852.
GIBBS, J. W., 1906, *Scientific Papers*, Vol. I, 324.
KOSSEL, W., 1928, *Phys. Z.*, **29**, 553 ; 1934, *Ann. Phys., Lpz.*, **21**, 457.
KOWARSKI, L., 1935, *J. Phys. Chem.*, **32**, 303, 395, 469.

Lassen, H., 1934, *Phys. Z.*, **35**, 172.
Lotmer, W., 1945, *Helv. Phys. Acta*, **18**, 369.
Marcellin, R., 1918, *Ann. Phys. Chem.*, **10**, 185.
Royer, L., 1928, *Bull. Soc. franç. Mineral.*, **51**, 7 - 159.
Rüdiger, O., 1937, *Ann. Phys., Lpz.*, **30**, 505.
Schwab, G. M., 1947, *Trans. Faraday Soc.*, **128**, 641.
Stranski, I. N., 1928, *Z. phys. Chem.*, **136**, 259 ; 1943, *Z. Kristallogr.*, **105**, 90.
Stranski, I. N. and Kaischew, R., 1934, *Z. phys. Chem.*, **26**, Abt. B.1, 100, 312, Abt. B.4–5, 317 ; 1935, *Phys. Z.*, **36**, 393, *Ann. Phys. Lpz.*, **23**, 330 ; 1937, *Z. phys. Chem.* B, **35**, 427.
Thomson, G. P., 1930, *Proc. Roy. Soc.* A, **128**, 641.
Thomson, G. P., and Cochrane, W., 1938, *Theory and Practice of Electron Diffraction* (London : Macmillan and Co.).
Usmani, I. H., 1941, *Phil. Mag.*, **7**, 32, 89.
Valeton, J. J. P., 1923, *Z. Kristallogr.*, **59**, 168, 335 ; 1924, *Ibid.*, **60**, 1.
Volmer, M., 1921, *Z. Elektrochem.*, **35**, 555.
Volmer, M., and Adhirkari, G., 1925, *Z. Phys.*, **35**, 170 ; 1926, *Z. phys. Chem.*, **119**, 46.
Volmer, M., and Estermann, I., 1921, *Z. Phys.*, **7**, 13.
Volmer, M., and Weber, A., 1926, *Z. phys. Chem.*, **119**, 277.
West, C. D., 1945, *J. Opt. Soc. Amer.*, **35**, 26.
Willems, J., 1943, *Z. Kristallogr.*, **105**, 149.
Wulff, G., 1901, *Z. Kristallogr.*, **34**, 449.

The Interpretation and Application of Electron-Diffraction "Kikuchi-Line" Patterns—
Part II. The Methods of Indexing the Patterns

By H. WILMAN
Applied Physical Chemistry Laboratories, Imperial College, London

MS. received 17 *October* 1947

ABSTRACT. Seven methods are described of indexing electron-diffraction Kikuchi-line patterns from single crystals for the purpose of practical applications of such patterns. The crystal lattice form and orientation can be determined by method 1 (see Part I), which also gives the indices of the diffractions relative to the chosen unit cell. The other six methods are in general only applicable in conjunction with a knowledge of the crystal lattice form and orientation, in which case any one of them, or more conveniently several in conjunction, can be used to index the lines.

§ 1. INTRODUCTION

The only generally applicable direct method, independent of information about the crystal other than that contained in the diffraction pattern and a knowledge of the diffraction conditions, is the method described by Wilman (1948)—to be referred to as Part I—involving a construction of the reciprocal lattice. When a suitable unit cell in this reciprocal lattice has been chosen, the crystal lattice orientation and Laue symmetry can be defined, and the Laue indices of the Kikuchi-line diffractions follow simply as the coordinates of the corresponding reciprocal-lattice points, relative to the chosen reciprocal axes.

The other methods described here may be useful, for example, when too small a range of diffracted beams is recorded, or is distinguishable, to apply the absolute method described in Part I, or when the crystal nature and structure are already known but it is required to explore the intensities of a large range of diffractions, or to define the orientation more precisely than can be done from the spot pattern when the spots are too diffuse or too few to apply the methods previously developed by the author (Charlesby, Finch and Wilman 1939).

One or other of these methods, or several in conjunction, can generally be applied successfully, so that the desired information about the relative orientations and relative reflecting powers of the different net planes can be derived and specified.

§ 2. OUTLINE OF THE MAIN FEATURES OF THE METHODS, AND SOME ESSENTIAL COMMON CONSIDERATIONS

(i) *The general characteristics of the methods*

The seven methods listed below are of three types. The first two methods are characterized by construction of a projection in which each net plane is represented by a point. It is only the first method, the reciprocal-lattice projection, which incorporates information on the net-plane spacings as well as on the directions of the net-plane normals represented in the second, gnomonic projection, method. The main feature of the second type of method is the derivation of the ratios of the net-plane or the Laue indices from the ratios of the intercepts cut off by the net-plane trace, i.e., the line-pair median, either on the three lines which are along the projections of the crystal axes on the plate (method 3), or (methods 4 and 5) on two perpendicular axes on the plate, one of which is along a definite $(h_1k_1l_1)$ net-plane trace on the plate. The third type of method uses either the zone relationships (method 6) or the closely related parabolic and circular envelope relationships (method 7). All the methods are developed for the general case of a triclinic crystal, and the expressions applicable to crystals of other systems can be derived by giving a, b, c, α, β, γ appropriate values.

Methods 2, 4, 5 and 6 supply only the Miller indices of the reflecting net plane as a first step, and the order number of the Bragg reflection must then be found from the calculated plane spacing d and the measured line-pair separation D. Methods 1, 3 and 7, however, provide the Laue indices of the line diffractions directly, the measurements of D being used in combination with the other data which define the net-plane direction.

The first method alone actually carries out a construction of the reciprocal lattice and thus an independent determination of the crystal lattice, assuming only a knowledge of the camera length L and the position of O_1, the foot of the perpendicular from the crystal origin O to the photographic plate. The wavelength must also be known if an estimation of the axial lengths a, b, c is required instead of just the axial ratios. Method 2 can also be used to a limited extent for a determination of the lattice form and orientation, but only in rather special cases where the crystal setting is a favourable one.

In all the other methods the further knowledge is assumed of the lattice constants a, b, c, α, β, γ and of the crystal orientation relative to the photographic plate or the primary beam. This information, if not definitely known or obtained by the method of Part I, can sometimes be inferred from the relative positions of the main bands in the pattern, possibly together with information provided by the geometrical form of the spot pattern and, if necessary, in conjunction with an examination of other patterns obtained at different settings, or patterns of other types such as powder and rotation patterns.

The various methods are mostly best suited to different spheres of application. Method 1 is the most fundamental, generally applicable and independent.

Method 2 is not usually so convenient as the other methods and is only readily usable when the polar direction of the projection is along or close to a crystal axis or a principal lattice row. Method 4 (Finch, Quarrell and Wilman 1935) was developed by the author to study the relationships between the Kikuchi lines and their parabolic and circular envelopes in reflection patterns at different azimuths; and method 5, also evolved in this laboratory (Thirsk and Whitmore 1940) is a form of method 4 more directly expressed for application to particular main azimuths. The neater and simpler method 3 was developed by the author in 1939 for easier practical use, especially when the crystal orientation is not very near to a main setting but is known relatively closely from the Laue spot positions as in the case of one of the anthracene patterns reproduced by Charlesby, Finch and Wilman (1939), where this method was first applied. Methods 6 and 7 are easy to apply and are often exceedingly useful, especially if only the intensified line of a pair is distinguishable; and when desirable these methods can be systematically applied in the way shown below.

(ii) *Preliminary considerations applicable to all methods*

The following considerations should be noted in indexing a pattern, whatever the method used.

(*a*) *Conventional viewpoint to be used in indexing prints.* The indexing of the pattern can be carried out on either a negative or a positive print; the latter is preferable for clearness. A positive print should be considered as corresponding to the electron distribution in the recording plane seen from the side of this plane opposite to that on which the electrons fall and on which the crystal lies (Part I). A negative print (or the initial "negative" recording observed from the sensitive emulsion side) should be regarded as corresponding to the electron distribution in the recording plane, viewed from the side on which the electrons fall and on which the crystal lies.

(*b*) *The Bragg-reflection positions at the band edges.* These have been shown in Part I to be at, or practically at, the points where the intensity is equal to the background intensity in the region considered.

(*c*) *The black and white line positions.* The positions of the Bragg reflection loci and the intersections of the net planes with the plate are determined by the orientation of the crystal relative to the plate, and are best specified relative to the foot O_1 of the normal from the crystal origin O to the plate. The primary electron beam OF is not in general along OO_1, and of a Kikuchi-line pair the one farthest from OF is the intensified line and the one nearest OF the absorption line relative to the general background intensity.

(*d*) *Convention for the sign of the Laue indices of the line diffractions.* The direction of a net plane is specified equally well by the Miller indices (hkl) or ($-h, -k, -l$), but in a Laue spot pattern the diffraction directions represented by the Laue indices hkl and $-h, -k, -l$ are different, and the sign of each index is fixed by the directions of this diffraction and of the primary beam relative to the corresponding crystallographic axis. In Kikuchi-line patterns, owing to the partial reciprocal relationships between the diffraction lines of a pair, there remains the question of which line of the pair is to be called the hkl diffraction and which the $-h, -k, -l$. It is important to adopt a convention to specify the sign to be used for each line, not merely for uniformity, but in order to be able to use the zone and envelope Laue-index relationships (methods 6 and 7) without errors arising from this cause.

A convention which is easy to apply, and which is now recommended, is the following : Consider the two lines of a pair as the intersection with the plate of the two halves of a cone whose apex is at the crystal origin O, each line of the pair corresponding to one half of the cone on one side only of the net plane (also through O) whose trace on the plate is the median of the line pair. Then, having chosen the positive directions of the axes a, b, c, the positive (hkl) plane normal is that from the origin O to the plane which cuts off intercepts a/h, b/k, c/l on a, b, c respectively, and the Kikuchi line which corresponds to the half-cone lying on the same side of O as this plane can be assigned the Laue indices hkl or the appropriate multiples nh, nk, nl. Conversely, the other line of the pair has Laue indices $-nh$, $-nk$, $-nl$ and corresponds to the half-cone lying on the opposite side of O, where also is the plane whose intercepts on a, b, c are $-a/h$, $-b/k$, $-c/l$ respectively. A paper or card model comprising the ab, bc, and ca faces of the unit cell is helpful in visualizing orientations of a particular net plane when the crystal orientation relative to the photographic plate is known.

The above convention is automatically followed if the indexing of the lines is done by method 1, but it has to be specifically applied in all the other methods of indexing.

(*e*) *Conversion of plane-trace and Kikuchi-line positions to those which would be obtained on a different recording plane.* The expressions derived below in methods 3, 4, 5 for the positions of the lines and the line-pair medians or plane normals take more convenient simple forms in the case where the known direction which defines the normal to the photographic plate has relatively small integral indices. If the plate normal OO_1 in any particular case does not approximately coincide, as it is usually arranged to do, with such a lattice row, the position that a line or a band median would have on a plate normal to any desired lattice row $[uvw]$ inclined at δ to the actual plate normal can be constructed as follows (figure 1).

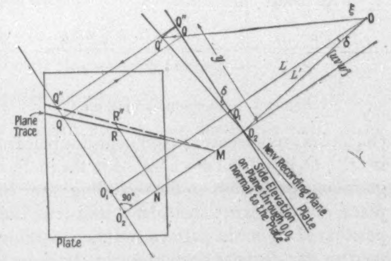

Figure 1.

Let O_2 be the (observed) intersection of the lattice row $[uvw]$ with the plate and O_2M be normal to O_1O_2. Let QM be a line-pair median, i.e., a net-plane trace on the plate, produced to meet O_2M at M and O_2O_1 at Q. Then, as can be seen from the side elevation in figure 1, the line OQ which lies in the net-plane under consideration is prolonged to meet at Q' the plane which is normal to OO_2, i.e., $[uvw]$. If this new recording plane is now rotated about the line O_2M so as to become coincident with the actual plate, O_2Q' rotates to the position O_2Q''; whence the position of Q'' is as shown in the plan part of figure 1. In the triangle OO_2Q, let angle $O_1OO_2 = \delta$, angle $O_2OQ = \xi$, and $O_2Q = y$, then

$$y/\sin\xi = L'/\sin\{180° - \xi - (90° - \delta)\},$$

and Q″ is given by

$$Q''O_2/QO_2=(y+\Delta y)/y=(L'/y)\tan\xi=\cos\delta/\{1-(y/L')\sin\delta\}.$$

The plane trace on the new recording plane is then the line Q′M, which becomes Q″M when rotated into the plane of the plate. It follows that any other ordinate RN is also changed to R″N where $R''N/RN=Q''O_2/QO_2$.

As a particular example it can be seen that if δ is less than about 5° and $L'\sim 20$ cm. with RN<6 cm., then $\Delta y/y<2\%$, thus under these conditions, to a first approximation, the pattern can be indexed as if OO_2 was the normal to the plate.

The new Kikuchi-line positions can be found, if necessary, by treating as plane appropriate small parts of the corresponding diffraction cones, and applying the above construction.

§ 3. THE METHODS OF INDEXING THE PATTERNS

(i) *The reciprocal-lattice projection method*

This has been fully described and illustrated in Part I and will not be discussed further here.

(ii) *The gnomonic projection method*

A gnomonic projection can be constructed very easily from the positions of the band medians. If any net plane is shown in side view by the line OP in figure 2 (K_1 and K_2 representing a Kikuchi-line pair from this plane), then the plane normal is OP′, $O_1P'=L\cot\phi=L^2/p$; ϕ is the inclination of the net plane to OO_1. The gnomonic projection on the recording plane comprises points such as P′ where the plane normals meet this plane, and it is thus simply obtained by marking the position of O_1 on the pattern and then marking a point corresponding to each band median, at a distance proportional to $1/p$ from O_1 on a line through O_1 normal to the band median, and on the opposite side of O_1 from the band median. The application to x-ray diffraction patterns has been illustrated by Wyckoff (1931), Bragg (1933), and others.

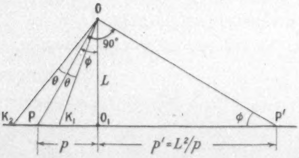

Figure 2. Gnomonic projection.

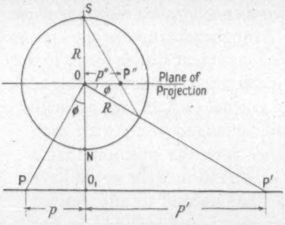

Figure 3. Stereographic projection.

Although stereographic projections are not easy to apply to the indexing of Kikuchi-line patterns, it may sometimes be desired to construct such a projection, and this can be done as follows. Representing a net plane in edge view by OP (figure 3) and its normal by OP′, meeting the plate at P′, its stereographic projection on a plane through O parallel to the plate is P″, of radius R. By joining the point where OP′ cuts the sphere to the opposite pole S, the point P″ is found as the intersection of this line with the equatorial projection plane. It is easy to show that the length OP″, i.e. p'', is

$$p'' = R\cos\phi/(1+\sin\phi) = R[\{1+(p/L)^2\}^{\frac{1}{2}} + p/L]^{-1}.$$

To construct a stereographic projection from a Kikuchi line pattern it is thus necessary to measure off from O_1 (or a point displaced suitably outside the pattern area) distances p'' in a direction opposite to that of the normal drawn from O_1 to each line-pair median.

(iii) *The method of intercepts on the three axial projections on the plate*

The Laue indices of the Kikuchi lines can be calculated directly from the bandwidth D and the intercepts which the band median cuts off on the projections $\mathbf{a}_p$, $\mathbf{b}_p$, $\mathbf{c}_p$ of the crystal axes $\mathbf{a}$, $\mathbf{b}$, $\mathbf{c}$, drawn from the point O_1 where a known lattice row $[uvw]$ meets the plate normally (or nearly so). In figure 4, let O be the origin in the crystal and OO_1, of length L, be the normal from O to the plate. Let $\mathbf{a}$, $\mathbf{b}$, $\mathbf{c}$ meet the plate at A, B, C, respectively, so that O_1A, O_1B, C_1C are in the directions of $\mathbf{a}_p$, $\mathbf{b}_p$, $\mathbf{c}_p$ and let the (hkl) plane through O cut O_1A, O_1B, O_1C at X, Y, Z, distant x, y, z from O_1. Also let $\mathbf{N}$ be the unit vector along OO_1 and $\mathbf{n}$ that along the normal from O outwards to the plane whose intercepts on $\mathbf{a}$, $\mathbf{b}$, $\mathbf{c}$ are $\mathbf{a}/h$, $\mathbf{b}/k$, $\mathbf{c}/l$; the angles between $\mathbf{N}$ and $\mathbf{a}$, $\mathbf{b}$, $\mathbf{c}$ are θ_a, θ_b, θ_c respectively. Then we have

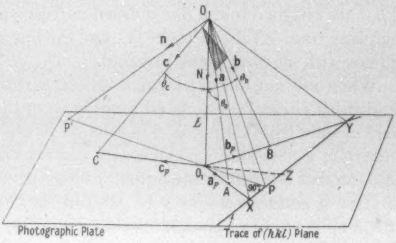

Figure 4.

$$\mathbf{O_1A} = \mathbf{OA} - \mathbf{OO_1} = (L/\cos\theta_a)(\mathbf{a}/a) - L\mathbf{N}.$$

The equation of the line O_1A relative to O as origin is thus

$$\mathbf{r} = L\mathbf{N} + mL\{(\mathbf{a}/a\cos\theta_a) - \mathbf{N}\},$$

where m is a parameter. Since the point X on this line lies in the (hkl) plane through O, its radius vector $\mathbf{r}$ must also satisfy $\mathbf{r}\,.\,\mathbf{n} = 0$.

Hence, with $\mathbf{a}\,.\,\mathbf{n} = hd$,

$$L\mathbf{N}\,.\,\mathbf{n} + mL[\{(\mathbf{a}\,.\,\mathbf{n})/a\cos\theta_a\} - \mathbf{N}\,.\,\mathbf{n}] = 0,$$

i.e. $$m = \cos\theta_p/\{\cos\theta_p - (hd/a\cos\theta_a)\},$$

where θ_p is the angle between $\mathbf{N}$ and $\mathbf{n}$. We now have, directly, $O_1A = L\tan\theta_a$,

whence $$O_1X = x + mO_1A = L\tan\theta_a\cos\theta_p/\{\cos\theta_p - (hd/a\cos\theta_a)\}$$

and $$h = (a/d)\cos\theta_p\,.\,[\cos\theta_a - (L/x)\sin\theta_a],$$

and there are similar expressions for k and l.

The values of d and $\cos\theta_p$ must be expressed in terms of the bandwidth D, the Laue indices hkl of the diffraction line, and the length p of the perpendicular from O_1 to the trace XYZ of the (hkl) plane (subtending $90° - \theta_p$ at O), thus

$$d = \lambda/(2\sin\theta) \simeq \lambda L/D\sin\theta_p; \quad \cos\theta_p = p/(L^2+p^2)^{\frac{1}{2}}; \quad \sin\theta_p = L/(L^2+p^2)^{\frac{1}{2}}.$$

Hence $$h=[pD/(L^2+p^2)](a/\lambda)[\cos\theta_a-(L/x)\sin\theta_a].$$

Similarly $$k=[pD/(L^2+p^2)](b/\lambda)[\cos\theta_b-(L/y)\sin\theta_b],$$
$$l=[pD/(L^2+p^2)](c/\lambda)[\cos\theta_c-(L/z)\sin\theta_c].$$

In order to calculate h, k and l for a line pair it is thus necessary to calculate θ_a, θ_b and θ_c and the directions of $\mathbf{a}_p$, $\mathbf{b}_p$, $\mathbf{c}_p$ for the known or estimated crystal setting (actually in most main settings these are almost obvious or very simply calculated), and to measure λL, x, y, z, p and D and then use these equations. λ need not be known if only $h:k:l$ is accepted as sufficient to determine h, k and l. The lengths x, y, z are positive or negative according to whether they are measured from O_1 along the "positive" or the "negative" direction of a_p, b_p or c_p. The signs of h, k and l also depend on p and θ_p. If p is always positive and thus θ_p always an acute angle, i.e. to the positive direction of the net-plane normal n always down from O towards the plate, then with the index convention stated in § 2 the indices h, k, l are assigned to the line diffraction (black or white) which lies on the side of the plane trace XYZ nearest to O_1, and the line on the opposite side XYZ has the indices with all three signs reversed.

When only one line of the pair is visible, so that p and D cannot be measured, the bandwidth D can be estimated roughly from the sharpness of the line, or much more exactly from its position in relation to other lines which form with the line concerned a parabolic envelope with the associated zone axis intersection at its focus, so that $D/2$ can be measured.

If $p=0$, and thus $x=y=z=0$, the only finite terms remaining in the equations for h, k and l are those containing the factors p/x, p/y and p/z which are the cosines of the angles between O_1P and O_1A, O_1B and O_1C respectively.

Calculation of θ_a, θ_b, θ_c *when* OO_1 *is along* $[uvw]$. If the angles θ_a, θ_b, θ_c are not directly known, but a lattice row $[uvw]$ is known to be along OO_1, the values of $\cos\theta_a$, $\sin\theta_a$ etc. can be calculated as follows for insertion in the above equations for h, k and l.

If $\mathbf{T}$ is the (positive) $[uvw]$ lattice translation,

$$\cos\theta_a=\mathbf{T}\,.\,\mathbf{a}/Ta=(ua+vb\cos\gamma+wc\cos\beta)/T,$$
$$\cos\theta_b=\mathbf{T}\,.\,\mathbf{b}/Tb=(ua\cos\gamma+vb+wc\cos\alpha)/T,$$
$$\cos\theta_c=\mathbf{T}\,.\,\mathbf{c}/Tc=(ua\cos\beta+vb\cos\alpha+wc)/T,$$

where $T^2=u^2a^2+v^2b^2+w^2c^2+2uvab\cos\gamma+2vwbc\cos\alpha+2wuca\cos\beta$.

Since $\sin^2\theta_a=1-\cos^2\theta_a$, this gives

$$\sin^2\theta_a=[v^2b^2\sin^2\gamma+w^2c^2\sin^2\beta+2vwbc(\cos\alpha-\cos\beta\cos\gamma)]/T^2,$$
$$\sin^2\theta_b=[u^2a^2\sin^2\gamma+w^2c^2\sin^2\alpha+2uwac(\cos\beta-\cos\gamma\cos\alpha)]/T^2,$$
$$\sin^2\theta_c=[u^2a^2\sin^2\beta+v^2b^2\sin^2\alpha+2uvab(\cos\gamma-\cos\alpha\cos\beta)]/T^2.$$

Thus, for example,

$$h=\{pD/(L^2+p^2)\}(a/\lambda)(1/T)\,.\,[(ua+vb\cos\gamma+wc\cos\beta)$$
$$-(L/x)\{v^2b^2\sin^2\gamma+w^2c^2\sin^2\beta+2vwbc(\cos\alpha-\cos\beta\cos\gamma)\}^{\frac{1}{2}}].$$

These expressions take much simpler forms in the more symmetrical crystal systems, thus for example for cubic crystals,

$$h=[pD/(L^2+p^2)](a/\lambda)(u^2+v^2+w^2)^{-\frac{1}{2}}[u-(L/x)(v^2+w^2)^{\frac{1}{2}}],$$
$$k=[pD/(L^2+p^2)[(a/\lambda)(u^2+v^2+w^2)^{-\frac{1}{2}}[v-(L/y)(u^2+w^2)^{\frac{1}{2}}],$$
$$l=[pD/(L^2+p^2)](a/\lambda)(u^2+v^2+w^2)^{-\frac{1}{2}}[w-(L/z)(u^2+v^2)^{\frac{1}{2}}].$$

Calculation of the angles between $\mathbf{a}_p$, $\mathbf{b}_p$, *and* $\mathbf{c}_p$ *and the normal to the trace of the* $(h_1k_1l_1)$ *plane passing through* $[uvw]$, *normal to the plate.* When the directions of the projections $\mathbf{a}_p$, $\mathbf{b}_p$, $\mathbf{c}_p$ are not conveniently determined by inspection from the known orientation or the geometry of the spot pattern, i.e. the Laue zones along the spot rows, they can be calculated from the known indices $[uvw]$ of OO_1 and those $(h_1k_1l_1)$ of a plane which passes through this zone axis and whose Kikuchi lines are identified in the pattern.

Thus, the vector $\mathbf{r}_1{}^* = h_1\mathbf{a}^* + k_1\mathbf{b}^* + l_1\mathbf{c}^*$ lies in the plate, normal to $(h_1k_1l_1)$, and since $\mathbf{a}_p = \mathbf{a} - (\mathbf{a}\,.\,\mathbf{N})\mathbf{N}$,

$$\cos(\mathbf{a}_p, \mathbf{r}_1{}^*) = (\mathbf{a}_p\,.\,\mathbf{r}_1{}^*)/a_p r_1{}^* = (d_1/a_p)\{\mathbf{a}\,.\,\mathbf{r}_1{}^* - (\mathbf{a}\,.\,\mathbf{N})(\mathbf{N}\,.\,\mathbf{r}_1{}^*)\} = h_1 d_1/a \sin\theta_a,$$

$$\cos(\mathbf{b}_p, \mathbf{r}_1{}^*) = k_1 d_1/b \sin\theta_b, \quad \text{and} \quad \cos(\mathbf{c}_p, \mathbf{r}_1{}^*) = l_1 d_1/c \sin\theta_c,$$

where $\sin\theta_a$, $\sin\theta_b$ and $\sin\theta_c$ are given by the expression stated above, in terms of u, v and w. For cubic crystals, for example, $\cos(\mathbf{a}_p, \mathbf{r}_1{}^*) = h_1/(h_1{}^2 + k_1{}^2 + l_1{}^2)^{\frac{1}{2}} \sin\theta_a$, etc.

It is desirable to check the relative positive directions of $\mathbf{a}_p$, $\mathbf{b}_p$, $\mathbf{c}_p$ carefully, preferably with the aid of a rough model, before proceeding to index the pattern.

(iv) *The method of intercepts on two perpendicular axes along and perpendicular to the trace of a plane* $(h_1k_1l_1)$, *in terms of the azimuth* ϕ *in this plane*

An analytical derivation of the equation of a net-plane trace or Kikuchi line has been given and illustrated previously (Finch, Quarrell and Wilman 1935), and it can also be obtained in a similar way by vector methods. The results are as follows.

First imagine the crystal unit cell to be mounted in a fixed, but at present unspecified, position relative to three orthogonal reference axes OX_3, OY_3, OZ_3. (A convenient setting is that shown in figure 5.) Now transfer the cell, together with these axes, to the diffracting crystal, and orientate it so that the axes $\mathbf{a}$, $\mathbf{b}$, $\mathbf{c}$ of the unit cell are parallel to the corresponding axes of the crystal, whose origin is at O (figure 6). Let OO_1 be the normal to the fluorescent screen or photographic plate and assume the known crystal orientation to be defined by the indices $(h_1k_1l_1)$ of a net-plane whose trace on the plate is the line $O_1{}'X$, and by the azimuth angle ϕ between two planes normal to $(h_1k_1l_1)$, one also normal to the plate and thus containing OO_1 and $OO_1{}'$, and the other containing OY_3 and intersecting $(h_1k_1l_1)$ in OY_2.

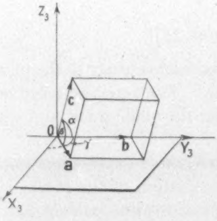

Figure 5.

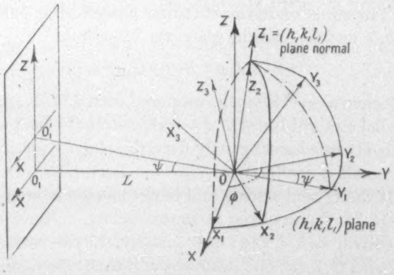

Figure 6.

The orthogonal set of axes OX_2, OY_2, OZ_2 is further defined by setting OZ_2 along the positive normal to the net plane $(h_1k_1l_1)$, i.e. from O to the plane which cuts off intercepts $\mathbf{a}/h_1$, $\mathbf{b}/k_1$, $\mathbf{c}/l_1$ on **a**, **b**, **c** respectively. A further orthogonal set of axes OX_1, OY_1, OZ_1 is such that OZ_1 coincides with OZ_2, and OX_1 is parallel to the plate and lies in the $(h_1k_1l_1)$ plane through O, i.e. $OX_2Y_1Y_2$. Finally the orthogonal axes OX, OY, OZ are such that OX is along OX_1 and OY is along O_1O; the angle YOY_1 is ψ.

On this basis, if the normals to the net planes $(h_1k_1l_1)$ and any other plane (hkl) have direction cosines λ_1, μ_1, ν_1 and λ, μ, ν relative to $OX_3Y_3Z_3$, the equation of the line where the plane (hkl) through O intersects the plate is, relative to O_1X and O_1Z on the plate (figure 6),

$$C_1z = -A_1x + B_1L,$$

where

$$\begin{aligned} A_1 &= A_2, & A_2 &= A_3\cos\phi - B_3\sin\phi, \\ B_1 &= B_2\cos\psi + C_2\sin\psi, & B_2 &= B_3\sin\phi + B_3\cos\phi, \\ C_1 &= C_2\cos\psi - B_2\sin\psi, & C_2 &= C_3, \end{aligned}$$

$$\begin{aligned} A_3 &= (\lambda\nu_1 - \nu\lambda_1)/(1-\mu^2)^{\frac{1}{2}}, \\ B_3 &= \{\mu - \mu_1(\lambda\lambda_1 + \mu\mu_1 + \nu\nu_1)\}/(1-\mu^2)^{\frac{1}{2}}, \\ C_3 &= \lambda\lambda_1 + \mu\mu_1 + \nu\nu_1, \end{aligned}$$

in which

$$1 = \lambda^2 + \mu^2 + \nu^2 = \lambda_1{}^2 + \mu_1{}^2 + \nu_1{}^2 = A_1{}^2 + B_1{}^2 + C_1{}^2 = A_2{}^2 + B_2{}^2 + C_2{}^2 = A_3{}^2 + B_3{}^2 + C_3{}^2.$$

If the origin of coordinates on the plate is transferred from O_1 to O_1', which is on the $(h_1k_1l_1)$ plane trace where it cuts O_1Z, the (hkl) plane trace has the equation $C_1z = -A_1x + B_2L/\cos\psi$, and if ψ is small this is approximately $C_2z = -A_2x + B_2L$, which is the same as the equation for the plane trace relative to O_1XZ with ψ put equal to zero.

The equation of the nth order Kikuchi-line pair from the (hkl) plane is, relative to O_1X and O_1Z on the plate, the hyperbola

$$(A_1x + B_1y + C_1z)^2 = (x^2 + y^2 + L^2)(n\lambda/2d)^2,$$

and when $x^2 + y^2$ is small compared with L^2 this approximates closely to the pair of parallel straight lines, $C_1z = -A_1x + \{B_1L - (n\lambda L/2d)\}$. The equation relative to O_1' is obtained analogously from the above equation for the plane trace, and when ψ is small it is effectively $C_2z = -A_2x + \{B_2L \pm (n\lambda L/2d)\}$.

If the crystal setting and lattice constants are known, these expressions can be evaluated, for example as shown below. Since the equation of the (hkl) plane trace involves h, k and l only linearly, the two intercepts of any line-pair median on O_1X and O_1Z (or one intercept and the slope) suffice to allow the ratios $h:k:l$ to be determined. The angle ϕ is taken here as the angle through which the crystal must be rotated in a positive direction (right-handed screw) about the positive direction of the $(h_1k_1l_1)$ plane normal, to bring the crystal from the setting where OY_2 is in the plane YOZ, into the actual crystal orientation.

The axes $OX_3Y_3Y_3$ can be chosen conveniently relative to a, b, c as shown in figure 4, such that OY_3 is along b and OX_3 is in the ab plane on the same side of b as is a. In this case, for the general triclinic crystal,

$$\lambda = [(h/a) + (k\cos\gamma)/b]d/\sin\gamma; \quad \mu = kd/b;$$

$$\nu = \{(h/a)(\cos\alpha\cos\gamma - \cos\beta) + (k/b)(\cos\beta\cos\gamma - \cos\alpha) + (l/c)\sin^2\gamma\}abcd/V\sin\gamma,$$

where $$d=(V/abc)/\{\Sigma(h^2/a^2)\sin^2\alpha+2\Sigma(hk/ab)(\cos\alpha\cos\beta-\cos\gamma)\}^{\frac{1}{2}},$$

and $$V=abc(1-\cos^2\alpha-\cos^2\beta-\cos^2\gamma+2\cos\alpha\cos\beta\cos\gamma)^{\frac{1}{2}}.$$

There are similar expressions for λ_1, μ_1, ν_1 in terms of h_1, k_1, l_1.

The angle ϕ is not in general known directly as part of the specification of the crystal orientation, but it can be calculated for example from the indices $[u_1v_1w_1]$ of the lattice row which is along OO_1' in the $(h_1k_1l_1)$ plane, since then we have

$$\cos\phi=(\cos\delta)/\mu_1=(u_1a\cos\gamma+v_1b+w_1c\cos\alpha)/\mu_1T_1,$$

where δ is the angle between $[u_1v_1w_1]$ and OY_2, i.e. b, and T_1 is the $[u_1v_1w_1]$ lattice translation given by $T_1{}^2=\Sigma u_1{}^2a^2+2\Sigma u_1v_1ab\cos\gamma$.

Thus in any particular case, knowing the crystal lattice constants, the orientation defined by the indices $(h_1k_1l_1)$ and $[u_1v_1w_1]$ and the angle ψ which can be measured from the pattern in terms of the position of the $(h_1k_1l_1)$ line-pair median relative to O_1, the procedure to index the pattern is as follows. First write down the values of λ_1, μ_1, ν_1 and λ, μ, ν from the above expressions by inserting the known indices h_1, k_1, l_1, and $a, b, c, d, V, \alpha, \beta, \gamma$, and calculate $\cos\phi$ and $\sin\phi$, as just described, from $[u_1v_1w_1]$. Then putting these values in the expressions for A_2, B_2, C_2 etc., the equation for the (hkl) line median is obtained, involving h, k, l linearly. Finally the position of each line-pair median in the pattern can be compared with this equation and two relationships between h, k and l thereby established which give $h:k:l$; from this the simplest integral value of h, k and l consistent with the band-width D must be deduced, bearing in mind the accuracy of the measurements.

This method, like the next, is unwieldy for crystals which have low symmetry, but it has been easily applied to the patterns from some cubic and hexagonal crystals (Finch, Quarrell and Wilman 1935, Finch and Wilman 1936, 1937 a, b). For cubic crystals, for example, the expressions take the simple general forms

$$\lambda=hd/a, \qquad \mu=kd/a, \qquad \nu=ld/a, \qquad d=a/(h^2+k^2+l^2)^{\frac{1}{2}},$$

$$\lambda_1=h_1d_1/a, \quad \mu_1=k_1d_1/a, \quad \nu_1=l_1d_1/a, \quad d_1=a/(h_1{}^2+k_1{}^2+l_1{}^2)^{\frac{1}{2}},$$

$$A_3=(hl_1-lh_1)/(h^2+k^2+l^2)^{\frac{1}{2}}(h_1{}^2+l_1{}^2),$$

$$B_3=[k-k_1(hh_1+kk_1+ll_1)]/[(\Sigma h^2)(\Sigma h_1{}^2)(h_1{}^2+l_1{}^2)]^{\frac{1}{2}},$$

$$C_3=(hh_1+kk_1+ll_1)/[(\Sigma h^2)(\Sigma h_1{}^2)]^{\frac{1}{2}},$$

$$\cos\phi=[v_1/(\Sigma u_1{}^2)^{\frac{1}{2}}][\Sigma h_1{}^2/(h_1{}^2+l_1{}^2)]^{\frac{1}{2}}.$$

The general analytical expressions derived above are also useful in studying the positional relationships between systems of net-plane traces or Kikuchi lines, such as the line envelopes.

(v) *The method of intercepts on two perpendicular axes along and perpendicular to the trace of an $(h_1k_1l_1)$ plane in which $[u_1v_1w_1]$ is normal to the plate*

Thirsk and Whitmore's (1940) expressions are given below, in a notation uniform with the above, and the equation of a line pair is added.

Figure 7 shows the disposition of the reference axes OX, OY and of the known plane $(h_1k_1l_1)$ normal to the plate, with positive direction of the known lattice row $[u_1v_1w_1]$ along the normal OO_1 from the crystal origin to the plate. The trace MN of any plane (hkl) then has, relative to OX and OY, the equation $Px+Ry+L=0$, where

$$P=\frac{d_1}{V(u_1h+v_1k+w_1l)}\begin{vmatrix} \begin{matrix} u_1a^2+v_1ab\cos\gamma \\ +w_1ca\cos\beta \end{matrix} & \begin{matrix} u_1ab\cos\gamma+v_1b^2 \\ +w_1bc\cos\alpha \end{matrix} & \begin{matrix} u_1ac\cos\beta \\ +v_1bc\cos\alpha+w_1c^2 \end{matrix} \\ h_1 & k_1 & l_1 \\ h & k & l \end{vmatrix},$$

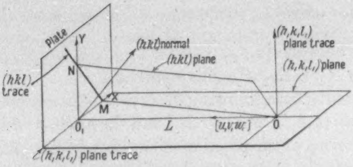

Figure 7.

Note: vertical through O should read "plane normal".

$$R=\{T_1d_1(a^2b^2c^2/V^2)/(u_1h+v_1k+w_1l)\}$$
$$\times[\Sigma(hh_1/a^2)\sin^2\alpha+\Sigma\{(hk_1+h_1k)/ab\}(\cos\alpha\cos\beta-\cos\gamma)],$$

$L=$ camera length,

$V=$ volume of cell $=abc(1-\cos^2\alpha-\cos^2\beta-\cos^2\gamma+2\cos\alpha\cos\beta\cos\gamma)^{\frac{1}{2}}$,

$d_1=(h_1k_1l_1)$ spacing $=(V/abc)/\{\Sigma(h_1{}^2/a^2)\sin^2\alpha+2\Sigma(h_1k_1/ab)(\cos\alpha\cos\beta-\cos\gamma)\}^{\frac{1}{2}}$,

$T_1=[u_1v_1w_1]$ lattice translation $=(\Sigma u_1{}^2a^2+2\Sigma u_1v_1ab\cos\gamma)^{\frac{1}{2}}$.

Thirsk and Whitmore give, as an example, the expressions for the case of a hexagonal crystal; in that for R, however, their $\nu c_0{}^2$ in the numerator should read $\nu^2c_0{}^2$.

The equation of the nth order Kikuchi-line pair from (hkl) is

$$Px+Ry+L\pm[(n\lambda L/2d_{hkl})\{1+(x^2+y^2)/L^2\}^{\frac{1}{2}}T_1/(\Sigma u_1h)d_{hkl}].$$

(vi) *The zone relation method*

The zone relationships. If a net-plane (hkl) is parallel to two lattice rows $[u_1v_1w_1]$ and $[u_2v_2w_2]$ whose lattice translations are T_1 and T_2, then r^*_{hkl} is perpendicular to T_1 and T_2; thus

$$u_1h+v_1k+w_1l=0;\qquad u_2h+v_2k+w_2l=0,$$

which gives $h:k:l=(v_1w_2-v_2w_1):(w_1u_2-w_2u_1):(u_1v_2-u_2v_1)$. Conversely, the zone axis $[uvw]$ parallel to two net-planes $(h_1k_1l_1)$ and $(h_2k_2l_2)$ is defined by $u:v:w=(k_1l_2-k_2l_1):(l_1h_2-l_2h_1):(h_1k_2-h_2k_1)$.

This zone relation method seems to have been the sole method applied before 1935 to index the line-pair medians in Kikuchi-line patterns, for example by Kikuchi (1928), Shinohara (1932), Kirchner (1932) and Shinohara and Matukawa (1933). Nevertheless, no general systematic method has hitherto been stated for indexing the various zone-axes corresponding to the points of intersection of line-pair medians on the plate, and the method has only been applied with relatively simple crystal orientations where an easy geometrical construction suffices to identify the main zone axes. General systematic methods of calculation are now outlined below.

Calculation of the position of the intersection of a zone-axis $[uvw]$ *with the plate.* Any lattice row $(uvw]$ along OP (figure 8), with lattice translation $\mathbf{T}$, makes with the plate normal OO_1 along the reciprocal-lattice direction $[h_0k_0l_0]^*$, i.e. $\mathbf{r}_0{}^*$, an angle η given by $\cos\eta = (\mathbf{T}\,.\,\mathbf{r}_0{}^*)/Tr_0{}^* = (uh+vk+wl)d_0/T$. The radial distance of P from O_1 in the plate is then $O_1P = L\tan\eta$. If the direction O_1X of the trace of a known plane $(h_1k_1l_1)$ through OO_1 is identified, and PQ is the normal from P to O_1X, then O_1P makes with O_1X an angle ξ_1 given by

$$\sin\xi_1 = QP/O_1P = (\mathbf{OP}\,.\,\mathbf{r}_1{}^*)/r_1{}^*O_1P = (uh_1+vk_1+wl_1)d_1/T\sin\eta.$$

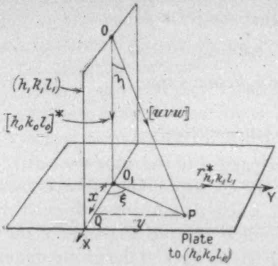

Figure 8.

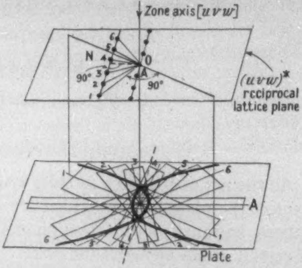

Figure 9.

The distance O_1P and the angle ξ_1 thus specify the point P where $[uvw]$ meets the plate. In the above expressions, $d_1 \simeq \lambda L/D_1$, where D_1 is the measured $h_1k_1l_1$ line-pair separation near O_1. From the above equations it follows also that $y_1 = QP = O_1P\sin\xi_1 = L\{(\Sigma uh_1)/\Sigma uh_0\}d_1/d_0$.

Calculation of the indices $[uvw]$ *of a zone axis from the position of its intersection P with the plate.* From the above equations, conversely,

$$uh_0+vk_0+wl_0 = (T/d_0)\cos\eta;\quad uh_1+vk_1+wl_1 = (T/d_1)\sin\xi_1\sin\eta;$$

but to determine $[uvw]$ uniquely it is necessary to measure also the angle ξ_2 made by O_1P with the trace of another net-plane, for example $(h_2k_2l_2)$, through O_1, whence

$$uh_2+vk_2+wl_2 = (T/d_2)\sin\xi_2\sin\eta.$$

Then $u:v:w =$

$$\begin{vmatrix} (\cos\eta)/d_0, & k_0, & l_0 \\ (\sin\xi_1\sin\eta)/d_1, & k_1, & l_1 \\ (\sin\xi_2\sin\eta)/d_2, & k_2, & l_2 \end{vmatrix} : \begin{vmatrix} h_0, & (\cos\eta)/d_0, & l_0 \\ h_1, & (\sin\xi_1\sin\eta)/d_1, & l_1 \\ h_2, & (\sin\xi_2\sin\eta)/d_2, & l_2 \end{vmatrix} : \begin{vmatrix} h_0, & k_0, & (\cos\eta)/d_0 \\ h_1, & k_1, & (\sin\xi_1\sin\eta)/d_1 \\ h_2, & k_2, & (\sin\xi_2\sin\eta)/d_2 \end{vmatrix}.$$

Alternatively, from the above expression for y_1 (and y_2), we have the following two equations, if $\rho_1 = d_1/d_0$ and $\rho_2 = d_2/d_0$:

$$u\{h_0y_1 - h_1L\rho_1\} + v\{k_0y_1 - k_1L\rho_1\} + w\{l_0y_1 - l_1L\rho_1\} = 0,$$
$$u\{h_0y_2 - h_2L\rho_2\} + v\{k_0y_2 - k_2L\rho_2\} + w\{l_0y_2 - l_2L\rho_2\} = 0,$$

which gives $u:v:w$ as in the case of a pair of zone-relation equations given above.

Calculation of $[h_0k_0l_0]^*$ *if this direction is initially specified by* $[u_0v_0w_0]$. If OO_1 is initially known to be the $[u_0v_0w_0]$ lattice direction, then the indices $[h_0k_0l_0]^*$ of this direction in the reciprocal lattice, required in the above calculations, may be obtained readily by comparison of the two equations

$$\mathbf{T}_0^* = h_1\mathbf{a}^* + k_1\mathbf{b}^* + l_1\mathbf{c}^*;$$

$$\mathbf{T}_0 = u_0\mathbf{a} + v_0\mathbf{b} + w_0\mathbf{c} \equiv (\mathbf{T}_0 \,.\, \mathbf{a})\mathbf{a}^* + (\mathbf{T}_0 \,.\, \mathbf{b})\mathbf{b}^* + (\mathbf{T}_0 \,.\, \mathbf{c})\mathbf{c}^*.$$

Thus,

$$h_0 = \mathbf{T}_0 \,.\, \mathbf{a} = a(u_0\, a + v_0 b \cos\gamma + w_0\, c \cos\beta);$$

$$k_0 = \mathbf{T}_0 \,.\, \mathbf{b} = b(u_0\, a \cos\gamma + v_0 b + w_0\, c \cos\alpha);$$

$$l_0 = \mathbf{T}_0 \,.\, \mathbf{c} = c(u_0\, a \cos\beta + v_0\, b \cos\alpha + w_0\, c).$$

(vii) *The envelope-relation method*

All the net planes such as (*hkl*) which are parallel to the same zone axis [*uvw*] intersect the plate in lines which are along the corresponding Kikuchi-line pair medians, and they all pass through one point, where the line [*uvw*] drawn through the crystal origin O meets the plate. The indices (*hkl*) of all planes of the zone satisfy the relation $uh + vk + wl = 0$, but the Kikuchi lines of the group of cozonal planes fall into subgroups, the lines of each subgroup being tangential to a common parabolic envelope.

The envelope curves themselves are not in general present in the pattern as true parabolic curves (black or white), though in the main subgroups where a large number of lines touch the envelope locus at frequent intervals, the polygonal nature of the apparent curves is only recognizable if the crystal is highly perfect and if a narrow well-focused monochromatic electron beam is used to obtain high resolution (Finch, Quarrell and Wilman 1935, Shinohara 1935, Finch and Wilman 1937 b). There is usually noticeable a characteristic weakening and curving away of Kikuchi lines just before they touch the envelope, also contributing to the prominence and appearance of continuity of the main envelope loci.

As Shinohara (1935) has shown, the lines associated with any one parabola arise from net planes such as (*hkl*) belonging to a zone [*uvw*]; the reciprocal-lattice points associated with these planes not only lie on the $(uvw)^*$ plane through the origin O, fulfilling the condition $uh + vk + wl = 0$, but also lie on a line, for example in an $[h_1k_1l_1]^*$ direction, lying in the $(uvw)^*$ plane parallel to the plate or nearly so, but not passing through the origin. (If it did, the lattice points along it would only correspond to the orders of diffraction from a single net-plane.) If this reciprocal-lattice line $[h_1k_1l_1]^*$ is densely populated, the approximation to the parabolic envelope curve will be prominent. It can be shown that, if the zone axis is normal to the plate, or nearly so, the axis of the parabola is parallel to the perpendicular ON to this reciprocal-lattice line $[h_1k_1l_1]^*$, and is thus, in the plate, along the trace of the net-plane $(h_1k_1l_1)$ (figure 9). The Laue indices of the successive Kikuchi lines touching the parabola differ by the same integers $h_1k_1l_1$ as the indices of this net-plane, or by a multiple of them.

Thus, if the indices of two or more lines touching a particular parabolic locus are known, those of the plane $(h_1k_1l_1)$ along its axis are the differences of these two sets or a sub-multiple of these differences; the indices of all the other lines touching the locus are also easily found even if only one line of each pair is distinguishable, and can be checked by the position or slope of the line (see methods 3, 4, 5).

Conversely, if the plane $(h_1k_1l_1)$ whose trace is along the parabola axis has been indexed and the indices hkl of any line touching the parabolic locus are known, then those of the other lines are of the form $h+nh_1$, $k+nk_1$, $l+nl_1$.

If the sign convention of § 2 is adopted in assigning the Laue indices hkl to any Kikuchi line, black or white, the above reciprocal-lattice interpretation shows (figure 9) that Kikuchi lines touching a parabolic locus on one side of its axial net-plane progressively further from its vertex have indices obtained from those of the previous one by *adding* the Laue indices (or a multiple) of the first-order Kikuchi line due to the axial plane of the parabola and lying on the same side of the net-plane trace, i.e. the parabola axis.

As has been shown (Finch, Quarrell and Wilman 1935), the parabolic envelopes in turn fall into groups whose envelopes are a system of circles with centres at the points where main lattice rows, if produced, would meet the plate. Shinohara (1935) has also shown that the circular envelopes represent the limiting loci outside which lie all Kikuchi lines characterized by the same Laue index h' relative to a lattice row meeting the plate at the centre of the circle, the lines all lying on the side of the net-plane traces, opposite to that on which the centre of the circle lies. The angular radii of such circles are given by $\cos\phi = 1-(h'\lambda/T)$, i.e. $\phi \simeq (2h'\lambda/T)^{\frac{1}{2}}$, where T is the lattice translation of the lattice row directed towards their centre and h' is any integer; thus the circles have radii nearly proportional to $\sqrt{h'}$, and have the same positions as the h'th-order Laue zones of reinforcement from the lattice row corresponding to an imaginary primary beam parallel to the row.

If the Laue indices of a Kikuchi line are hkl relative to the axes $\mathbf{a}$, $\mathbf{b}$, $\mathbf{c}$, and the lattice row is $[uvw]$, the line belongs to the group associated with the h'th-order circle round the $[uvw]$ trace on the plate, where h' is the Laue index of the diffraction direction hkl relative to the lattice row $[uvw]$, that is $hu+kv+lw=h'$. Many of the lines of a group will not touch the circle nor even lie close to it, but they fall into subgroups as above, touching parabolic envelopes which do touch the circle; the connection between any particular line and one of these circles is thereby established, and if $[uvw]$ and h' are known, the above linear relation between h, k and l is obtained. A line may be seen to belong to two or more non-coaxial parabolae or circles, and in this case several relations such as the above hold simultaneously and allow hkl to be determined without difficulty, on this basis alone, without reference to the bandwidth.

ACKNOWLEDGMENTS

The author thanks the Council of the Royal Society for a Moseley Research Studentship held from 1938–1940, during which period the third of the above methods was developed.

It is a pleasure also to thank Professor G. I. Finch for his interest and encouragement.

REFERENCES

Bragg, W. H., and Bragg, W. L., 1933, *The Crystalline State*, Vol. I (London: G. Bell and Sons).

Charlesby, A., Finch, G. I., and Wilman, H., 1939, *Proc. Phys. Soc.*, **51**, 479.

Finch, G. I., Quarrell, A. G., and Wilman, H., 1935, *Trans. Faraday Soc.*, **31**, 1051.

Finch, G. I., and Wilman, H., 1936, *Proc. Roy. Soc.* A, **155,** 345 ; 1937 a, *Trans. Faraday Soc.*, **33,** 1435 ; 1937 b, *Ergebn. exakt. Naturw.*, **16,** 353.
Kikuchi, S., 1928, *Jap. J. Phys.*, **5,** 83.
Kirchner, F., 1932, *Ergebn. exakt. Naturw.*, **11,** 64.
Shinohara, K., 1932, *Sci. Pap. Inst. Phys. Chem. Res., Tokyo,* **18,** 223, 315, **20,** 39 ; 1935, *Phys. Rev.*, **47,** 730.
Shinohara, K., and Matukawa, K., 1933, *Sci. Rep. Inst. Phys. Chem. Res., Tokyo,* **21,** 21.
Thirsk, H. R., and Whitmore, E. J., 1940, *Trans. Faraday Soc.*, **36,** 565.
Wilman, H., 1948, *Proc. Phys. Soc.*, **60,** 341.
Wyckoff, R. W. G., 1931, *The Structure of Crystals* (New York : Chemical Catalog Co.).

Electron Diffraction from Anthracene with Special Reference to the Diffuse Background*

By J. SKREBOWSKI
Physics Department, Imperial College †

MS. received 25 *June* 1947; *read at Science Meeting*, 31 *October* 1947

ABSTRACT. The object of the research was to examine the diffuse pattern obtained when an electron beam is transmitted through a crystal of anthracene. A special camera adapted for low temperature work is described. It has been found that the diffuse pattern has a fine structure which is more apparent in the case of thick crystals. The changes in intensity of the diffuse pattern with temperature have been established experimentally and it is shown that the phenomenon of the diffuse scattering is analogous to that found in x rays.

§ 1. INTRODUCTION

Electron diffraction transmission photographs from single crystals of anthracene show, besides a cross-grating pattern, a superimposed pattern which appears to be that of diffuse bands and areas. These bands and areas are related to the orientation of the anthracene molecule within the crystal lattice and to the separation of carbon atoms in the anthracene molecule; this led Charlesby, Finch and Wilman (1939) to the assumption that the diffuse areas are due to what they call "molecular scattering".

The following is a brief summary of their theory. The molecules are vibrating independently of each other in the crystal lattice and their vibrations have no definite phase relationship with each other. Although built in the crystal lattice they are producing an effect similar to that of a gaseous mass of oriented molecules in the electron beam. In the consideration of the vibrations the intramolecular heat motion is neglected. Molecules are thus vibrating as rigid units about their mean positions in the crystal lattice. As the anthracene unit cell contains two molecules in different orientations the authors proceed to construct qualitatively a molecular scattering pattern such as would be given by two independent molecules in these orientations. This diffuse pattern is to be superimposed on the cross-grating pattern of the crystal. It is claimed that the calculated diffuse pattern agrees well with the observed positions of diffuse areas and bands and gives the correct intensity distribution. Furthermore,

---

[*] Part of Thesis submitted to London University for Ph.D. degree examination.
[†] Now at Imperial Chemical Industries, Billingham.

they have derived an expression for the dependence on temperature of the intensity of the molecular pattern, on the assumption that the thermal displacement of any molecule from its mean position is given by the Maxwell-Boltzmann law.

No confirmation for either the theory or the experiments of Charlesby, Finch and Wilman has been found in recent x-ray work. In this field another temperature-dependent phenomenon was found. It was examined experimentally by Laval, Preston, Lonsdale and Smith, and others, and it received theoretical treatment by Faxen, Waller, Born, Zachariasen *et al.* (see review by Lonsdale 1943). The experimental researches of Lonsdale and Smith (1941) were carried out on organic as well as inorganic crystals. No x-ray investigations have been reported on anthracene, but benzil, sorbic acid, hexamethyl-benzene, urea nitrate and urea oxalate have been studied. A very brief outline of the work of Lonsdale and Smith will be given here.

A simple theory of diffraction of monochromatic x-rays by a crystal lattice predicts that with most crystal orientations (where the Ewald sphere of reflection misses all the reciprocal lattice points) no trace of any pattern should be found on photographs, no matter how long the crystal is exposed to x-rays. Experimentally, however, it was found that, with long exposures or very powerful x-ray sources, some definite pattern of diffuse spots of various shapes, and streaks of different types (sometimes connecting the diffuse spots), could be seen on the photographic plate. The effect was specially clear when highly monochromatized radiation was used. The intensity of the diffuse pattern was greatly diminished when the specimen was cooled with liquid air. The temperature change was reversible.

The diffuse pattern varied considerably from substance to substance and showed very interesting features for some chain and layer structures—for chain structures a characteristic sharp streak and for layer structures a large diffuse spot. The diffuse streaks connecting diffuse spots are found to lie along or nearly along some reciprocal lattice axes. Generally the intensity of the diffuse spot is largest near the position of a Bragg spot, and although the intensity diminishes with crystal rotation from this position, diffuse reflections could sometimes be observed when the crystal was turned as much as 30°. The intensity of a diffuse spot is related to the intensity of the corresponding Bragg reflection; thus no diffuse spots were observed corresponding to reflections forbidden by structure-factor considerations.

The phenomenon of diffuse scattering is accounted for by the Faxen-Waller theory which not only predicts its existence but also gives the formulae for the shape of the diffuse spots and accounts for the dependence of their intensity on temperature. The Faxen-Waller theory assumes that atoms are vibrating thermally in the crystal lattice and that the vibrations are harmonic. As the maximum frequency of atomic vibrations ($\sim 10^{13}$ sec.$^{-1}$) is much lower than that of x-rays (10^{18} sec.$^{-1}$) the atoms or molecules in a crystal will appear stationary as far as the passage of x-rays is concerned but slightly displaced from their mean positions. It is possible to consider the atomic displacement as due to superimposed, standing, elastic waves in the crystal which can be of acoustical or optical type. Although the complete theory must take into account both acoustical and optical branches of the vibrational spectrum, nevertheless the acoustical, which corresponds to larger amplitudes, is of primary importance. The theory shows that a single stationary wave of this type would produce two extra points very near each main reciprocal lattice point. The shorter the wavelength the larger the distance of these extra spots from the main spot. The effect of thermal motion can be represented by a cloud of such extra points, giving extra reflecting power (or diffuse reflection) to every region surrounding a reciprocal lattice point. The shape of this extra reflecting cloud is dependent, among other factors, on the elastic constants (Lonsdale 1943). So far, the Faxen-Waller theory has not been worked out in detail for organic crystals but it explains qualitatively the peculiar diffuse reflections from chain-like molecules and layer structures and also the diffuse streaks extending between two spots.

The results predicted by the molecular scattering theory of Charlesby, Finch and Wilman, and those predicted by Faxen and Waller are essentially different. While, according to the molecular scattering theory, it should only be possible to observe relatively large diffuse areas or bands without any associated fine structure, the Faxen-Waller theory predicts diffuse spots and streaks. Later, Charlesby and Wilman (1942), on re-examining their plates, found evidence of diffuse streaks as well as diffuse areas on the electron diffraction pattern of anthracene. There is also an attempt by Charlesby (1942) to reconcile the molecular scattering theory with that of Faxen-Waller, on theoretical grounds.

The aim of the present research is to study the diffuse areas observed by Charlesby, Finch and Wilman, and to see whether these can be interpreted in terms of the Faxen-Waller theory which has been used successfully in the X-ray work.

§ 2. APPARATUS

A camera of the type designed by Thomson and Fraser (1930) was modified so as to accommodate four photographic plates. This design of camera uses a cold-cathode discharge as electron source and a fine beam is obtained by pinhole collimating, no magnetic focusing being employed. The accelerating voltage of the electrons was usually in the region of 28 kv. The distance from specimen to photographic plate was 42 cm.

As the experiments were to be carried out at low temperatures, the main cone was redesigned to enable the specimen to be cooled down to the temperature of liquid air (figure 1). A large brass cone B is bored out. Inside it a tube T, about 3 cm. in diameter and 25 cm. in length, made of German silver, is soldered at its upper end to a flexible bellows C, which in turn is soldered to the main cone. The position of the tube can be adjusted by three screws. The tube T at its lower end is closed by a brass disc D. A part of the specimen holder H is tightly screwed into D so as to ensure good thermal contact between these two pieces. The specimen holder, made of copper, consists of two thick plates H and F, both with hemispherical cavities. These are put together with four screws. A thick ring with a rod-like extension A, on either side in the plane of the ring, is enclosed between the plates and can be rotated about its axis. After H, A and F are put together, a short cylinder R can be inserted into the ring from outside and, as the cylinder R fits tightly into the ring, good contact is ensured between them. The specimen-carrying cylinder R is a piece of thick copper tube with a fine wire gauze soldered over the top. On this gauze a transmission specimen can be placed. In the main cone there is a small cone M which can be rotated about its axis. To its lower end a violin string is attached and also fixed to a small wheel W at the end of the axis A. Thus by rotating cone M, A can also be rotated. With these arrangements it is possible to ensure all the necessary movements, viz. up and down by three screws, rotational movement of the whole cone B, and rotational movement of the specimen-cylinder R. A calibrated copper-constantan thermocouple is soldered to H. All the temperature measurements were made with a potentiometer bridge.

After the camera was evacuated, liquid air was introduced into the tube T and it generally took 5–10 minutes to cool the specimen. The amount of liquid air necessary to keep the specimen at low temperature is small. In the initial experiments at low temperature it was found that the pattern observed on the fluorescent screen became blurred after a few minutes. It was probably due to condensation of organic vapour from the diffusion pump on cold crystal surfaces and it was necessary to introduce on both sides, H and F of the specimen holder, two shields Z in the form of tubes about 2·5 cm. long. After this modification the crystal could be kept for a long time without any appreciable change in the diffraction pattern.

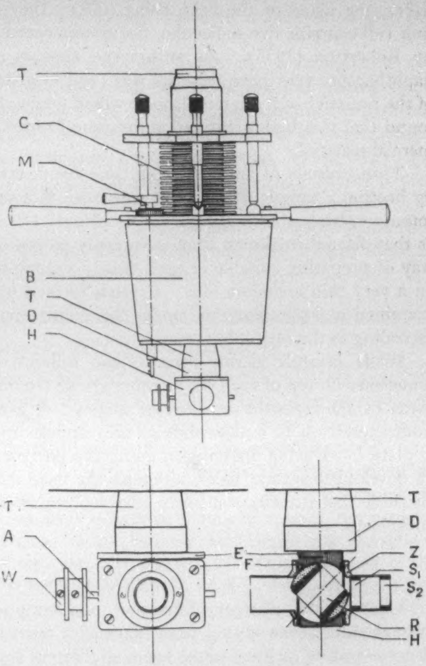

Figure 1. Specimen holder arrangements for orienting specimen and cooling device.

It should be noted, however, that as soon as the apparatus is cooled, a thermal contraction takes place and removes the observed crystal from the beam. Although it should be possible with screws to bring the specimen holder back to its previous position, in practice it was found impossible to find a very small crystal again once it was lost from the beam. A slightly different arrangement was therefore tried. Two pin holes, S_1 and S_2, were fitted into the shielding tube on the side from which the beam is incident, so that the nearest hole was only about 0·5 cm. from the carrier R. The distance between the holes was about 3 cm. and their diameter was 0·1 mm. With this arrangement it was possible to find the same crystal after lowering its temperature. It also produced a very fine beam and reduced the area of the crystal upon which the beam was falling. The experiments with this device proved particularly successful in elucidating the problem of the fine structure of the diffuse areas.

§ 3. CRYSTALLOGRAPHIC DATA. PREPARATION AND MICROSCOPIC EXAMINATION OF ANTHRACENE CRYSTALS

Anthracene ($C_{14}H_{10}$) has a melting point of 217° C. and sublimes slowly *in vacuo* at room temperature. It belongs to the monoclinic system, the elementary cell having the following dimensions :—$a = 8{\cdot}58$ A., $b = 6{\cdot}02$ A., $c = 11{\cdot}18$ A., with $\beta = 125°$. Anthracene crystals occur in the form of hexagonal flakes, the plane of the flake being (001) ; they can easily form twins. The unit cell contains two molecules, the atomic coordinates of which were obtained by Robertson (1933). As anthracene crystals are often contaminated with naphthacene, very pure material was used in order to eliminate the possibility of the presence of foreign molecules which might affect the diffuse areas. It was found that this highly purified anthracene formed better crystals than the commercial material.

Thin crystals of anthracene suitable for electron diffraction were prepared by heating a sample of the pure substance in a test tube. A large number of minute crystals showing interference colours was formed from the vapour and as they floated in the air they were easily picked up on a fine gauze. Another way of preparing suitable crystals was to evaporate xylene solution very slowly on a very thin collodion film. Crystals formed by each of these methods were examined and photographed under the microscope. Their appearance differed according to the method of preparation.

While crystals grown from xylene solution formed regular flakes lying sometimes on top of each other, those grown from vapour often formed clusters, twins or intergrowths at different angles. A general view of crystals grown from vapour on to a glass slide as they appear under the microscope is shown in plate 1. During observation under the microscope the crystals disintegrated by developing several holes, although the flake itself was still thick. It seems plausible that the electron beam covers portions of the crystal of very different thicknesses.

§ 4. GENERAL DESCRIPTION OF THE SPOT PATTERN OF ELECTRON DIFFRACTION PHOTOGRAPHS

Most of the electron diffraction photographs obtained by transmission through anthracene crystal flakes showed a fairly extensive pattern due to the *ab* cross-grating inclined to the beam at different angles. Sometimes the pattern was very extensive. This corresponded to a very thin crystal, possibly only a few molecules thick. Other photographs showed only a few intense spots and were correspondingly due to much thicker crystals. The pattern on the photographs was mainly rectangular, or nearly so. Most photographs, whether corresponding to thick or thin crystals showed irregularities in the cross-grating array of spots, frequent doubling or tripling of the spots, convergence of some rows, and generally untidy and irregular grouping of spots. From a large number of photographs taken with crystals grown from vapour, only a few showed a perfect cross-grating pattern such as would be expected from a single crystal; even on these a very noticeable regular doubling of spots was observed. Crystals grown from xylene solution on to collodion did not show these double spots, but unfortunately the rings due to the collodion film tended to obscure considerably the details of the anthracene pattern, especially near the centre.

It is of interest to note that spots forbidden by the structure factor, of the type $(2n+1, 0, m)$, $(0, 2n+1, 0)$, where n and m are integers, appeared on all photographs. They were rather faint and quite sharp.

§ 5. PATTERN INDEXING AND ESTIMATION OF CRYSTAL THICKNESS

The plates were indexed by assuming the values for the cell dimensions given by Robertson (1933). Sections of the reciprocal lattice were drawn to scale and to allow for the crystal being thin, lines were added to every lattice point in a direction perpendicular to the surface of the crystal. This was taken to be an (001) face. The sphere of reflection was then orientated to give the observed pattern.

Crystal thickness can be estimated from the length of the extension of the reciprocal lattice points. If some spots fail to appear on the photographic plate then the reflection sphere misses the corresponding (extended) reciprocal lattice point because its extension is too short. Once the length of the extension is found the crystal thickness is estimated from the formula: $l=1/t$, where t is the crystal thickness and l is the length of the extension measured from the centre. It may be remarked that the reciprocal lattice points of anthracene are fairly close together. Hence, with crystal thickness below 20 A., the reciprocal lattice points are so much extended that they form continuous lines. Thus it is not possible to estimate crystal thickness below that value.

§ 6. DESCRIPTION OF THE DIFFUSE PATTERNS

(a) *Experimental results at room temperature*

The character of the diffuse background in the diffraction patterns appeared at first to depend on the crystal thickness and the plates were accordingly classified in this way. The deductions below were made from a large number of plates of which examples, illustrating the salient points, are reproduced.

(i) *Thick crystals* ($t > 200$ A.). Thick crystal patterns are characterized by relatively few Laue spots, most of which are intense. These patterns show, on well exposed photographs, an array of diffuse spots and streaks, but nothing which can be termed a diffuse area. Plate 2 shows conclusively that the diffuse background has a well defined structure, the details of which can be seen in the enlarged portion (plate 3). These bear a striking likeness to the diffuse background of benzil, in plate 10 *b* of the paper by Lonsdale and Smith (1941). To obtain detail, it is particularly important to use plates which show good contrast (e.g. photomechanical plates show more detail than process plates). It is also necessary to use a fine electron beam to avoid the pattern being a composite one of a number of crystals. In these composite patterns the superposed diffuse background may have the appearance of a diffuse area, as the detailed structure tends to be blurred. That the diffuse pattern is very faint, can be seen by comparing its intensity with that of Laue spots visible in the same photograph (plate 3). The dependence of the pattern on temperature will be discussed below.

Another feature which has been noticed on a large number of plates is that some of the diffuse spots are elongated and not circular. In special cases these are very elongated and are found on both sides of the central beam. Plate 4 shows a typical example of this. These elongated spots were fairly persistent when the orientation of the crystal was changed.

(ii) *Thin crystals* ($t \sim 100$ A.). Thin crystal patterns are characterized by an extensive array of cross-grating spots. These spots vary a great deal in intensity (roughly in accordance with the structure factor) and forbidden spots are also present. A typical example of the thin crystal pattern is shown in plate 5:

this shows also the type of background called diffuse areas by Charlesby, Finch and Wilman (1939). This is a composite pattern due to a number of crystals in more or less the same orientation. Both the print and the plate show some signs of fine structure, though it is not so evident as for the thick crystals.

In order to eliminate one disturbing factor—the composite nature of the specimen—a special arrangement described in § 2 was introduced which ensured a very fine electron beam. This did not result in perfect single crystal patterns but under the best conditions clearer photographs were made possible. Further, particular care was taken in the time of exposure. Too short exposure gives very little contrast resulting in vague patches of background and a loss of detail. Excessive exposure leads to halation and again loss of detail. The choice of the right exposure time is thus essential.

Plates 6 and 8 are patterns of the same crystal and practically the same orientation taken at two different times (see below) with a fine beam. In the first case, plate 6, the exposure is rather short, and though a fine structure can be seen on the original plate, it is not very evident in the reproduction; in plate 8, on the other hand, the exposure is stronger and the fine structure of the background (for instance the streaking between spots) prominent.

(b) *Experimental results at low temperatures*

The object of the experiments at low temperatures was to find whether the diffuse background disappears or weakens at the temperature of liquid oxygen.

An ideal experiment would be to take a photograph at room temperature and then, with unchanged crystal setting and the same beam intensity, to cool the crystal down to the temperature of liquid oxygen and take another photograph. This was, in fact, done by Lonsdale and Smith with organic crystals using x rays. Unfortunately, in electron diffraction with the present experimental arrangement, it proved to be impossible, as neither the setting of the crystal nor the beam intensity could be strictly controlled. The procedure adopted was to take a photograph at room temperature, cool the specimen-holder to the temperature of liquid oxygen, find the same crystal and take several photographs with different exposures but using the same voltage. It was difficult to find two photographs which were exactly comparable; very slight movement of a specimen could change the spot pattern, though the new pattern could be identified as being due to the same crystal with slightly different orientation or a slightly different thickness.

Plate 6 taken at room temperature shows diffuse patches which, on the original plate, have a fine structure consisting of diffuse streaks joining cross-grating spots. The pattern indicates that the crystal is thin. Plate 7 shows the same crystal cooled to the temperature of liquid oxygen. Although the exposure is stronger than that of plate 6 very little diffuse streaking is visible on the original plate and the strength of the whole background is considerably reduced. The cross-grating spots are also stronger than in plate 6. Plate 8 shows the same crystal warmed to room temperature again; the background is more prominent than in plate 7, and the fine structure more obvious than in plate 6. These three photographs show that the temperature phenomenon is reversible. A number of sets of photographs of the above type were taken, all of which showed the same features.

§7. DISCUSSION

The existence of diffuse spots and streaks, observed with anthracene crystals, suggests that the effect is the same as that found by Lonsdale and Smith (1941) in their investigation on the X-ray diffuse scattering from some organic crystals. As mentioned above, the X-ray diffuse pattern of benzil (Lonsdale and Smith 1941, plate 10 *b*) bears a striking resemblance to the pattern shown in plate 3. In other photographs, e.g. plate 4, the characteristic elongated streaks on either side of the central beam, and their observed persistence with tilt of the crystal are similar to the streaks observed in X rays with sorbic acid (Lonsdale and Smith 1941, plates 12 *b* and 21 *a*, *b*, *c*).

The temperature effect cannot be demonstrated as clearly as with X rays because of considerable experimental difficulties, but the examination of several sets of photographs, e.g. plates 6, 7, 8, shows conclusively that the diffuse pattern intensity diminishes considerably at the temperature of liquid oxygen. This decrease is especially well marked in the case of diffuse streaks joining the diffuse spots; the streaks disappear almost completely at low temperature. Thus it can be concluded that the effect of diffuse scattering as found in X rays has a close analogy in electron diffraction.

The diffuse scattering in X rays was interpreted successfully in terms of the crystal vibrations and it is reasonable to conclude that a similar phenomenon in electron diffraction is due to the same cause. It is, therefore, unnecessary to assume that the diffuse spots and streaks are due to the molecules vibrating independently, which has been postulated by Charlesby, Finch and Wilman (1939); indeed, the fine structure observed, plates 2, 3, 4 cannot be reconciled with their theory.

Emphasis has been placed by Charlesby, Finch and Wilman (1939) on the fact that the diffuse patches observed on their patterns from anthracene crystals are due to independent scattering from anthracene molecules, and that, therefore, the molecular structure of anthracene can be deduced from the relative positions of the diffuse areas on the patterns. While it is possible that some molecules at the surfaces and edges of the solid may scatter independently, the molecules forming the lattice do not.

Examination of the patterns obtained in the present work showed that in general, the diffuse background was strongest in those positions where Laue spot intensities were strongest; this is to be expected on the Faxen-Waller theory. It can be shown on this theory (Born 1942–43) that for any crystal the intensity of the diffuse scattering is directly proportional to the square of the lattice structure factor, in the region near the Laue spot. One would therefore expect that an examination of the structure factor, F, would show where the diffuse background would be most intense. Contour lines of F^2, for anthracene, corresponding to the orientation in plate 5, have been drawn, and are shown in figure 2. The positions of the strong regions coincide reasonably well.

On the molecular scattering theory, the intense regions of the background should be given by each molecule scattering independently. This results in a slightly different set of contour lines from the previous set (see figure 3) but they are not significantly better as a rough representation of the intensity distribution found on the plate.

The orientation chosen in plate 5 is a fair one from the point of view of the molecular scattering theory, since the cross-grating spots are grouped, as regards intensity, into only three regions. Neither set of contour lines (figures 2 and 3) shows any detailed structure over a region comparable with the cross-grating unit. A careful examination of plate 5, however, shows that there is a streaking between spots and a fine structure. The molecular scattering theory fails, therefore, to provide a basis for a full description of the experimental results.

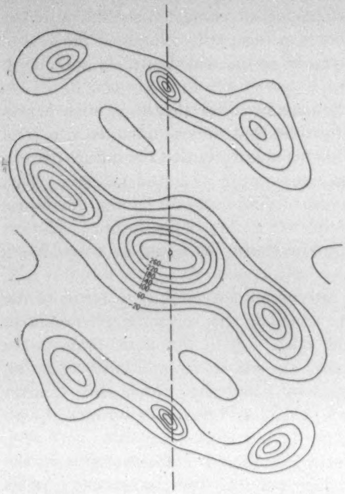

Figure 2. Contour lines of intensity scattered from a unit cell of anthracene. Beam direction as in plate 5.

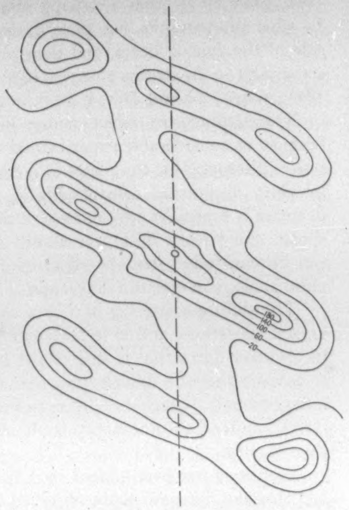

Figure 3. Contour lines of intensity scattered from two independent molecules oriented as in the anthracene cell. Beam direction as in plate 5.

ACKNOWLEDGMENTS

The author wishes to express gratitude to Professor Sir George Thomson, F.R.S., for providing facilities for the research, and for his great help and interest in these investigations, to Dr. M. Blackman and Dr. W. Cochrane for their valuable help and interest throughout the whole period of the research. He also wishes to thank Mr. B. K. Johnson of the Technical Optics Department of the Imperial College of Science and Technology for the microscopic photographs, Mr. L. J. Bowen, F.R.S., of the Physical Chemistry Laboratory, Oxford, and Dr. Schnurmann and Dr. Boyd-Barrett of the Manchester Oil Refinery Ltd. for examples of pure anthracene.

REFERENCES

Born, M., 1942–43, *Rep. Prog. Phys.*, **9**, 294.
Charlesby, A., 1942, *Proc. Phys. Soc.*, **54**, 379.
Charlesby, A., Finch, G. I., and Wilman, H., 1939, *Proc. Phys. Soc.*, **51**, 479.
Charlesby, A., and Wilman, H., 1942, *Nature, Lond.*, **149**, 411.
Lonsdale, K., 1942–43, *Rep. Prog. Phys.*, **9**, 256.
Lonsdale, K., and Smith, H., 1941, *Proc. Roy. Soc.* A, **179**, 8.
Robertson, J. M., 1933, *Proc. Roy. Soc.* A, **140**, 79.
Thomson, G. P., and Fraser, C. G., 1930., *Proc. Roy. Soc.* A, **128**, 641.

DISCUSSION

Dr. K. **Lonsdale**. Mr. Skrebowski's paper is of great interest, in that it suggests that experimental data on diffuse scattering, which appeared to have been satisfactorily accounted for by the assumption of independently vibrating molecules, can be explained equally well by assuming that the diffuse intensity is dependent upon the ordinary structure factor, being greatest in the neighbourhood of reciprocal lattice points with the largest reflecting power. That this is true in general is quite clear to anyone who has worked in this field; it may be seen illustrated in plates 5 and 6 of Lonsdale and Smith, *Proc. Roy. Soc.* A, 1941, **179,** 8, for X ray diffuse scattering; although of course the rule cannot be applied in detail for all structures.

It is interesting also that the photograph (author's plate 7) taken at liquid air temperatures shows very clearly not only the decrease of intensity of the diffuse pattern but also the increase of intensity of the Laue spots (especially of those at large diffraction angles), which is a necessary corollary. This fact has misled Dr. Wilman into thinking that plate 7 must have been taken using a thinner part of the crystal than that which gave plates 6 and 8.

Another point which comes out more clearly perhaps from the electron diffraction photographs than from X rays (although quantitative ionization spectrometer measurements given by Laval for KCl, and Geiger counter measurements on urea and on oxalic acid dihydrate shortly to be published in the *Acta Crystallographica,* do prove this fact without any doubt) is that the falling off of diffuse intensity with increasing angle of diffraction is markedly less than that of the Laue intensities. This also follows from the Faxen-Waller theory, as extended by Born and others.

I see no particular significance, however, so far as this controversy on interpretation is concerned, in the presence or absence of diffuse " areas ", meaning by these the overall blackening of considerable regions of the photographic plate. The practical applications of the Faxon-Waller theory so far made have only considered the parts of reciprocal space in the neighbourhood of reciprocal lattice points, but in all but the simplest cases (and anthracene is not a simple case) it is quite certain that optical waves will have to be taken into account, and that the effect of these will be greatest *between* the reciprocal lattice points. In one sense the effect of these optical vibrations is likely to be much more like that of independent molecular vibrations than the acoustical vibration effects would be, but I am not clear that the present method really provides a crucial experiment by means of which a distinction can be made. The presence or absence of diffuse scattering in the neighbourhood of reciprocal lattice points of zero Laue intensity is not such a criterion, for any vibration or distortion which disturbs the crystal lattice will necessarily also disturb the conditions which cause the Laue reflection to disappear. The surprising thing, perhaps, is that such " forbidden " reflections do not appear more often in diffuse form. Some unpublished work by Mr. P. G. Owston on the diffuse pattern of ice shows that such forbidden reflections do appear in that case, where the intermolecular forces are much stronger than they are in anthracene, and independent molecular vibrations are very unlikely.

My opinion is that the electron diffraction photographs of thick anthracene crystals are the most useful for comparison with X-ray diffraction effects, because the use of very thin crystals will necessarily introduce a possible confusion between surface and internal structure, and because with very thin crystals some of the long wavelength standing waves will no longer exist.

Professor Sir **George Thomson**. This is a paper which raises an interesting theoretical issue. It is one of those cases in which two widely different theories lead to nearly the same answer. Born's theory has been well confirmed for X rays by the work of Dr. Lonsdale and others, and there can be no doubt of its essential truth. Unfortunately it is very complicated, and involves a number of elastic constants. For substances as complicated and crystal forms as unsymmetrical as anthracene, it is not possible to work it out in detail. One is therefore driven to qualitative predictions, as, for example, that the diffuse effects are most marked near points of the reciprocal lattice with large structure factor. It is inherently extremely probable that the Born effects will also occur with electron diffraction, and I am convinced that the effects first observed by Finch and Wilman and studied in this paper are the electron analogue of those studied for X rays by Dr. Lonsdale. The general agreement in appearance, the close correlation with structure factor, the character of the fine structure observed by Dr. Skrebowski, all confirm this. But that is not to say that the theory put forward by Charlesby, Finch and Wilman, which ascribes the effect to diffraction from molecules vibrating independently under thermal agitation, is necessarily wrong. The Born theory is a theory, and I believe a complete one, of the effect of thermal agitation on the scattering of x rays. It is expressed in terms of certain elastic constants. These elastic constants are determined by the structure of the crystal and the forces between the atoms in it. If certain groups of atoms are held together very strongly so as to form molecules, and if the forces between molecules are relatively weak, these facts will be reflected in the values of the elastic constants, and by the time you have gone through all the mathematics it is probable you will get roughly the same answer as if you had started by assuming the molecules to be independently moving rigid solids as Charlesby, Finch and Wilman have done. Only you will not get the fine structure which only the more refined theory is capable of predicting. I regard the independent rigid motion of the molecules as inherently probable though not certain; a flat molecule like anthracene might easily bend, but I do not think that experiments of this kind are capable of proving it, since there is so little difference, at least in the cases tried so far, between the distribution of intensity deduced from the structure factor and that deduced from the hypothesis of independent molecular motion.

Dr. A. CHARLESBY. The problem with which Mr. Skrebowski deals, i.e. the presence of diffuse bands in electron diffraction, is of considerable value in the determination of molecular structure. Under certain conditions it enables the arrangement of atoms in the molecule to be determined directly, without going through an elaborate Fourier analysis of Laue spot intensities. Several papers have shown their occurrence and their correlation with molecular structure.

Mr. Skrebowski attempts to explain away the existence of these diffuse bands by ascribing them to the blurring or smearing out of relatively sharp streaks. These sharp streaks are, however, quite distinct and have indeed been previously observed in electron diffraction and x-ray work. I fail to see how photographic plates can smear out a streak perhaps 1 mm. wide into a band 5 mm. in width, while yet reproducing sharp spots less than 0·1 mm. across.

Using Process plates, the author was unable to obtain diffuse bands, but observed sharp streaks. This does not disprove the existence of these diffuse bands. His observation arises simply from the sharp contrast and limited intensity range of these plates, which suppress low intensities. It is for this reason that after experimenting, we preferred Special Rapid to Process plates. Obviously it is not a sufficient explanation to show that under unsuitable conditions of exposure a phenomenon does not appear. It is far more important to explain why it does appear under other conditions.

I would like to refer to another question raised in the paper, namely the comparison of diffuse streaks and diffuse bands. On the basis of rather superficial similarities, mainly that both phenomena are more diffuse than the spot pattern, Mr. Skrebowski draws the conclusion that bands and streaks are identical, whereas a closer examination reveals wide differences between them.

My conclusion is that we are dealing with three distinct sets of phenomena : (*a*) sharp spots corresponding to the crystal structure; (*b*) diffuse streaks and spots, observed both in x-ray and electron diffraction work; these streaks arise from thermal motion and correspond to elastic waves throughout the crystal; (*c*) diffuse bands, so far only observed in electron diffraction, whose non-appearance in present-day x-ray work is readily explained (Charlesby, *Proc. Phys. Soc.*, 1942, **54**, 379).

In the case of a few simple structures, the effect on the diffraction pattern of elastic vibrations throughout the crystal may be evaluated. These vibrations give rise to streaks and spots, the presence of which is confirmed by x rays. In the case of more complex crystals the mathematical difficulties appear insuperable, and one is obliged to proceed by qualitative comparisons. Similar streaks and diffuse spots have been observed in electron diffraction patterns and reported in *Nature*. It may be presumed that they arise from the same continuous type of thermal vibration.

Instead of considering these continuous thermal vibrations throughout the crystal, one can go to the opposite extreme, and consider each molecule as vibrating independently of its neighbours. On this alternative assumption, the mathematical calculation can be readily completed even for a complex crystal such as anthracene. There is very good

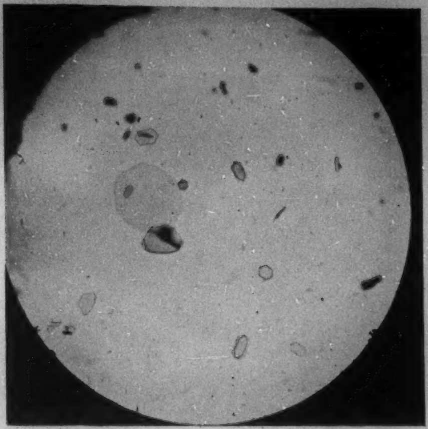

Plate. 1. Anthracene crystals grown from vapour. Magnified × 50.

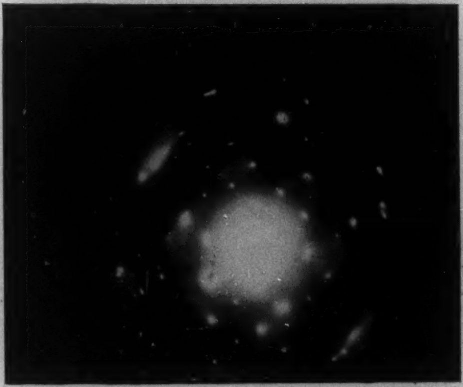

Plate 4. Thick crystal pattern of anthracene showing fine structure and two elongated diffuse streaks.

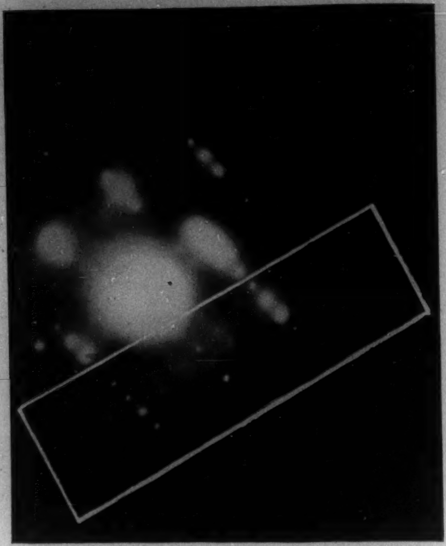

Plate 2. Thick crystal pattern of anthracene showing fine structure.

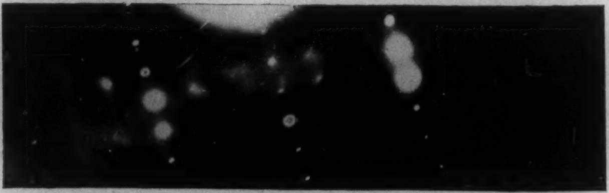

Plate 3. Enlargement of a portion marked on photograph 2, showing details of the fine structure.

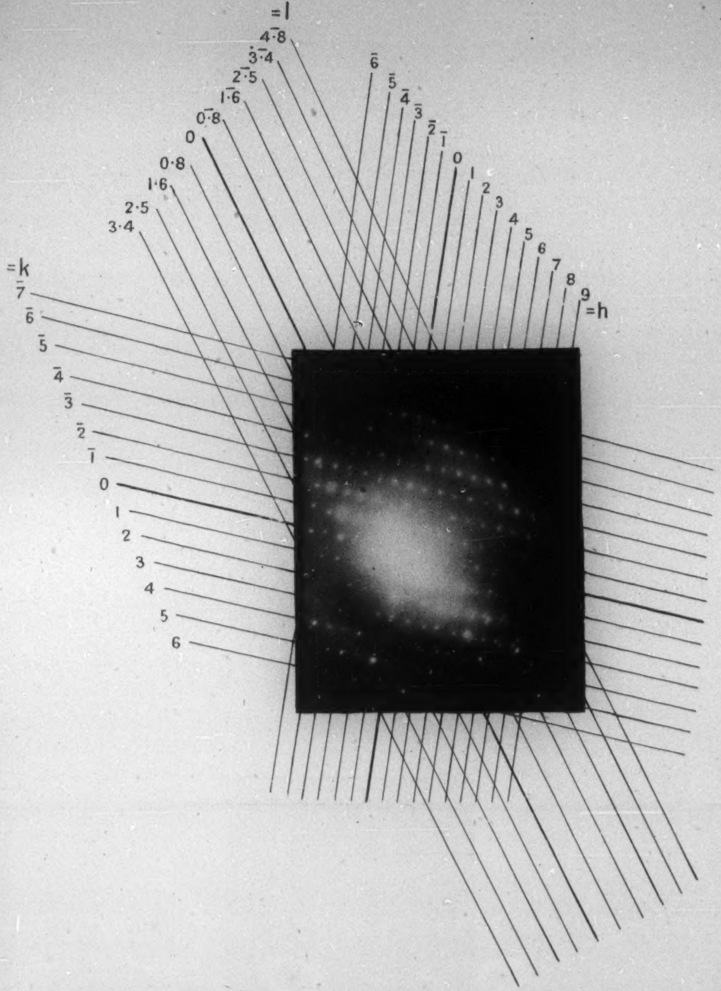

Plate 5. Indexed pattern of a thin crystal of anthracene showing diffuse background. Incident beam making angles with axes *a*, *b*, *c*, $\theta_a=107°$, $\theta_b=105°$, $\theta_c=18°$.

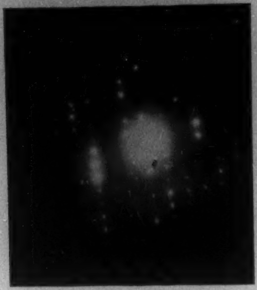

Plate 6. Thin crystal of anthracene at room temperature.

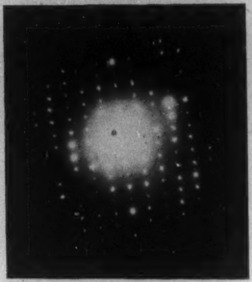

Plate 7. Same crystal as on plate 6 at temperature of liquid oxygen.

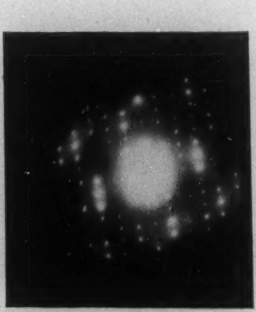

Plate 8. Same crystal as on plate 7 warmed up again to room temperature.

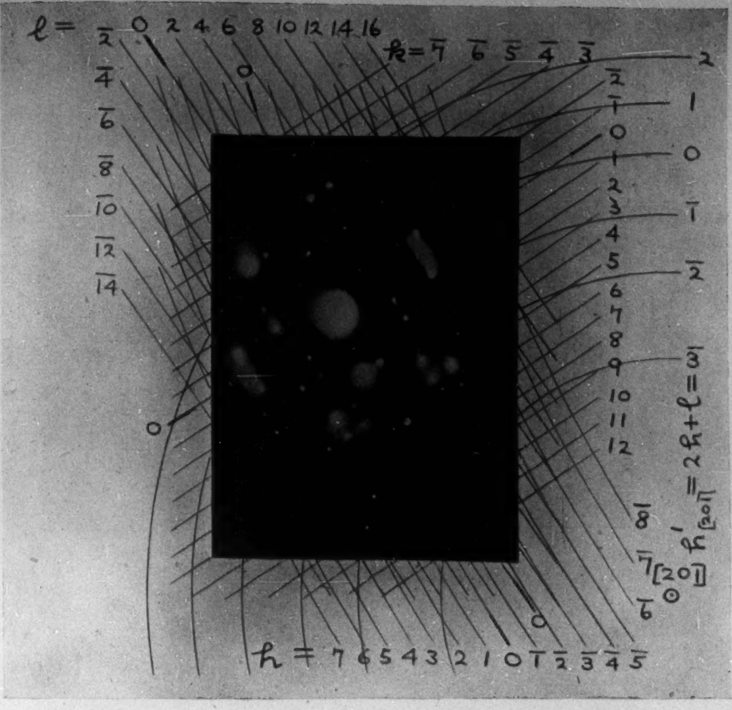
$l = \bar{2}$ 0 2 4 6 8 10 12 14 16
$k = \bar{7}\ \bar{6}\ \bar{5}\ \bar{4}\ \bar{3}$
$\bar{4}$
$\bar{6}$
$\bar{8}$
$\overline{10}$
$\overline{12}$
$\overline{14}$
0
0
0
0
$\bar{2}$ $\bar{1}$ 0 1 2 3 4 5 6 7 8 9 10 11 12
2
1
0
$\bar{1}$
$\bar{2}$
$\bar{3}$
$\bar{8}$
$\bar{7}$
$\bar{6}$
$0\ [20\bar{1}]$
$h'_{[20\bar{1}]} = 2h + l = \bar{3}$
$h = 7\ 6\ 5\ 4\ 3\ 2\ 1\ 0\ \bar{1}\ \bar{2}\ \bar{3}\ \bar{4}\ \bar{5}$

Top:—Diffraction pattern obtained from an anthracene crystal, orientated so that the two molecules in the unit cell are approximately at right angles to the incident beam.

Opposite right is a sketch of the pattern to be expected from independent molecules, orientated as in the crystal. The contributions of the two separate molecules are distinguished by vertical and horizontal shading. This sketch is not the same as that of the structure factor.

Points to note are :

i. The large dimensions (especially width) of the bands,

ii. the occurrence of strong bands at points where the spot pattern disappears owing to the structure factor,

iii. the absence of any marked interference effects when the contributions from two separate molecules overlap.

Reproduced from *Proc. Phys. Soc.*, 1939, **51**, 479 (Charlesby, Finch and Wilman).

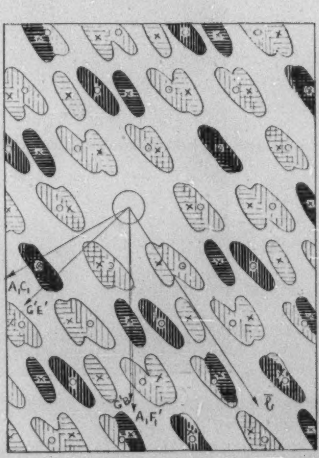

Plate A.

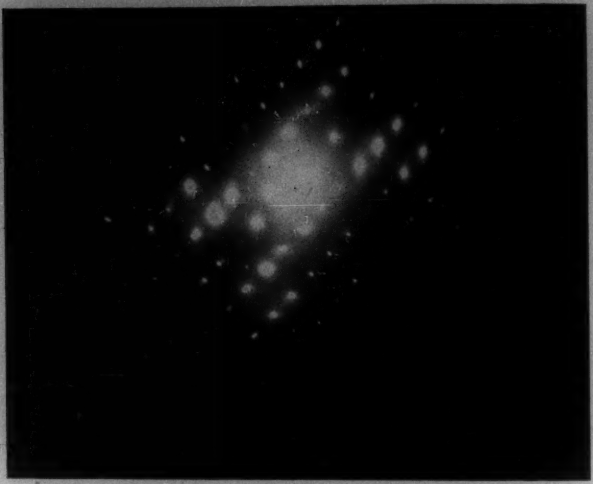

Plate B.

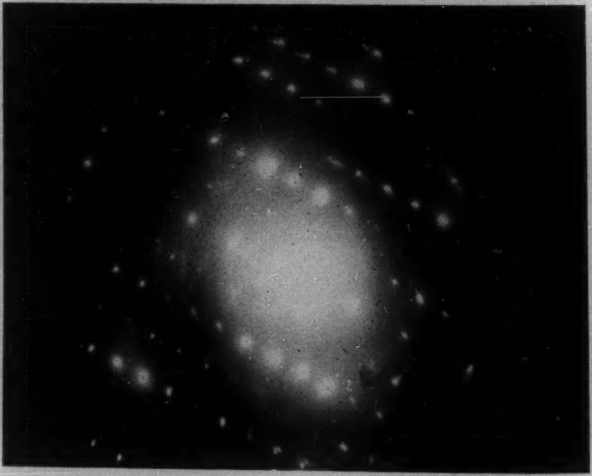

Plate C.

agreement between the calculated pattern and the diffuse bands observed. This theory was put forward in 1939 by Charlesby, Finch and Wilman. It was realized that this explanation was only a first approximation, since it did not account for the presence of diffuse streaks and spots, which could often be observed superimposed on the diffuse bands.

It appears to me that both theories are necessary to account for the full pattern. Of the total thermal motion of a molecule one component can be considered to form the elastic waves continuous throughout at least fairly large areas of the crystal. This component leads to streaks and diffuse spots. The remaining component is independent of that of other molecules and gives rise to the diffuse bands. But I must emphasize that an independent component must be accepted to account for the diffuse bands.

Mr. Skrebowski assumes that for a complex crystal such as anthracene the intensity of diffuse streaks follows the structure factor of the unit cell. No such calculation has been made, nor does the diffuse pattern observed in simpler crystals such as diamond follow this intensity distribution.

In his remarks the author points out that the structure factor for the unit cell is not very different from that calculated from each molecule separately, and attempts to substantiate this statement with a direct comparison between the two. Unfortunately the single orientation he has shown is very badly chosen to make this comparison. In other orientations the difference is much greater, and in such orientations the observed diffuse pattern does not agree with that calculated from the structure factor, but rather with that calculated for each molecule separately.

Anthracene provides a good example of this distinction. In certain directions the amplitudes scattered by the two molecules are equal but opposite in phase so that the resultant intensity is zero. Spots should therefore vanish (forbidden reflections), as should any diffuse streaks in the immediate neighbourhood. Observations of the area where diffuse patterns from different molecules overlap show no such phenomenon of interference. Strong diffuse bands occur in areas where the interference between the two molecules in the unit cell should eliminate them, and does in fact eliminate the Laue spots. On the other hand the theory of independent molecular scattering accounts both for the appearance and extent of diffuse bands in these areas (plate A).

In view of the importance of this argument, it is worth considering it in further detail. On page 522 of the original paper by Charlesby, Finch and Wilman (*Proc. Phys. Soc.*, 1939, **51,** 479) the difference was pointed out between the two factors in the expressions for the spot and diffuse band intensities.

The expressions for the intensity distribution of the spot and diffuse band pattern respectively in a direction h, k, l were given as

$$I_1=(A^2+B^2)\pi(\sin^2 M_1 h\pi/\sin^2 h\pi)\exp(-16\pi^2\sin^2\theta kT/\lambda^2 f),$$

$$I_2=N\sum_p(A_p{}^2+B_p{}^2)\{1-\exp(-16\pi^2\sin^2\theta kT/\lambda^2 f)\}.$$

A_p+iB_p is the amplitude of the wave scattered by molecule p in the unit cell. In the expression for the spot pattern (A^2+B^2) is equal to $(\Sigma A_p)^2+(\Sigma B_p)^2$ summed over all molecules in the unit cell, the phase difference between different molecules being taken into account. In the corresponding expression for the diffuse bands $\Sigma(A_p)^2+\Sigma(B_p)^2$ no phase difference between molecules is involved.

In the particular case of anthracene there are two molecules per unit cell p, q. As the molecules are symmetrical $B_p=B_q=0$. The structure factor for the spot pattern—and according to Mr. Skrebowski for the diffuse streaks—is

$$(A_p+A_q)^2 \text{ or } A_p{}^2+A_q{}^2+2A_pA_q\cos\pi(h+k).$$

According to the theory of independent molecular vibration the structure factor for the diffuse bands is $A_p{}^2+A_q{}^2$.

The distinction between these two expressions is best seen in diffractions for which $A_p=A_q$ (eg. $h0l$ and $0k0$). The intensities are then proportional to $4A_p{}^2\cos^2\pi h/2$ or $4A_q{}^2\cos^2\pi k/2$ (spots and diffuse streaks) and $2A_p{}^2$ (diffuse bands). In the theory of independent molecular scattering the intensity of the diffuse bands is modified by the molecular structure factor and by a thermal factor while that of Laue spots and diffuse streaks in addition depends on the value of the expression $\cos^2\pi h/2$ or $\cos^2\pi k/2$.

If the author's thesis is correct, the intensity distribution within a diffuse band which extends over an area corresponding to several Laue diffraction spots should show characteristic fluctuations from $4A_p{}^2$ to 0. Although certain diffuse bands do show some variations in intensity, there is no doubt that many bands occur with high intensities at points where the factor $\cos^2 \pi h/2$ or $\cos^2 \pi k/2$ would cause them to disappear. Diffuse bands are often observed at points where the spot pattern is eliminated by the structure factor, e.g. ($h0l$) diffraction with h odd, or ($0k0$) diffraction with k odd. In fact the intensity distribution in the diffuse bands is proportional to the structure factor of each molecule, and not to the structure factor of the unit cell.

One is therefore driven to the conclusion that the diffuse bands although dependent on the atomic arrangement in the molecule are not dependent on the arrangement of the molecules in the unit cell. As has long been suggested—and verified by the author—the appearance of diffuse bands is a temperature-dependent phenomenon. It seems difficult to escape the conclusion that these bands derive from that component of the thermal motion of each molecule which is independent of that of its neighbours.

I have mentioned the existence of a number of characteristic differences between diffuse bands and diffuse streaks. The following observations summarize these differences :

(i) In the patterns shown to us the streaks run from one sharp spot parallel to one of the spot arrays. The bands on the other hand bear no obvious relationship to the direction of the spot pattern. (ii) The intensity of the streaks is modified in the proximity of a diffraction spot. The bands appear to be quite independent of spot intensity except in so far as they both vanish in directions in which the structure amplitude from each molecule is low. (iii) Each streak is relatively narrow. Bands have a width often equal to several times the distance between Laue spots. (iv) The intensity of the streaks, in the photographs shown, is less than that of spots in the neighbourhood. Diffuse bands at some distance from the central spot are far more intense than Laue spots. (v) Although diffuse streaks may be observed superimposed on diffuse bands near the central part of the pattern where they can be readily distinguished, only diffuse bands are observed further away from the centre. (vi) The diffuse streaks are related to the direction of thermal vibrations in the crystal, and hence to the crystalline axes. Their intensity is mainly dependent on the direction of these thermal vibrations. The diffuse bands are independent of crystal orientation except in so far as this determines the molecular orientation.

In conclusion, I would like to state that the assumption of independent vibration leads to a number of deductions which may be readily verified in the diffraction patterns. These include (i) the distribution and dimension of diffuse bands in the diffraction pattern; (ii) the relative intensity distribution within the bands; (iii) the increased intensity of the bands relative to the spot pattern as the angle of diffraction is increased; (iv) the non-occurrence of interference between bands from different molecules.

A simple extension of this idea provides an explanation of the diffuse spots seen by Preston and Bragg in inorganic crystal diffraction patterns.

The theory in the simple form in which it was first presented does not explain the occurrence of diffuse streaks or spots.

The alternative theory of continuous thermal vibrations as propounded by Mr. Skrebowski explains the appearance of diffuse streaks and spots, though only qualitatively. It does not explain the following observations :

(i) the non-intensification of bands near Laue spots;
(ii) the non-interference of diffuse bands;
(iii) the occurrence of strong diffuse bands in areas where the structure factor eliminated the spot pattern;
(iv) the appearance of diffuse bands at large diffraction angles, when the spot pattern has vanished.

The most likely assumption appears to be that the thermal vibration of each molecule can be split into two components :

a component dependent on elastic vibrations throughout the crystal and giving rise to diffuse streaks and spots;
a component which is independent of that of its neighbours, leading to diffuse bands.

From the practical point of view, the latter component is of greater importance in so far as it provides a simple and effective method of molecular analysis.

In view of the increasing interest shown in these extra diffraction phenomena, might I suggest that some less confusing terms be applied to diffuse streaks, diffuse spots and diffuse bands, now that their causes are being separated. Much confusion in this paper arises from the use of a single adjective to describe such diverse phenomena.

Dr. H. **Wilman.** Although it seems reasonable, as we have said before, to expect the diffuse maxima to become weaker relative to the Laue spot intensity at low temperature, comparison of plate 7 with 6 and 8 is largely vitiated because plate 7 appears to correspond to a thinner part of the crystal, and the print of plate 7 seems to have had a longer exposure than those of plates 6 and 8. The plate itself still contains considerable intensity of diffuse maxima. This may be due to considerable heating of the crystal by the rather low energy (28 kv.) electrons used. Mr. Skrebowski has thus not conclusively shown the dependence on temperature. I have no doubt, however, but that such a temperature effect must exist.

The apparatus is not new in type. No references to previous work with liquid-air cooled specimens are given, though essentially identical apparatus, avoiding impurities condensing on the specimen, was described by Gen, Zelmanoff and Schalnikoff in 1933, Hass in 1937, 1938, Was in 1939, and Charlesby in 1945 (*Proc. Phys. Soc.*, **57**, 510).

The author suggests that he has discovered pattern details which had, in fact, already been described by Charlesby and Wilman (1942). In plate 5 Mr. Skrebowski has drawn three sets of parallel equidistant straight lines through the spots as the Laue zones—this would mean that the three crystal axes were all co-planar and normal to the beam, which is impossible and inconsistent with the spot intensities even as an approximation. Further, the crystal appears imperfect and the electron beam too broad.

In the introduction and discussion, Mr. Skrebowski expresses views which contradict facts published by Charlesby, Finch and Wilman (1939), and Wilman in 1942 (*Proc. Phys. Soc.*, **54**, 350), Charlesby (1942) and Charlesby and Wilman (1942), which we now illustrate again with slides. The X-ray patterns cannot confirm our electron diffraction results or otherwise, owing to the difference in wavelength, energy, crystal thickness etc. K. Lonsdale (*Proc. Phys. Soc.*, 1942, **54**, 352) has pointed out that the different crystal thickness in the two cases will probably lead to a different distribution of the thermal waves. The theory of thermal-elastic waves in the crystal can account for the diffuse spots in the X-ray patterns and also for the similar spots in the electron diffraction patterns, but has not been able to account for the more diffuse bands and areas of intensity hitherto only observed in the latter. Both the thermal-elastic wave theory and our molecular scattering theory fail to explain the whole of the electron diffraction phenomena, though a mixture of the two does appear to account for the main characteristics (plate A).

Mr. Skrebowski confuses groups of the thermal-elastic spots with the broad diffuse maxima on which they often, but by no means always, lie and which he has not effectively recorded owing to under-exposure and use of plates with unsuitable characteristics. Similarly, the X-ray patterns do not show even the thermal-elastic spots if under-exposed. Our experimental proof of the correspondence of the diffuse maxima with the patterns which would arise from the separate molecules orientated as in the crystal is a fact which he seeks to interpret as due to the thermal-elastic spots being strongest (and the weaker outer parts tending to coalesce) where the normal structure factor is high. He admits his F^2 contour diagram, figure 2, is not significantly different from that for F_1 and F_2, figure 3, and that neither show subsidiary maxima within the broad diffuse maxima. In most orientations the F^2 distribution *should*, however, in certain regions show maxima and minima separated by distances of the order of that between the Laue spots. This has not so far been reliably observed—we see no appreciable interference of this sort where the maxima of the two differently orientated molecules overlap. Moreover, the diffuse bands and areas are still relatively strong, as expected from the independent-molecule theory, in parts of the pattern distant from the undeflected spot, where the Laue and Bragg spots are no longer strong enough to be visible. Hence, it seems to be the F_1+F_2 diagrams, as we used them, which apply.

Professor G. I. **Finch.** In discussing this paper I should like in the first place to outline the history of the discovery of these thermal effects in electron diffraction patterns. The diffuse areas of intensity were first recorded by Finch, Quarrell and Wilman (*Trans. Faraday Soc.*, 1935, **31**, 1051). In 1937, Finch and Wilman (*Ergebn. exakt. Naturwiss*, 1937, **16**, 353) were able to say that these areas were associated with the molecular structure rather than with the crystal lattice; and in 1938, Finch and Tyson (15th *Ann. Rep. British Emp. Cancer Campaign*, 1938) accounted in a similar manner for the diffuse area patterns they had obtained from a variety of carcinogenic compounds. In 1939, Charlesby, Finch and Wilman (*Proc. Phys. Soc.*, 1939, **51**, 479), made a comprehensive study of the anthracene pattern and gave detailed proof that the diffuse areas originate from the molecules. In 1942, Wilman (*Proc. Phys. Soc.*, 1942, **54**, 350) published a pattern from an inorganic substance, cadmium iodide, showing diffuse lines along the main spot rows similar to those found with phthalimide (Finch and Wilman 1937) and later, in 1942, Charlesby and Wilman (*Nature, Lond.*, 1942, **149**, 411) pointed out that these diffuse lines correspond to the diffuse spots or lines which had then recently been found in X-ray patterns, and that they occur together with these still more diffuse areas of intensity in electron diffraction patterns obtained from a wide variety of molecular aliphatic and aromatic compounds, including anthracene.

The first clear recording of the coherent thermal scattering effects with X rays was by Preston in July, 1939, some four or five months after the first full publication of our results and four years after we first announced their discovery. It is remarkable that since then the rôle played by electron diffraction in recording thermal scattering effects seems to have been largely overlooked by X-ray workers—I have seen only two references to it, by Mrs. Lonsdale and the late Sir William Bragg.

Thus in 1942, it was clearly shown by us that electron diffraction patterns may exhibit three main types of features, (i) normal Laue spots together with, in thicker crystals, more or less well-developed Kikuchi lines of normal type, (ii) more diffuse spots due to coherent thermal vibrations, like those now so much studied in X rays and, finally, (iii) diffuse areas of intensity due to molecules scattering as independent units as a result of incoherent thermal motion. Mr. Skrebowski, as far as I can see, has added little or nothing to this picture and indeed seems to me to have closed his eyes to the facts which show the occurrence of independent molecular scattering.

I need only draw your attention to the much larger thickness of the crystals used in X rays to show that the absence of these incoherent thermal-motion effects in the X-ray pattern is not surprising. The molecules at or close to the surface of a crystal are obviously subject to unsymmetrical forces resulting from atoms (or molecules) being on each side of them and below, but not above, them in the crystal, so that their motion must be less regular than that of the molecules deeper inside a large crystal; and, moreover, there must be an absence of the longer standing waves in directions steeply inclined to the main surface of a thin crystal sheet. In large crystals there is a small ratio of surface to mass, and the relative importance of the diffraction from the surface layers is small, but with the very thin crystals necessarily used in electron diffraction it will be much larger, and may even predominate in crystals which are only a few molecules thick. This is indeed precisely what is found experimentally, when an adequate technique is employed, not only in production of the pattern, but also in its scrutiny.

I have hinted elsewhere at the potential value of this independent molecular pattern to molecular and crystal-structure analysis. The coherent thermal-motion pattern has been in this respect, as far as I am aware, of only limited value in X-ray analysis. It will therefore, be of some interest if I tell the meeting that Miss Fisher, working in my laboratory, has in proof with the Society*, a paper which describes how an appreciation of the independent molecular scattering pattern has enabled her to make a valuable advance in our knowledge of the molecular and crystal structure of rubber, a field in which hitherto we have had to rely only on X rays as a tool.

AUTHOR's reply. Some misunderstanding has arisen about part of my paper which I should like to correct. Contour lines of the intensity scattered from a unit cell (figure 2) are drawn for the purpose of indicating where the cross-grating spots (if they appear) are strongest. Thus a cross-grating spot lying between, say, lines 140 and 180 will have an intensity between these values. These contour lines tell nothing about the diffuse background between cross-grating spots. Their sole purpose is to show where strong cross-grating spots will tend to group, as well as the shape of these groupings. Thus Dr. Charlesby's discussion on this part of my paper is inapplicable.

Owing to the length of the discussion I should like to recapitulate briefly the issues involved. Charlesby, Finch and Wilman claim the following :

1. The diffuse areas are primary phenomenon.
2. They are without any detailed structure.
3. They can be explained by the molecular scattering theory which predicts their positions and shapes.

---

* Now published (*Phys. Soc. Proc.*, 1948, **60**, 99).

4. Sometimes diffuse streaks and spots appear, but these have nothing to do with the diffuse areas. These streaks and spots can be explained in terms of the Faxen-Waller theory and are similar to those found in x rays recently.

In my paper I attempted to show :

1. The diffuse areas (in the Charlesby, Finch and Wilman sense) are secondary phenomena.
2. They always have a definite fine structure which is more prominent in thick crystals.
3. With thin crystals this fine structure is very often smeared out and the appearance of diffuse bands or areas without any fine structure prevails.
4. The diffuse streaks and spots are grouped into bands or areas and the position and shape of these groups is equally well (if not better) predicted by structure factor considerations than by the molecular scattering theory.

The Charlesby, Finch and Wilman view has many conflicting elements. If the diffuse streaks and spots exist independently, then why do their contour lines drawn for the diffuse areas include these streaks (figures 10 *a*, 14 *a*) ?

In the discussion there was no mention of the different appearance in the pattern for thick and thin crystals. This is, however, an important point in the present controversy. The pattern in plate 2 might be taken for the diffuse areas (in the Charlesby, Finch and Wilman sense) but for plate 3 which shows that these areas have a fine structure. If, however, the crystal shown on plate 2 were thinned a large number of cross-grating spots would appear. This would tend to obliterate the fine structure and produce something like that observed by Charlesby, Finch and Wilman (1939), i.e. diffuse areas. In the discussion none of these authors attempted to explain the absence of diffuse areas on plates 2 and 4.

One of the main claims of the molecular scattering theory is that it can predict the position of the diffuse areas satisfactorily. In my paper I have shown that these can be found equally well from the structure factor consideration. They coincide with the regions where the structure factor values are high. This is not a coincidence as Dr. Charlesby suggests, for I have calculated this with widely different crystal orientations. Unless he produces quantitative contour lines for a particular photographic plate his argument will have little value. In fact, the qualitative treatment adopted by Charlesby, Finch and Wilman (1939) is open to criticism. Often their diffuse areas are very small (figures 10 *a*, 14 *a*) and cover 1–2 reciprocal lattice cells. A quantitative treatment would give a different result. The diffuse areas in the latter case are much broader (figure 3) and are without sharply defined limits, in contrast to the Charlesby, Finch and Wilman estimations.

Drs. Charlesby and Wilman in interpreting the diffuse pattern apply either the Faxen-Waller theory or the molecular scattering theory or a mixture of both without proving first that these can be applied simultaneously and are not mutually exclusive.

Experiments have been performed on other molecules in order to test the molecular scattering theory further, for this theory requires large and highly symmetrical molecules to produce the effect (Charlesby 1942). Now phenanthrene is not a symmetrical molecule and its unit cell contains four molecules. If, as the molecular scattering theory requires, each of these molecules were scattering independently, one would expect the resulting pattern to be a maze of diffuse bands and areas. Experimentally, however, the pattern is very simple and highly symmetrical (plate B). It appears to follow the structure factor and is composed of diffuse streaks (visible on the original plate). Naphthalene was the other compound examined. Its crystalline structure is almost a replica of anthracene somewhat reduced. According to the molecular scattering theory, the naphthalene molecule, being much shorter than anthracene, should give very broad diffuse areas. The pattern observed (plate C) has diffuse areas (with fine structure) of the same angular spread as anthracene.

I found Dr. Charlesby's argument about the use of photographic plates in electron diffraction unconvincing.

In replying to Dr. Wilman, I would point out that he has misunderstood the indexing shown on my plate 5. The lines shown are not Laue zones. His comment regarding my apparatus is ill-founded in view of the statement made by his collaborator, Dr. Charlesby (*Proc. Phys. Soc.*, 1942, **54**, 383, § 2), “ Experimental difficulties have so far prevented direct investigation of the effect of temperature on the diffuse band pattern ”.

Delayed Fracture of Materials under Tension, Torsion and Compression

By C. GURNEY and Z. BORYSOWSKI
Royal Aircraft Establishment, Farnborough

MS. received 1 *December* 1947; *in final form* 8 *April* 1948

ABSTRACT. Delayed fracture experiments were made in tension, torsion and compression, the times to fracture under a series of constant loads being determined. The materials tested were brass in ammonia vapour, polymerized methyl methacrylate (p.m.m.) in liquid carbon tetrachloride, and glass in air.

In all cases delayed fracture is attributed to the gradual spread of cracks caused by the preferential attack by the surrounding medium of the highly stressed material at the ends of the cracks. In tension, fractures were transverse and in torsion they were helical. In the case of brass and glass, subjected to tension and torsion, fracture of the respective materials occurred in not greatly differing times when the materials were subjected to the same maximum nominal principal tensile stresses. P.m.m. withstood higher nominal principal stress in torsion than in tension for equal times to fracture. The p.m.m. results were complicated by the absorption of carbon tetrachloride, which was greatly accelerated by tension or torsion stresses. During the time occupied by the tests, absorption was inappreciable when the p.m.m. was stress-free or stressed in compression.

In no case did delayed fracture occur in compression.

---

§ 1. INTRODUCTION

Many materials if left under constant load will ultimately fracture. The delayed fracture is usually associated with attack of the substance under stress by the surrounding atmosphere. In the absence of stress, the attack may be inappreciable, but when the substance is stressed, very localized attack may take place, leading to the formation of cracks and ultimately to fracture. For metals, the phenomenon is usually called stress corrosion cracking. Under certain conditions of heat treatment, many aluminium- and magnesium-rich alloys suffer from stress corrosion cracking when exposed under stress to atmospheres containing chlorides; copper alloys are attacked by ammonia, and iron alloys by many salt solutions (Mears *et al.* 1944). The very remarkable delayed fracture of glass in air, for which a three-fold reduction in stress leads to a proportional increase in time to fracture of $10^6 : 1$, has been shown by Preston and his collaborators (1946) to be mainly due to the attack of the atmosphere. Organic plastics also give rise to delayed fracture, especially if surrounded by organic liquids or vapours. A good example is delayed fracture of polymerized methyl methacrylate (p.m.m.) when immersed in carbon tetrachloride, which gives inappreciable attack during the same period when the p.m.m. is stress free.

In nearly all the delayed fracture experiments so far made the materials have been tested in either tension or bending, whereas in practice materials have to withstand other stress systems. In the present experiments delayed fracture of materials subjected to tension, torsion and compression, has been investigated.

§ 2. MATERIAL

In the present series of experiments three materials were tested. The first was brass to Spec. B.S.251 of the following composition: Cu 62·4, Sn 1·2, Zn 36·4. Before machining, the material was heat-treated in air at 500° c. for 45 minutes and then cooled in air. After machining, the test pieces were heat-treated in air at 270° c. for one hour and cooled in the furnace. Control tests were made in tension, torsion and compression. The nominal ultimate tensile stress when tested in air was 24·9 ton/in^2 and the 0·1% proof stresses were 9·5 tons/in^2 (tension) and 9·6 tons/in^2 (compression). The figures quoted are the means of four tests. The delayed fracture experiments were done in an atmosphere saturated with the vapour of aqueous ammonia solution of 35% w/w. NH_3.

The second material tested was polymerized methyl methacrylate (p.m.m.) sheet *. After machining, all test pieces were heated in air at 80° c. for half an hour and cooled in the oven. The ultimate tensile strength at a rate of increase of stress of about 5000 lb/in^2/min. was about 10,000 lb/in^2. Delayed fracture experiments were made with the test pieces immersed in carbon tetrachloride.

The third material was a soda-lime glass in the form of ¼ in. diameter rods, the chief ingredients of which were present in the following percentages: silica 69, alumina 3, lime 6, magnesia 3, soda 18. It was annealed by the manufacturer, and subsequent measurements of internal stress by photoelastic methods indicated a mean value of surface compressive stress of about 600 lb/in^2 with a standard deviation of about 400 lb/in^2. The rods were packed without wrapping and tested without previous surface treatment. Delayed fracture experiments were made in air.

§ 3. APPARATUS

For delayed fracture experiments in tension and compression a spring-loaded cage was used. The test piece was screwed into plates at each end. Three screwed rods fitted with nuts and springs passed through each end plate. For the tension tests the springs were between the plates, one end of each bearing on an end plate and the other bearing on nuts screwed on to the rods. By tightening the nuts, the tension on the test piece was increased. For compression tests the springs were outside the end plates. In both tension and compression tests three Huggenberger tensometers were mounted on each test piece at angles of 120° to each other, and the nuts which loaded the springs were adjusted until the readings on each tensometer corresponded to the strain corresponding to the required stress. This arrangement ensured axial loading. For the torsion tests pulleys were screwed on to each end of the test pieces and located by lock nuts. Each pulley carried two separate cables attached to its rim at each end of a diameter. The cables were in contact with the pulley rims for an arc of about 90°, and then they left the pulley in opposite parallel directions. The directions of the cables on the pulleys at each end of a test piece were parallel and were arranged so that when all four cables were under equal tension the test pieces was subjected to equilibrating end torques. The equality of the tensions was arranged by attaching the two upward cables to the opposite ends of a beam and by attaching the two downward cables to the opposite ends of another beam ; the whole apparatus could be put inside the cages used for the tension and compression experiments, which were adapted to apply central loading to the two beams. For small loads the beams were pulled apart by dead loading.

The brass test pieces were 2¾ in. long threaded ½ in. B.S.F. for a length of ¾ in. at each end, and reduced to 5/16 in. diameter over a central length of ⅝ in. They had a central axial hole of 3/16 in. diameter running the full length of the test piece. The p.m.m. test pieces were 3 in. long threaded ½ in. B.S.F. for a length

---

* Containing 8% dibutyl phthalate as plasticizer.

of 1 in. at the ends and reduced to ¼ in. diameter over a central length of ⅝ in. The glass test pieces were round parallel rods of ¼ in. diameter. They were tested in bending instead of in tension, on account of the difficulty of obtaining axial loading. A four-point loading rig was used, the length subjected to uniform bending moment being 3 in. For torsion, the glass rods were cemented into 3 in. long steel sleeves with an organic cement. Pulleys were screwed on to the sleeves, and the tests were made in the same rig as that used for brass and p.m.m.

§4. EXPERIMENTS

The test pieces were set up in the apparatus already described and the times to fracture under a series of constant loads were recorded. The mean temperature during the tests was 22° c. This was thermostatically maintained to within ± 1° c. for the p.m.m. tests, but for the brass and glass tests the temperature was not so closely controlled. Figure 1 shows the results for brass, figure 2 those for p.m.m. and figure 3 those for glass. For the torsion tests the nominal maximum principal stress computed on the basis of a linear stress distribution is plotted against the logarithm of the time to fracture. For the tension tests the nominal average tensile stress has been plotted. There were five repetitions of each brass experiment, three repetitions of each p.m.m. experiment and twelve repetitions of each glass experiment. The points shown in figures 1, 2 and 3 are median points (half the test pieces failed at a lower stress). The median was chosen rather than the mean, as the former can be computed without waiting for all test pieces to break. The standard error of the median of a normal population is about 1·25 times that of the mean, so that the median is not a greatly worse statistic than the mean. The standard errors of the median points (on the log (time) scale) varied somewhat with stress, the standard error increasing with decreasing stress, and becoming very large at the lowest stresses where the curves tend to become parallel with the time axis. Except at the lowest stresses, the standard errors did not vary greatly with stress, and average standard errors of the median points have been computed from the mean of the ranges of results for each stress, omitting the results for the lowest stresses. The values for tension and torsion respectively were 0·09 and 0·08 for brass, 0·10 and 0·05 for p.m.m., and 0·5 and 0·5 for glass.

When brass in ammonia and p.m.m. in CCl_4 were stressed in compression at the highest stresses which could be applied without buckling the test pieces, no delayed fractures occurred and no cracks were noticed. Even when a short cylindrical piece of p.m.m. was immersed in CCl_4 and compressed so that it was deformed into a barrel shape, no cracking was observed. Compression tests on glass were not made, but it is known that glass is many times stronger in compression than in tension, so that delayed fracture in compression would not occur at stresses at which it occurred in tension.

When stress-free brass was left in the ammonia vapour it became covered with a blue deposit of more or less uniform thickness. When stress-free p.m.m. was left in CCl_4 no attack was detectable during the time occupied by the delayed fracture experiments, but after some months immersion at 22° c. the surface of the p.m.m. was seen to be swollen and covered with a gelatinous layer and the test piece had lost weight, showing that solution was taking place. The soda-lime glass was not noticeably attacked by the atmosphere when stressed or unstressed, but it is known that attack takes place after prolonged exposure. At elevated temperatures glass is rapidly attacked by steam.

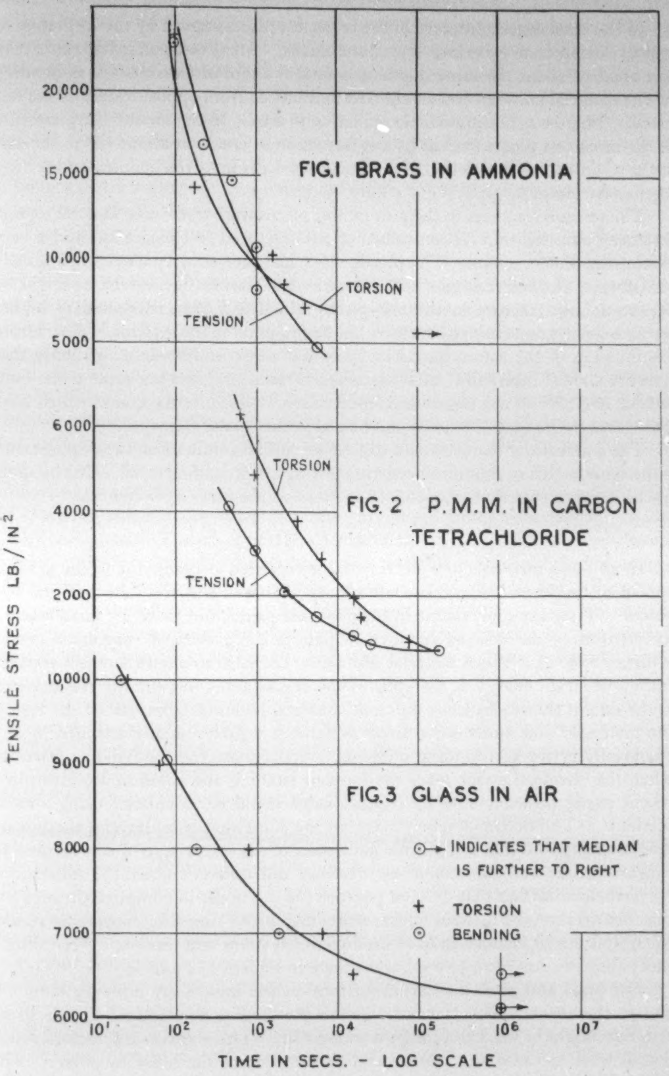
FIG.1 BRASS IN AMMONIA
TORSION
TENSION
20,000
15,000
10,000
5000
FIG. 2 P.M.M. IN CARBON TETRACHLORIDE
TORSION
TENSION
6000
4000
2000
FIG.3 GLASS IN AIR
⊙→ INDICATES THAT MEDIAN IS FURTHER TO RIGHT
+ TORSION
⊙ BENDING
10,000
9000
8000
7000
6000
TENSILE STRESS LB/IN²
10¹
10²
10³
10⁴
10⁵
10⁶
10⁷
TIME IN SECS. - LOG SCALE

§ 5. APPEARANCE OF FRACTURES

In the tension tests fracture of the brass test pieces started by the formation of approximately transverse intercrystalline cracks. Many test pieces had more than one crack of about the same depth, and final fracture often consisted in bending off the material between two cracks that had started from opposite sides of the test piece. There was no appreciable reduction in area. In the torsion tests, fracture of the brass test pieces started by the formation of cracks at about 45° to the axis at the test piece. Completion of the fracture usually involved bending and tearing of the test piece.

The tension fractures in the p.m.m. test pieces were transverse and the torsion fractures were helical. Examination of the fractured test pieces showed a very interesting phenomenon. Test pieces which had been subjected to comparatively low stresses showed fractures which appeared to start at the surface, as might be expected; but fracture in the test pieces which had been subjected to higher stresses started, not from the surface, but from a point in the interior. Apart from examination of the actual fractures, there was other unmistakable evidence that fracture started internally; after tests had been in progress for some time, both tension and torsion test pieces developed clearly visible internal cracks which were transverse in the case of tension and helical in the case of torsion.

The fractures of the glass rods call for no special comment as their appearance is the same as that of fractures occurring during quick-loading tests. The bending fractures were usually S-shaped and the torsion fractures were helical.

§ 6. DISCUSSION

In all three materials delayed fracture is regarded as being due to the gradual spread of cracks. The cracks were clearly visible in the brass and p.m.m. test pieces. They were not visible in the glass test pieces, but there are good reasons for attributing the delayed fracture of glass to the growth of very small cracks (Gurney 1947 a). When material containing cracks is stressed there is a concentration of strain energy at the ends of the cracks and consequently the material at the end of the cracks has a different chemical potential from that of the rest of the material; and under some stress systems it is preferentially attacked by any chemically active surrounding medium. Appropriate thermodynamic relations when the chemical attack takes the form of swelling and solution are given in a recent paper (Gurney 1947 b). Other cases could be calculated using similar methods. The thermodynamic relations are somewhat complex and there is no reason to suppose that any simple parameter of the stress system can be used to express results for different stress systems and different chemical substances. Nevertheless the fact that delayed fracture did not occur in compression suggests that the maximum principal tensile stress may prove useful in expressing results for simple stress systems such as unidirectional stress and torsion. Accordingly this parameter has been plotted as ordinate in figures 1, 2 and 3.

For brass and glass the curves for tension and torsion are not very different, and in the absence of better information the maximum principal tensile stress criterion might be used as a rough working rule. There are several factors which would tend to cause the tension and torsion curves for brass to differ. The assumption of linear stress distribution in torsion would be in error at the higher stresses. At the lower stresses cracks occupying a considerable part of the cross-section developed before fracture occurred. The nature of the stress distribution would be entirely altered by the presence of these large cracks. In particular, the stress at the ends of the cracks, which presumably is an important factor affecting the rate of crack growth, might be very different in the torsion tests and the tension tests, even though the nominal maximum principal tensile stresses assuming uncracked material were equal. In the case of glass these factors are inoperative as the assumption of linear stress distribution in torsion is probably accurately fulfilled, and fracture occurs before cracks of appreciable length compared with the diameter of the test pieces have developed. The experimental points for glass in torsion and bending are not significantly different, and a single curve has been drawn to represent the results.

The difference between the tension and torsion curves for p.m.m. is greater than that between the corresponding curves for brass or glass. The factors which have been suggested to account for the difference in the case of brass are also operative for p.m.m., but it seems doubtful that these effects would be so much greater for the p.m.m. test pieces than for the brass test pieces as to account for the large difference. Examinations of the fractured p.m.m. test pieces showed the peculiarity already mentioned—that at high stresses fracture started internally. This is evidence for an additional factor affecting the p.m.m. results which finds a ready explanation. When stress-free p.m.m. is immersed in CCl_4 for prolonged periods, it is found that the surface is swollen by absorption of CCl_4, and that some of the p.m.m. has actually gone into solution in the liquid. The first effect of immersing stress-free p.m.m. in CCl_4 therefore will be a gradual absorption of the CCl_4 accompanied by swelling, but after prolonged immersion solution in the CCl_4 takes place. The effect of stress of the effects can be deduced from general thermodynamic reasoning. Natural processes tend to a reduction of the free energy of systems, and part of the free energy of a system under load lies in the potential energy of the external forces. If a rod under tension absorbs fluid, the external forces do positive work, and therefore reduce their potential energy for two reasons. Firstly, there is a direct increase in the length of the rod due to swelling, and secondly, there is an increase in the length of the rod due to the reduction in Young's modulus consequent upon swelling. The effect of tension, therefore, is to increase the rate of swelling. The effect of torsion is also to increase the rate of swelling; the reduction in shear modulus of the swollen test pieces allows the end couples to rotate and do work.

The swelling of the surface material of a rod under tension or torsion causes two effects. The swollen material is weakened and therefore more likely to fracture; but its size is increased and its elastic moduli (E and G) are reduced, while the elastic constants and dimensions of the unswollen interior material remain the same. The swelling of surface material tends to set up a system of internal stress in which the surface material is in two-dimensional compression. Both in tension and torsion, therefore, the maximum principal tensile stress in the surface is reduced. A further reduction is caused by the change in elastic moduli. Absorption of liquid by surface layers therefore weakens them, but at the same time causes a reduction in the stress they have to withstand.

These ideas lead to a plausible explanation of the experimental results that at low stresses fracture of the p.m.m. test pieces started from the outside, and at high stresses fracture started from the inside. It is only necessary to assume that at low stresses the weakening of surface material by absorption of CCl_4 exceeds the reduction in the stress associated with the absorption; fracture would then start from the outside. On the other hand, at high stresses the reduction in stress due to swelling and change in elastic moduli exceeded the weakening of the material due to absorption, so that fracture started in the interior, where the stress was already increased by the internal tension stress caused by the swelling of the surface layers.

The broad conclusions to be drawn from the experiments are that delayed fracture does not occur in compression. For brass in ammonia and glass in air, delayed fracture in tension and torsion occurs in approximately equal times at equal principal tensile stresses. P.m.m. in carbon tetrachloride will withstand higher principal tensile stresses in torsion than in tension for equal times to fracture.

ACKNOWLEDGMENT

The delayed fracture experiments on glass were made by Mr. S. Pearson. Measurement of internal stress was done at the Research Laboratories of the General Electric Company.

REFERENCES

Gurney, C., 1947 a, *Proc. Phys. Soc.*, **59**, 169 ; 1947 b, *Ibid.*, **59**, 629.
Mears, R. B., Brown, R. H., and Dix, E. H., 1944, *Symposium on stress corrosion cracking of metals* (Philadelphia : A.S.T.M.).
Preston, F. W., Baker, T. C., and Glatshart, J. L., 1946, *J. Appl. Phys.*, **17**, 162.

β-Disintegration and the Sargent Diagram

By N. FEATHER and H. O. W. RICHARDSON
Department of Natural Philosophy, University of Edinburgh

MS. received 6 *May* 1948; *to be read* 5 *November* 1948

ABSTRACT. Sargent diagrams constructed for negative-electron-active species having $80 < Z < 94$ (as also for the restricted group with $80 < Z < 84$), and for both negative-electron-active and positron-active species having $Z < 22$, are discussed in the light of theory. The majority of first-forbidden transitions in the group of heaviest radioelements give a Sargent line parallel to the allowed line, corresponding to disintegration constants smaller by a factor of roughly 10 only than the disintegration constants of allowed transitions of equal energy. Transitions with no parity change between states of zero spin appear to give a second-forbidden line also parallel to the allowed line.

With the lightest radioelements "super-allowed" transitions are identified which require Wigner selection rules for their interpretation, but there is also a group of transitions which appears to be ordinarily allowed (i.e. subject to spin and parity selection rules only). Compared with these allowed transitions in the lightest elements, allowed transitions in the heaviest radioelements are less probable by a factor of about three only, when comparison is made for equal energy release and account is taken of the effect of the coulomb field of the nucleus.

On the assumption that all $\binom{\text{even}}{\text{even}}$ nuclei have even parity and zero spin in the ground state it is concluded that the β-particles of maximum energy observed with RaB, RaC and MsTh_1 are emitted in transitions to excited states of the final nuclei RaC, RaC′ and MsTh_2, respectively. This conclusion makes it likely that the accepted value of the total γ-ray emission from RaB (Gray 1937) is too small, that the total disintegration energy Ra.C.C′ is 3·78 Mev. and that MsTh_1 emits a low-energy γ-radiation which has not as yet been detected. On the same assumption it is concluded that the disintegrations $\text{UX}_1 . \text{UX}_2'$ and $\text{UX}_2 . \text{U}_{\text{II}}$ possess features at present unknown or insufficiently understood.

A REVISED Sargent diagram for the heavy radioelements has recently been published by one of us (Feather 1948) showing strong evidence for a hitherto unidentified " line ", almost parallel to the line for allowed transitions, and not very distant from that line. If the suggestion that the new line can belong only to first-forbidden transitions be accepted, then obviously the degree of forbiddenness corresponding to the other lines, previously identified, and lying lower on the diagram, must be revised—the first-forbidden line of the old diagram becoming the second-forbidden line of the new diagram, and so on. It is one object of this note to point out that this assignment has the support of theory : the occurrence of first-forbidden transitions, differing relatively little in probability from allowed transitions of the same energy, has been predicted by Konopinski and Uhlenbeck (1941), at least for the heavy elements. For the lightest radioelements, according to these authors, such transitions should not occur : the calculations show that a much larger difference in transition probability is to be expected as between allowed and first-forbidden disintegrations of equal energy.

The formal predictions of the theory are briefly as follows. Let R_{01} be the ratio of the disintegration constants, $\lambda_0(W)$, $\lambda_1(W)$, for allowed and first-forbidden transitions in which the total disintegration energy (including the rest-energy of the electron) is $W\boldsymbol{mc}^2$. Let Z be the charge number of the β-active nucleus, and let the nuclear radius be $\rho \boldsymbol{h}/2\pi \boldsymbol{mc}$. Then when

$$\alpha Z \gg 2\rho W, \qquad \ldots\ldots(1)$$

α being the fine-structure constant, 1/137, we have, alternatively,

$$R_{01} \sim (\alpha Z/2)^{-2} \qquad \ldots\ldots(2)$$

or

$$R_{01} \sim (\rho W)^{-2} \qquad \ldots\ldots(3)$$

depending upon the change of spin in the transition. If I is the total spin quantum number of the nucleus, (2) applies to those transitions which involve a change of parity of the nuclear state and for which $\Delta I = 0$ or ± 1 and (3) applies when $\Delta I = \pm 2$. (Here it might be noted that first-forbidden transitions with $\Delta I = \pm 2$ are possible only on the basis of the axial vector and tensor forms of interaction, which are governed by Gamow-Teller selection rules.) The theory also predicts that the shape of the energy spectrum should approximate to the allowed shape when (2) applies, and differ considerably from this shape, showing a deficit of medium-energy β-particles and an excess of high-energy particles, when (3) is valid.

For the heavy elements ($80 < Z < 94$) for which (1) is amply fulfilled, (2) points to a first-forbidden line parallel to the line for allowed transitions and distant, approximately, by $\Delta \log \lambda = 1{\cdot}0$ ($8{\cdot}5 < (\alpha Z/2)^{-2} < 11{\cdot}7$)—and (3) to a lower-lying line, quite steeply inclined to the allowed line at its upper end, but still representing transitions which are only once forbidden. On this analysis of the situation there is clearly a good case for our identifying the newly-recognized line with the first-forbidden line predicted by (2) : it exhibits the close parallelism with the experimental line for allowed transitions which is required, and the absolute value of the mean separation ($0{\cdot}75 < \Delta \log \lambda < 1{\cdot}1$) agrees remarkably well with prediction.

Having elicited this measure of agreement, the next object of this note is to continue the comparison of experiment and theory in respect of transitions of higher degrees of forbiddenness.

The theoretical result concerning R_{02}, the ratio of the disintegration constants for allowed and second-forbidden transitions of energy $\boldsymbol{W}\boldsymbol{mc}^2$, is that

$$R_{02} \sim (\alpha Z \rho W/2)^{-2} \qquad \ldots\ldots(4)$$

or

$$R_{02} \sim (\rho W)^{-4} \qquad \ldots\ldots(5)$$

depending upon whether, without change of parity, $\Delta I = \pm 2$ or ± 3. (Again, the higher value of the spin-change, as in the case of first-forbidden transitions, is permissible only under Gamow-Teller selection rules.)

In order to make further comparison with least ambiguity due to variations in Z and ρ, we restrict consideration at this stage to disintegrations of β-active nuclei having $Z = 81$, 82 and 83 ($204 \leqslant A \leqslant 214$). Figure 1 contains the 27 representative points for these disintegrations, now considered separately from the 23 points for $87 \leqslant Z \leqslant 93$ with which they were combined in the Sargent diagram recently published. As starting point we take the point for RaE. Here $Z = 83$, $A = 210$, $W = 3{\cdot}29$ and $R_{02} = 616$ ($\Delta \log \lambda = 2{\cdot}79$). Writing (4) for this disintegration in the form

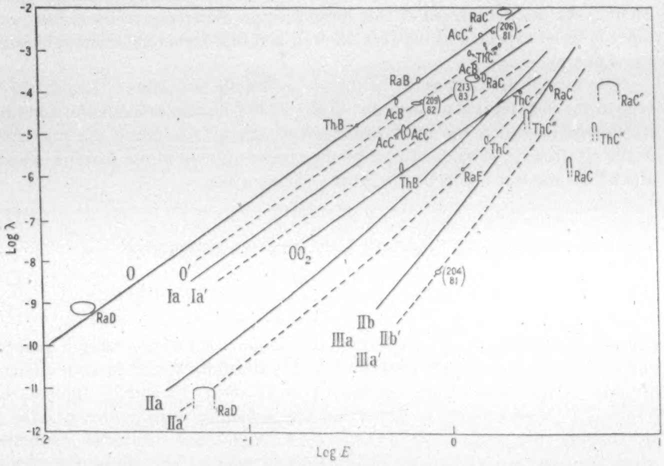

Figure 1. λ in sec⁻¹; E in Mev.

$$R_{02} = 5a(\alpha Z/2)^{-2} . (\rho W)^{-2} \qquad \ldots\ldots(6)$$

on the assumption that a second-forbidden transition, $I = 2 \rightarrow I = 0$, is involved (Greuling 1942), with $(\rho \boldsymbol{h}/2\pi \boldsymbol{mc}) = 1{\cdot}5 \times 10^{-13} A^{\frac{1}{3}}$ (cm.), giving $\rho^{-1} = 43{\cdot}2$, we obtain $a = 0{\cdot}066$. The factor 5 (the value of $2|\Delta I| + 1$, for RaE.F) has been introduced into the equation for R_{02} because the transition is taken as one in which the total spin decreases (to zero) rather than increases (Marshak 1942, Greuling 1942); the constant a then refers to the most probable type of second-forbidden transition (having $\Delta I = +2$). We do not comment further on the absolute value of a, which appears as considerably smaller than " of the order of magnitude unity "—this aspect of the problem has already been treated in detail by others

(Marshak 1942, Greuling 1942), who find in it evidence for narrowing the choice of possible interaction forms to the polar vector (Fermi rules) or tensor (Gamow-Teller rules) forms—but we attempt to follow the assumption that a closely similar value of a is appropriate to the other second-forbidden transitions to which (4) applies (within our chosen range of Z). Curves IIa and IIa′, therefore, have been constructed, the latter according to (6) through the representative point for RaE, and the former parallel to it and higher in the diagram by $\Delta \log \lambda = 0{\cdot}699$ ($= \log 5$). In constructing these curves, which are of course drawn with respect to the allowed curve O as reference curve, the small variations in Z and ρ, possible for the various points in the diagram, have been neglected. Curve O, it should be pointed out, is appropriate only when $\Delta I = 0$ or $+1$; curve O′ belongs to those allowed transitions for which $\Delta I = -1$ ($\Delta \log \lambda = 0{\cdot}477$). Similarly for the curves Ia and Ia′ which belong to the first-forbidden transitions governed by (2): Ia is applicable when $\Delta I = 0$, $+1$ and Ia′ when $\Delta I = -1$ *.

In considering the whole diagram at this stage it will be seen that one point only lies between curves Ia′ and IIa, and that not more than two " observed " points lie below curve IIa′. Formally, therefore, at least 19 of the 22 " observed " points would appear to be satisfactorily accounted for—even though four of the five " unobserved " points, which lie below curve IIa′, require further consideration. We shall return later to the general question of the " unexplained " points, for the present we direct attention to the group of four transitions which has emerged as second-forbidden according to (4), through our construction of curves IIa and IIa′ as above described. In addition to the ground-to-ground state transition RaE.F, we have the " unobserved " ground-to-ground state transition RaD.E (for which a disintegration energy of 60 ± 4 kev. and an intensity of $< 0{\cdot}01$ has been assumed) and two transitions ThC.C′ (those leading to the ground state of ThC′ and to the excited state of 726 kev. energy, respectively).

In the first place it is extremely satisfactory that the two ground-to-ground state transitions belonging to the successive disintegrations RaD→RaE→RaF should be found grouped together in this way. The initial and final nuclei, ${}^{210}_{82}\mathrm{RaD}$ and ${}^{210}_{84}\mathrm{RaF}$, are both $\binom{\text{even}}{\text{even}}$ nuclei, and in the ground state each would be expected to have $I = 0$ and even parity. Thus the β-disintegrations RaD.E, RaE.F which involve the same intermediate state (the ground state of RaE) must be expected to be characterized by equal and opposite values of ΔI and by the same parity-change (either each " yes " or each " no "). The two transitions should, in short, be forbidden to identical degree. This is exactly what is found. (To be precise, the point for the ground-to-ground state transition RaD.E ought to lie on curve IIa, if that for RaE.F is on curve IIa′, but it cannot be held that the distinction is important having regard to the uncertainty as regards intensity and the extent of the extrapolation involved in the comparison just made.)

We next discuss the two points for ThC.C′. In the successive disintegrations ThB→ThC→ThC′ the situation in respect of A and Z is similar in all respects to that just considered: ${}^{212}_{82}\mathrm{ThB}$ and ${}^{212}_{84}\mathrm{ThC'}$ are each of them $\binom{\text{even}}{\text{even}}$ nuclei †,

---

* According to Marshak (1942) curves O′ and Ia′ belong strictly to those transitions characterized by $I = 1 \rightarrow I = 0$. Other transitions for which $\Delta I = -1$ should have representative points between curves O and O′, if allowed, or, if first-forbidden, between Ia and Ia′. See letter by Strachan in this issue, p. 481.

† The classification $\binom{\text{even}}{\text{even}}$, $\binom{\text{even}}{\text{odd}}$, etc., of this paper refers throughout to neutron and proton numbers, i.e. is a classification in respect of $\binom{A-Z}{Z}$, not of $\binom{A}{Z}$.

thus we should expect the ground-to-ground state transitions ThB.C, ThC.C′ to be identically forbidden. We have mentioned that the point for ThC.C′ falls within the limits of curves IIa and IIa′, but in this case the corresponding point for the previous disintegration does not. In fact the point for the ground-to-ground state transition ThB.C is the single point which on figure 1 lies mid-way between curves Ia′ and IIa. Formally this point might be interpreted as being on a curve Ib, determined by (3)—then $|\Delta I|$ would have the same value, 2, for the transitions which are thus associated—but we should not in this way solve the problem, for the parity changes would then be different. If our assumptions regarding spin and parity of the ground states of $\binom{\text{even}}{\text{even}}$ nuclei are correct, there would, in fact, appear to be only one solution—the ground-to-ground state transitions ThB.C, ThC.C′ must be of a special type which we have not hitherto considered. This suggestion might be thought to be strengthened by the empirical fact that the two representative points concerned are very closely the same distance below the line for allowed transitions, and, from the point of view of theory, by the fact that transitions $I=0$ [illegible] constitute a naturally special class when certain of the five standard [illegible] are employed (this is untrue only with the scalar and polar vec[illegible] which carry the Fermi rules). We adopt this suggestion, then, dr[illegible] parallel to O and distant by $\Delta \log \lambda = 1{\cdot}85$—and we make the [illegible] assumption that the new line (OO_2) is characteristic of a whole class [illegible] 0 transitions generally (within the chosen range of Z). That this class of 0→0 transitions is that for which there is no change of parity may be deduced from the following considerations. The representative point for the main ThB.C transition falls on the allowed line. Thus there is no parity change in this β-transition, which leads to the 238 kev. state of ThC. The γ-ray emitted in transition from this state to the ground state is converted internally as a magnetic dipole radiation. The excited and ground states, therefore, have like parity. The ground-to-ground state β-transition ThB.C is likewise, therefore, a transition without change of parity.

Now 0→0 transitions without change of parity are permitted according to the scalar and polar vector forms of interaction as ordinary allowed transitions, and such transitions are completely forbidden according to the axial vector and pseudoscalar forms of interaction. On the tensor form only are they permitted merely as (second) forbidden transitions. It appears therefore that our line OO_2 can only be explained, on the basis of a single (unmixed) interaction, as a "second-forbidden" line for 0→0 transitions obeying Gamow-Teller selection rules and describable in detail using the tensor form of interaction. It is satisfactory that theory in this case predicts a line which is parallel to the allowed line (Konopinski 1943). It is also satisfactory that the distance of OO_2 from the allowed line is approximately twice the distance of Ia from this line, for amongst the transitions to which Ia might belong are the 0→0 transitions with change of parity which, on the basis of the tensor form of interaction, behave as first-forbidden. Using an obvious notation we might in fact say that a line OO_1 coincides roughly with the line labelled Ia in figure 1.

We have obviously digressed from our discussion of the two points for ThC.C′; returning now to this specific topic we may note that whilst one of them has been taken out of the group to which the curves IIa and IIa′ apply, there is nothing to contradict the identification of the other as the representative point of a second-forbidden β-disintegration having $|\Delta I| = 2$.

A third case of successive β-disintegrations for which the initial nucleus is an $\binom{\text{even}}{\text{even}}$ nucleus is provided by the sequence RaB→RaC→RaC′. Although it cannot be claimed that sufficient is known regarding these much-studied disintegrations to provide full information for a discussion, if we make the same assumptions as before regarding spin and parity certain conclusions follow without question. The most important of these is that the ground-to-ground state transition RaB.C is " unobserved ". This is in line with the opinion originally held (cf. Ellis 1934), but it has been rendered doubtful by results of Gray (1937). The present argument is as follows. We may assume for the moment that it is not certain whether the ground-to-ground state transition RaC.C′ is that of 3·173 MeV. maximum energy given by the experimentally determined end-point of the RaC β-particle spectrum, or an unobserved transition of 0·606 MeV. higher energy (Ellis 1934, Bothe and Maier-Leibnitz 1937), but in either case it appears that the transition is at least second-forbidden. On the other hand, the experimentally determined end-point of the RaB β-particle spectrum at 0·72 MeV. energy (Constantinov and Latyschev 1941) belongs to a transition which is obviously allowed. This is enough to show that the two transitions are not consecutive ; they cannot have the ground state of RaC as a common intermediate state; in other words the ground-to-ground state transition RaB.C is "unobserved".

Concerning the disintegration RaC.C′ again, it has just been stated that it is not certain, on the direct experimental evidence, whether or not the ground-to-ground state transition is observed. We can now use figure 1 to establish the conclusion that it is almost certainly not observed. Evidence from the long-range α-particles of RaC′.D shows that a state of RaC′ of 2·88 MeV. energy is excited in the previous β-disintegration, and it is practically certain that de-excitation of this state involves the emission of the strong (quadrupole) γ-rays of 1·12 and 1·76 MeV. energy in cascade (Rutherford, Lewis and Bowden 1933). The absolute intensities of these γ-radiations have been shown to be closely the same (Latyschev 1947) and calculated values are such that an initial excitation of the 2·88 MeV. state of at least 20% must be assumed. If the total energy of disintegration is 3·17 MeV., excitation of the state in question involves a β-particle partial spectrum of 0·29 MeV. maximum energy only, and the highest excitation possible (assuming an allowed transition) is then about 1·5%. On the other hand, a partial spectrum of $(0{\cdot}29+0{\cdot}606)$ MeV. maximum energy would in fact give 22·5% or 67·5% excitation, depending upon whether curve O′ or O were appropriate to the case. Curve O′ would apply if the transition were one for which $\Delta I=-1$; on this matter all that can be said is that it is very unlikely that ΔI is positive, though it might be zero. In any case, however, the indication is clear enough ; the total disintegration energy must be considerably greater than 3·17 MeV. ; thus the ground-to-ground state transition RaC.C′ is not observed.

It is worth while discussing the unobserved transitions in this disintegration somewhat further—for there is clear evidence that there are many of them. Thus Rutherford, Lewis and Bowden (1933) detected twelve groups of long-range α-particles from RaC′—in this way providing evidence for the excitation, direct or indirect, of twelve states other than the ground state in the disintegration RaC.C′—and the same authors were forced to postulate the excitation of at least four other states in order to account even for the stronger lines in the γ-ray spectrum of RaC. Now, we have already suggested somewhat more than 20% excitation for the state of highest energy (2·88 MeV.), and the general shape of the β-particle spectrum (Constantinov and Latyschev 1941) is inconsistent with the direct excitation of more than a few other states to any comparable extent (say about 25% for the state of 0·606 MeV., and roughly 50% for a state or states at about 2·2 MeV. excess energy). So our statement may be made more precise: probably not more than four of the sixteen excited states which are regarded as definitely established are excited by direct β-transition RaC.C′ to more than 10%. Several of these states cannot be excited to more than a few tenths per cent at the most. Assuming that in the ground state the nucleus ${}^{214}_{84}\mathrm{RaC}'$ has $I=0$ and even parity, we thus conclude that there are probably other states, of higher energy than that of 1·41 MeV., which like the latter state (Fowler 1930) also have $I=0$. Some of these may not be involved in γ-ray emission to any appreciable extent. Depending upon whether $\Delta I=0$ or -1 for the transition exciting the 2·88 MeV. state, bearing in mind the nature of the cascade γ-ray emission from this state, we are led to assign $I=4$ or $I=5$ to the ground state of RaC. Thus these unobserved transitions must be at least third-forbidden ($|\Delta I|\geqslant 4$).

The general features of the level scheme begin to emerge from this discussion, but clearly it would be unprofitable to continue it further until the results of experimental studies of β–γ and γ–γ correlation provide more detailed information. Here it should merely be remarked that only three points are plotted for RaC on figure 1 ($E=3{\cdot}173$ MeV., $23\pm5\%$; $E=1{\cdot}51\pm0{\cdot}02$ MeV., $40\pm10\%$; $E=3{\cdot}78$ MeV., $<0{\cdot}5\%$): to have included all the " unobserved " points would have been neither practicable nor very helpful at this stage.

It has already been stated that not more than two of the " observed " points of figure 1 lie below the line IIa′. One of these is the point for the 3·173 MeV. transition RaC.C′ which has just been discussed at length, the other is the point for the ground-to-ground state transition ${}^{204}_{81}\mathrm{Tl}\xrightarrow{3\cdot5y}{}^{204}_{82}\mathrm{Pb}$. This point almost certainly belongs either to curve IIb′ or to curve IIIa′—the accents reflecting the fact that since the final nucleus is an $\binom{\text{even}}{\text{even}}$ nucleus ΔI is presumably negative in this case. On the basis of either attribution $\Delta I=-3$ (parity being unchanged if IIb′ applies and changing if IIIa′ is in question). Again, since the energy dependence of λ is the same according to either assumption (compare (5) with $R_{03}\sim(\alpha Z/2)^{-2}(\rho W)^{-4}$ which is applicable to curve IIIa′) we may, without further decision between the possibilities, construct a curve through the point under consideration and another curve representing values of λ greater by a factor of 7 ($2|\Delta I|+1$, with $|\Delta I|=3$). These curves are shown on figure 1 and appropriately labelled. It will be noted that they intersect curve IIa′ in the general region of the point for RaC ($E=3{\cdot}173$ MeV.), thus no definite assignment of this point appears possible on the basis of the diagram alone. A similar remark is obviously true of the unobserved point representing the 2·38 MeV. transition ThC″. D. As regards the " unobserved " points for the ground-to-ground state transitions RaC″. D, ThC″. D and RaC . C′ (see above), it would appear from their positions on the diagram very likely that these belong to transitions which are at least fourth-forbidden (see Richardson 1948).

Figure 1, it will be remembered, was constructed by omitting the 23 points representing β-transitions in elements having $87\leqslant Z\leqslant 93$ from the Sargent diagram recently published. We may reconsider these transitions briefly now, making the following general observations:

(1) 7 of the omitted points would lie, on figure 1, either between curves O and O′ or somewhat above curve O.

(2) 8 of them would lie between curves Ia and Ia′ (thus it happens that the evidence that these curves are significant is statistically stronger on the basis of the higher-Z group data than on the lower-Z group data).

(3) 1 point (belonging to a rare mode of the disintegration $UX_2 . U_{II}$) would appear to lie on the line OO_2.

(4) 4 points would lie between curves IIa and IIa′.

(5) 1 point would be found somewhat below the line IIb′ – IIIa′ (this is the only point plotted for $MsTh_2$, the disintegration of which is obviously almost as complex as that of RaC but much less thoroughly studied).

(6) The remaining two (" unobserved ") points would appear to belong to transitions which are third- or fourth-forbidden (these are the points for the ground-to-ground state transitions $UZ.U_{II}$ and ${}^{238}_{93}Np$. ${}^{238}_{94}Pu$).

Clearly there is nothing in these general observations to suggest that our detailed treatment of the points included in figure 1 would fail if applied to the omitted points ; the effect of the change in average Z value between the two groups (from $Z = 82$ to $Z = 91$) in fact appears to be even smaller than might have been predicted.

But there is one particular case which merits further discussion, for on the evidence at present available it seems that a real difficulty is involved. The disintegration sequence $UX_1 \rightarrow UX_2 \rightarrow U_{II}$ between the $\binom{\text{even}}{\text{even}}$ nuclei ${}^{234}_{90}UX_1$ and ${}^{234}_{92}U_{II}$ provides the case in point. These disintegrations have been very carefully studied by Bradt and others (Bradt, Heine and Scherrer 1943, Bradt and Scherrer 1945, 1946), and, in spite of the complications due to the $UX_2 - UZ$ isomerism, experimentally it would seem that the evidence is definite and in the main complete. But the positions of the representative points for the partial spectra of highest energy in the disintegrations $UX_1 . UX_2$, $UX_2 . U_{II}$ certainly lie on different Sargent curves on the revised diagram—the former between curves Ia and Ia′ and the latter on curve O. There is no evidence at present against the obvious assumption that the partial spectra in question characterize truly consecutive transitions, or against the assumption that the nucleus U_{II} is left in the ground state after the second of these transitions, yet the Sargent diagram analysis points to a change of parity in the first transition ($UX_1 . UX_2$) and no change of parity in the second ($UX_2 . U_{II}$). The apparent overall change of parity as between the initial and final $\binom{\text{even}}{\text{even}}$ nuclei disclosed by this analysis is the difficulty already mentioned.

There is another more subtle difficulty which concerns the disintegration $UX_2 . U_{II}$ considered in isolation from the preceding transformation. If the two component radiations of about 0·95 MEV. and 1·5 MEV. energy identified by Bradt and Scherrer (1945, 1946) were the only γ-radiations emitted by UX_2 the difficulty would not arise : observed intensities fit well with the assumption that for these radiations excitation of the γ-emitting states (of U_{II}) is by first-forbidden transitions, " excitation " of the ground state being by an allowed transition as above described. But there are two or three other radiations (of 782, 822 and possibly 806 kev. energy, respectively) to be taken count of, and there is strong circumstantial evidence that some or all of these radiations are emitted in $0 \rightarrow 0$ transitions leading to the ground state. The serious difficulty in this interpretation is that, if the emitting states and the ground state have the same spin ($I=0$) and parity, excitation of the emitting states by β-disintegration should be to the extent of about 20% whereas in fact it is almost certainly less than 0·5%. Even the assumption of different parities would not entirely remove the discrepancy. Empirically the representative points for the β-transitions exciting the emitting states in question (only one such point was plotted in the Sargent diagram recently published) appear to lie on the curve OO_2 ($0 \rightarrow 0$ transition, no parity change), as mentioned in our general observation (3) above. This, of course, is consistent with the assumption that the subsequent radiations involve $0 \rightarrow 0$ transitions to the ground state of the $\binom{\text{even}}{\text{even}}$ nucleus ${}^{234}_{92}\mathrm{U}_{\mathrm{II}}$: it is rather the main β-transition $\mathrm{UX}_2 . \mathrm{U}_{\mathrm{II}}$ which does not appear to fit into the general interpretative scheme—it cannot similarly be described as a $0 \rightarrow 0$ transition between states of even parity in view of the position of the representative point on the allowed curve O of the revised diagram. It would seem, therefore, that unless our general assumption regarding spin and parity of $\binom{\text{even}}{\text{even}}$ nuclei in the ground state is at fault, some new feature of the $\mathrm{UX}_1.\mathrm{UX}_2$, $\mathrm{UX}_2.\mathrm{U}_{\mathrm{II}}$ disintegrations remains to be discovered. More detailed studies of the known γ-radiations in emission, and a search for a possibly highly converted low-energy γ-radiation of high intensity, would appear to be called for. It might be mentioned here that no difficulty arises in assigning degrees of forbiddenness to the various β-transitions in the associated disintegration $\mathrm{UZ} . \mathrm{U}_{\mathrm{II}}$: energies and intensities of excitation, and the nature of the γ-radiations, can be satisfactorily explained on the assumption that the β-transition of energy 0·45 MeV. is allowed, that of energy 1·2 MeV. second-forbidden and the unobserved ground-to-ground state transition of about 1·95 MeV. energy third- or, more probably, fourth-forbidden.

There remains finally the case of the successive disintegrations $\mathrm{MsTh}_1 \rightarrow \mathrm{MsTh}_2 \rightarrow \mathrm{RdTh}$, the last case amongst the "classical" radioelements of successive β-disintegrations between initial and final nuclei which are both $\binom{\text{even}}{\text{even}}$ nuclei. Here, as already mentioned, information is far from complete, but it is complete enough to sustain one clear prediction, so long as our basic assumptions remain valid. According to Lee and Libby (1939) the maximum energy of the β-particles of MsTh_1 is 54 ± 4 kev. On the basis of a single disintegration mode this implies a first-forbidden transition according to our revised diagram. On the other hand, the ground-to-ground state transition $\mathrm{MsTh}_2.\mathrm{RdTh}$ is at least second and probably more highly forbidden (see our general observation (5) above). Thus we must anticipate that the ground-to-ground state transition $\mathrm{MsTh}_1.\mathrm{MsTh}_2$ is unobserved, that is, that there is an intense (soft) γ-radiation from MsTh_1 still to be discovered.

Our discussion of the Sargent diagram for the heaviest radioelements has been based on the tacit assumption that the only selection rules involved are those concerned with the parity and total angular momentum of the nucleus—and empirically there is no indication that these rules are inadequate. With the lightest elements, however, there is abundant evidence that further rules are required, and Wigner (1939) and others have formulated such additional rules employing a "super-multiplet" classification of nuclear energy states. The empirical evidence for the necessity of some such extension of theory is obvious from figures 2 and 3. These diagrams refer, respectively, to electron-active and positron-active species having $Z < 22$*. In the absence of additional selection rules we should expect the allowed curves to be well-defined, and that they should occupy identical positions on the two diagrams, the effect of the coulomb field of the nucleus being all but inappreciable for elements in this range of *Z*.

---

* No point is plotted on figure 2 for ${}^8\mathrm{Li}$, the β-spectrum of which cannot be resolved into a finite number of discrete partial spectra because the disintegration energy varies continuously from zero to about 12 MeV. For a full discussion see Wheeler (1941).

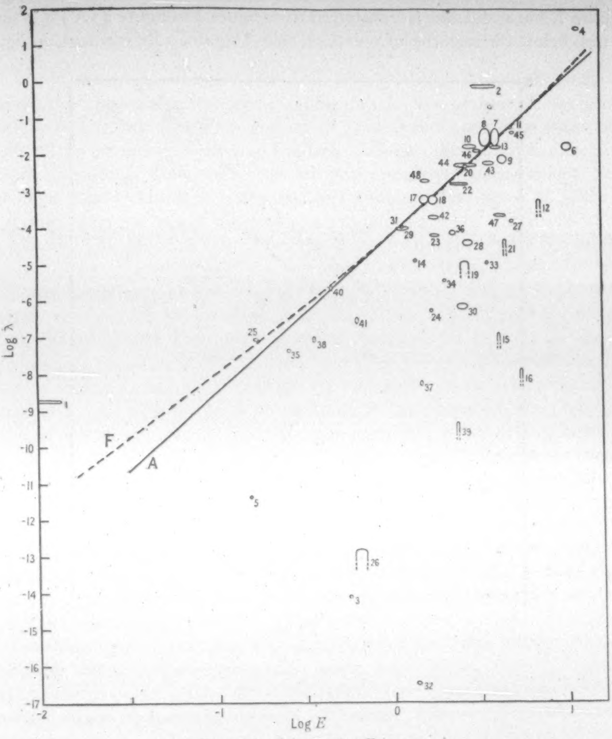

Figure 2. λ in sec^{-1}; E in MeV.

Key for figure 2

Species	Points	Species	Points	Species	Points	Species	Points
$^{3}_{1}$H	1	$^{23}_{10}$Ne	13	$^{34}_{15}$P	45, 46	$^{45}_{20}$Ca	35
$^{6}_{2}$He	2	$^{24}_{11}$Na	14, 15, 16	$^{35}_{16}$S	25	$^{49}_{20}$Ca	36
$^{10}_{4}$Be	3	$^{25}_{11}$Na	43, 44	$^{37}_{16}$S	47, 48	$^{46}_{21}$Sc	37, 38, 39
$^{12}_{5}$B	4	$^{27}_{12}$Mg	17, 18, 19	$^{36}_{17}$Cl	26	$^{47}_{21}$Sc	40
$^{14}_{6}$C	5	$^{28}_{13}$Al	20, 21	$^{38}_{17}$Cl	27, 28, 29	$^{48}_{21}$Sc	41
$^{16}_{7}$N	6, 7, 8	$^{29}_{13}$Al	22	$^{41}_{18}$A	30, 31	$^{49}_{21}$Sc	42
$^{19}_{8}$O	9, 10	$^{31}_{14}$Si	23	$^{40}_{19}$K	32		
$^{20}_{9}$F	11, 12	$^{32}_{15}$P	24	$^{42}_{19}$K	33, 34		

Comparison of the diagrams shows, however, that these predictions are far from the truth. There is the appearance of an allowed line (A) in figure 2—if we leave on one side for a moment the points for the β-active species ^{3}H, ^{6}He and ^{12}B—though it is not so well defined as the allowed line for the heavy radioelements in figure 1, but if this line is transferred from figure 2 to figure 3 (A′) it is seen to fall well below the majority of points on that diagram. By contrast, in figure 3 there is a perfectly well-defined line (S) parallel to A′, which line we can only classify empirically as "super-allowed". In this connection the treatment of Wigner is obviously significant: of the 15 points defining our super-allowed line, 12 belong to the ground-to-ground state transitions of 12 of the 16 $\left({}^{2Z-1}{}_{Z}\right)$ species $^{11}_{6}$C to $^{41}_{21}$Sc (and there is fairly clear indication from the known periods that the corresponding points for three at least of the remaining four species of this

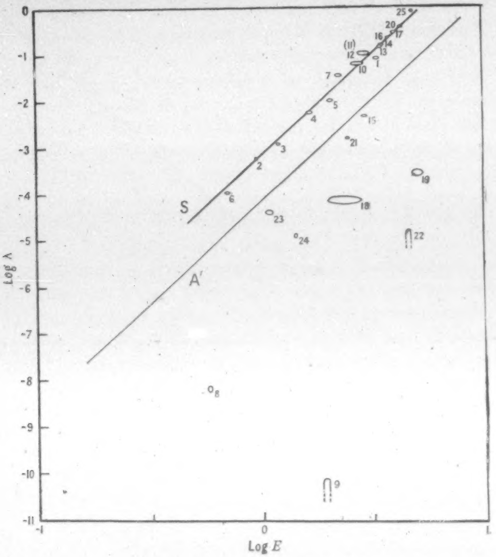

Figure 3. λ in sec⁻¹; E in Mev.

Key for figure 3.

Species	Points	Species	Points	Species	Points	Species	Points
$^{10}_{6}$C	1	$^{19}_{10}$Ne	7	$^{29}_{15}$P	14	$^{38}_{19}$K	21, 22
$^{11}_{6}$C	2	$^{22}_{11}$Na	8, 9	$^{30}_{15}$P	15	$^{41}_{21}$Sc	25
$^{13}_{7}$N	3	$^{23}_{12}$Mg	10	$^{31}_{16}$S	16	$^{43}_{21}$Sc	23
$^{15}_{8}$O	4	$^{25}_{13}$Al	(11)	$^{33}_{17}$Cl	17	$^{44}_{21}$Sc	24
$^{17}_{9}$F	5	$^{26}_{13}$Al	12	$^{34}_{17}$Cl	18, 19		
$^{18}_{9}$F	6	$^{27}_{14}$Si	13	$^{35}_{18}$A	20		

sequence, viz. $^{21}_{11}$Na, $^{25}_{13}$Al and $^{39}_{20}$Ca—only $^{37}_{19}$K is at present unknown—also fall on this line)—and the other three represent the ground-to-ground state transitions of $^{10}_{6}$C, $^{18}_{9}$F and $^{26}_{13}$Al. According to Wigner, only transitions belonging to the classes

$$\binom{2Z-1}{Z} \underset{\beta-}{\overset{\beta+}{\rightleftarrows}} \binom{2Z-1}{Z-1} \quad \text{and} \quad \binom{2Z}{Z+1} \underset{\beta-}{\overset{\beta+}{\rightleftarrows}} \binom{2Z}{Z} \underset{\beta-}{\overset{\beta+}{\rightleftarrows}} \binom{2Z}{Z-1}$$

with Z odd are not necessarily forbidden by any rules. It would appear that for $Z<22$ * all positron-active species falling into the first of these classes undergo super-allowed transitions (from ground to ground state) and that some of the species of the second class behave similarly, though others do not. No super-allowed transitions, however, occur for positron-active species which belong to neither class. Amongst the partially forbidden transitions of species of the second class we might mention the ground-to-ground transitions of $^{22}_{11}$Na, $^{30}_{15}$P, $^{34}_{17}$Cl and $^{38}_{19}$K—though apart from the Wigner rules the case of $^{30}_{15}$P might be regarded as that of an ordinarily allowed transition (see figure 3).

Because practically all species of the type $\binom{2Z-1}{Z-1}$ with $Z<22$ are stable species, examples of super-allowed transitions are much less frequent amongst negative-electron-active bodies than with positron-emitters. In fact $^{3}_{1}$H is the only representative of the first Wigner class, and $^{6}_{2}$He, $^{10}_{4}$Be and $^{14}_{6}$C are the sole representatives of the second class, amongst the radioelements for which figure 2 has been drawn. As with the positron-emitters, $^{3}_{1}$H, as a class I body, undergoes a transition which empirically appears super-allowed †, whilst $^{6}_{2}$He of class II is, but $^{10}_{4}$Be and $^{14}_{6}$C are not, in the super-allowed group according to the diagram. In this connection it may be mentioned that although the very varied behaviour of the different class II species has yet to receive a satisfactory explanation on any theory, the fact that super-allowed transitions occur with some species of this class is unambiguous proof that for these species the Fermi-type interactions are inadmissible (Konopinski 1943, Wigner and Feenberg 1942). A final obvious remark is that the position of the point for $^{12}_{5}$B (figure 2) is entirely anomalous according to the Wigner rules.

Summing up, we may say that the Wigner rules claim evident success in describing the otherwise inexplicably short lifetimes of the $\binom{2Z-1}{Z}$ positron emitters, but to be set against this is the very considerable concentration of points about what appears to be the ordinary allowed line A for negative-electron-active species in figure 2. There would appear to be some consideration which restricts the effect of these rules even in the class of the lightest elements to which they should most clearly apply. In this connection the exact lie of the line A of figure 2 is of some importance. This line has been drawn purely empirically as the best straight line having regard to the experimental points. As transferred to figure 3 (A′) it is seen to represent equally closely the slope of the super-allowed line S. Furthermore it may be shown to be the straight line which best approximates to the theoretical predictions of the Fermi theory. The dotted line F in figure 2 gives the Fermi function $f(0, W_0)$ (Konopinski 1943) fitted to A in the region of $E=1$ MeV. The theoretical line obviously appears as in many ways an even better representation of the experimental results than is our empirical line A;

---

* The choice of this particular range of Z for figures 2 and 3 was made precisely because no species belonging to the first Wigner class are at present known for $Z>21$.

† The β-disintegration of the neutron should also be super-allowed: in this case interpolation from figure 2 would indicate a half-value period of 7±1 minutes.

thus the well-determined point for ^{35}S is no longer significantly out of place, and the super-allowed points for ^{3}H and ^{6}He are more nearly the same distance above the line. Also, the anomaly regarding the point for ^{12}B is clearly reduced.

Having established the significance of the allowed line A in this way by comparison with theory, it is of interest to discuss the exact lie of the empirically-drawn allowed line O of figure 1 in a similar manner. We can do this most easily by reference to line F, figure 2, which provides the normalization for the theoretical results. In the table we give the difference of the ordinates ($\Delta = \log\lambda(\mathrm{O}) - \log\lambda(\mathrm{F})$, for E constant) of corresponding points on the two lines as a function of the disintegration energy E. The theoretical differences, $\Delta'(81)$, $\Delta'(93)$, defined by $\Delta'(Z) = \log[f(Z, W_0)] - \log[f(0, W_0)]$ (see Konopinski 1943) are given for comparison *. In the last line of the table the quantity δ is the second difference $\frac{1}{2}[\Delta'(81) + \Delta'(93)] - \Delta$. The constancy of δ over the range 0·2 MeV. $< E <$ 2·0 MeV. indicates that the straight line O, figure 1, has the full support of theory as representing the variation of λ with E over the range in question. This conclusion may be stated conversely and expanded as follows: the Fermi theory of allowed transitions appears to be entirely adequate so far as predictions of the dependence of disintegration constant on energy and charge number are concerned. The latter point is of interest, and the numerical value of δ over the range of E for which it is constant indicates that allowed transitions of the heaviest elements are less probable than the transitions which we have now with some confidence identified as "ordinarily allowed" for the lightest elements (see lines A and F, figure 2) only by a factor of roughly 3 (for the same energy release). This is of importance in relation to the problem of the extent to which the wave-functions of initial and final nuclear states "overlap" for nuclei of such different degrees of complexity.

Table

E(MeV.)	0·0158	0·0511	0·158	0·307	0·511	1·022	1·533	2·044
$\log E$	$\bar{2}$·20	$\bar{2}$·708	$\bar{1}$·20	$\bar{1}$·487	$\bar{1}$·708	0·009	0·185	0·310
Δ	1·47	1·47	1·32	1·16	1·13	0·97	0·84	0·69
$\Delta'(81)$	2·52	2·23	1·82	1·51	1·45	1·27	1·20	1·10
$\Delta'(93)$	2·91	2·58	2·14	1·81	1·72	1·51	1·42	1·30
δ	1·25	0·94	0·66	0·50	0·46	0·42	0·47	0·51

The increase of δ for $E <$ 0·2 MeV. which is evident from the table implies that the theoretical allowed line for the heaviest elements lies above the empirical straight line O of figure 1 at the low-energy end, the deviation being somewhat similar to the deviation of the theoretical line F from the straight line A of figure 2. This conclusion is not surprising and does not invalidate any of our previous discussions, for the purpose of which the empirical allowed line has been taken as reference line. Only with the heaviest elements it should be pointed out that for the extreme low-energy end of the line ($E <$ 0·02 MeV.) the predictions of the simple theory are obviously inadequate, since they do not take count of the energy derived from the "adiabatic" reorganization of the extranuclear electrons which for these elements is of the order of 0·01 MeV.

---

* In this calculation we have falsified theory only to the extent of using p_0, the maximum momentum, instead of p, an undefined mean momentum which enters as a slowly-varying term in the expression for $f(Z, W_0)$.

There is just one feature of figures 2 and 3 which remains to be considered. We have so far concentrated attention on the identification of a number of transitions which appear to be allowed according to the spin and parity rules and for which there is no empirical evidence of the intervention of the Wigner rules. It will be obvious, however, that there are many points, particularly on figure 2, which do not come within the scope of this identification. Some of these may refer to transitions on which the Wigner rules impose increased forbiddenness—some of them, therefore, may be allowed points so far as spin and parity changes are concerned—others may represent transitions which are " ordinarily " forbidden to first or higher degree. In this connection, since the condition expressed by (1) is no longer fulfilled, we should not expect to find an ordinary first-forbidden line parallel to the allowed line A. Also, since fairly large relative changes in ρ are involved, as between the lightest and the heaviest radioelements in the range $Z<22$, there is further reason why the higher-order Sargent lines should not stand out so obviously in the diagram. The question of order of forbiddenness must therefore be settled on other evidence for a number of transitions before much progress can be made in empirical classification.

Partial evidence of one kind is already provided by the experimental results considered in this paper. Figure 2 includes the representative points for 13 radioelements of which the β-disintegration is known to be complex, and with these species some transitions occur which would appear to be ordinarily allowed. In two cases of two-component spectra ($^{25}_{11}$Na and $^{34}_{15}$P) each of the observed components appears to result from such an allowed transition; in six other cases ($^{16}_{7}$N, $^{20}_{9}$F, $^{27}_{12}$Mg, $^{28}_{13}$Al, $^{38}_{17}$Cl and $^{41}_{18}$A) one or more allowed components are present together with another component or components which are to some degree forbidden. It seems reasonable to assume that in these cases the other β-transitions are ordinarily forbidden, that is, that the Wigner rules are of no more effect for them than they are for the allowed transitions with which they compete. If we make this assumption, we can at once identify the representative points numbered 6, 12, 19, 21, 27, 28 and 30 on figure 2 as ordinarily forbidden. On the further likely assumption that some of these points, at least, represent transitions which on spin and parity rules alone are first-forbidden, we then have a general impression of the lie of the second Sargent curve on our diagram *. With this approximate curve in mind we can recognize a further group of points (e.g. 14, 23, 35, 38, 41) which lie between the ordinarily allowed and first-forbidden lines—and we are led to conclude that these belong to species ($^{24}_{11}$Na, $^{31}_{14}$Si, $^{45}_{20}$Ca, $^{46}_{21}$Sc, $^{48}_{21}$Sc) for the β-transitions of which the Wigner forbiddenness is greater, and more varied, than it is for the other transitions which we have been considering. It is somewhat surprising to find the heavier species predominant in this group, but this is clearly the division to which our tentative considerations lead.

REFERENCES

BOTHE, W., and MAIER-LEIBNITZ, H., 1937, *Z. Phys.*, **104**, 604.

BRADT, H., HEINE, H. G., and SCHERRER, P., 1943, *Helv. Phys. Acta*, **16**, 455.

BRADT, H., and SCHERRER, P., 1945, *Helv. Phys. Acta*, **18**, 405; 1946, *Ibid.*, **19**, 307.

CONSTANTINOV, A. A., and LATYSCHEV, G. D., 1941, *J. Phys. U.S.S.R.*, **5**, 249.

ELLIS, C. D., 1934, *Internat. Conf. Phys., London*, **1**, 43.

---

* It is tempting to see this curve as passing through 5, the point for $^{14}_{6}$C, for the β-disintegration of which a recent determination of nuclear spin (Jenkins 1948) gives $\Delta I=1$.

Feather, N., 1948, *Nature, Lond.*, **161**, 431.
Fowler, R. H., 1930, *Proc. Roy. Soc.* A, **129**, 1.
Gray, L. H., 1937, *Proc. Roy. Soc.* A, **159**, 263.
Greuling, E., 1942, *Phys. Rev.*, **61**, 568.
Jenkins, F. A., 1948, *Phys. Rev.*, **73**, 639.
Konopinski, E. J., 1943, *Rev. Mod. Phys.*, **15**, 209.
Konopinski, E. J., and Uhlenbeck, G. E., 1941, *Phys. Rev.*, **60**, 308.
Latyschev, G. D., 1947, *Rev. Mod. Phys.*, **19**, 132.
Lee, D. D., and Libby, W. F., 1939, *Phys. Rev.*, **55**, 252.
Marshak, R. E., 1942, *Phys. Rev.*, **61**, 431.
Richardson, H. O. W., 1948, *Nature, Lond.*, **161**, 516.
Rutherford, Lord, Lewis, W. B., and Bowden, B. V., 1933, *Proc. Roy. Soc.* A, **142**, 347.
Wheeler, J. A., 1941, *Phys. Rev.*, **59**, 27.
Wigner, E. P., 1939, *Phys. Rev.*, **56**, 519.
Wigner, E. P., and Feenberg, E., 1942, *Rep. Prog. Phys.*, **8**, 274.

Investigations using a Permanent-magnet Double β-Ray Spectrograph with Coincidence Counting—I. Experiments with Thorium Active Deposit

By N. FEATHER, J. KYLES and R. W. PRINGLE
Department of Natural Philosophy, University of Edinburgh

MS. received 27 March 1948

ABSTRACT. A detailed description is given of a semicircular focusing β-particle spectrograph in which a thin source is centrally placed and sheaves of oppositely moving electrons are investigated using two thin-windowed Geiger counters. These counters can be used in a coincidence arrangement, and each is capable of movement so as to accept electrons which have been focused with any radius of curvature between 2·5 cm. and 6 cm.

The arrangement was tested using sources of thorium active deposit. During this work the (coincidence) β-particle spectrum for the ThB.C transition leading to the 238 kev. state of ThC was obtained separately for the first time and its end-point determined as 355 kev. A feeble higher-energy β-component due to ThB was also detected and the end-point estimated at 589 kev.

Redeterminations of the end-points of the β-particle spectra of ThC and ThC″ (by β–γ coincidences) gave values of 2·256 Mev. and 1·805 Mev., respectively. The intensity of the F-line of ThB was found to be 0·288 photoelectrons per disintegration.

§ 1. INTRODUCTION

The coincidence counting method of investigating time-correlations in the emission of particles and quanta by unstable nuclei has already become one of the standard techniques in the study of radioactivity (Dunworth 1940, Feather 1940 a). A development of this technique, first proposed by Feather (1940 b), has now been realized in practice: in the present paper the method will be described in detail and the results which have been obtained in its initial application to the active deposit of thorium will be presented and discussed.

The essential feature of the new method is the study of coincidences between the various components of the particle radiations emitted by a radioactive source, e.g. between the internal conversion electrons (belonging to the β-ray "lines") and the disintegration electrons (of the continuous spectra). For this purpose a special form of semicircular focusing spectrometer is employed, designed so that (for example) a β-line may be focused on one Geiger counter while another counter is used to scan the continuous spectrum. The spectrum of coincidences will then be the continuous spectrum of those disintegration electrons time-correlated with the photoelectrons of the β-ray line, and thus, by inference, with the γ-ray quanta of corresponding energy.

It is well known that magnetic analysis by semicircular focusing is inconsistent with the use of large solid angles for collection—in our particular arrangement (as shown in § 2) these are of the order of 10^{-3}–10^{-2} depending upon position; on the other hand, the sensitivity of any coincidence experiment increases rapidly with the collection angles which can be employed. A natural development will therefore be to use the present method with other types of β-particle spectrograph of greater collecting power (see e.g. Roberts, Elliott and Deutsch 1944). Nothing new in principle would necessarily be involved in such a development.

§ 2. THE SPECTROGRAPH

A detailed description of the spectrograph has already been given (Feather 1940 b). The essential features of construction are illustrated in figure 1. Slits S_1 and S_2 select two sheaves of oppositely moving β-particles coming from the source A situated midway between the slits. The two sheaves of electrons are focused by a magnetic field, perpendicular to the plane of the diagram, in the horizontal planes containing respectively the windows of the counters C_1 and C_2 and the defining slits.

The counters can be moved independently in the planes of focusing thus allowing the radius of curvature of either sheaf of electrons to be varied between 2·5 cm. and 6 cm. Electrical connections to each counter are made by two spring strips attached to the counter carriage. One of the strips bears against the side wall of the box and serves to earth the cathode. The other strip makes a sliding contact with a copper wire insulated from the box and supplies the anode voltage (see also figure 8).

A shutter B can be moved down to cover the slit S_1 and so to cut off the electrons from C_1. Movement of the counters and the shutter is obtained by means of screws which can be rotated from outside the vacuum box by keys turning in ground joints. The inside of the box is covered with aluminium and the slits are bevelled to reduce scattering as much as possible. The box is evacuated to a pressure of 10^{-4} mm. Hg by a three-stage oil diffusion pump and is locked in position in the 5·5 cm. gap between the poles of a large permanent magnet (Cockcroft, Ellis and Kershaw 1932). The use of a permanent magnet allows the magnetic field to be kept constant over the long periods necessary for coincidence counting and the provision of field coils enables the field strength to be set at any value up to 2000 gauss in a few minutes. To avoid opening the box in order to measure the magnetic field a search coil is mounted on the top of the spectrograph box and the change of flux produced when the coil is rotated through 180° in the stray field of the magnet is measured with a fluxmeter. For standardization this change of flux can be compared with that measured with a search coil of known area-turns inside the box. An accuracy of better than 1 % can be obtained in this way. A still more accurate value for the effective field strength can be obtained by finding the position of one or other of the prominent β-ray lines in the spectrum of the thorium active deposit. The $H\rho$ values of these lines have been measured with great care (Ellis 1932, Arnoult 1939, Siegbahn 1944) and since the position of the counters can be determined to 0·01 cm., the effective field strength can be obtained to an accuracy of 0·25% by dividing the accepted value of $H\rho$ by the observed value of ρ. Since several lines can usually be obtained for one field setting, a check on the accuracy of the measurements is generally possible.

The profile of a β-ray line as observed with a constant field setting (figure 2) extends over an appreciable range of ρ. It is necessary to determine which point on the counting-rate–position curve is to be taken as fixing the position of the line, and what correction is necessary in order to obtain the true value of ρ from the value corresponding to the position so fixed. If in figure 3 (which is drawn in perspective) we consider the source Q as emitting electrons of one momentum only, P, then the trajectories in a plane perpendicular to the magnetic field will be circles of radius $\rho_0 = P/He$. An electron from the centre of the source passing through O, the centre of the slit, will arrive at R on the centre line of the plane of focusing at a distance a_0 from O, where $4\rho_0^2 = a_0^2 + b^2$. Taking axes X, Y at R as shown, we may calculate the intensity at a point (x, y) by a method similar to that employed by Li (1937), for a source of dimensions given below.

The variation of intensity with y for fixed values of x is shown for a typical case in figure 4. If we integrate one of these curves with respect to y between the limits $+l$ and $-l$, we obtain the intensity over a narrow strip of width dx and length $2l$ for a fixed value of x, $2l$ being the length of the counter window. This is in effect the solid angle, expressed as a fraction of 4π, subtended by the narrow strip $2l dx$ at the source, for electrons of momentum P. The variation of this solid angle with x is shown in figure 5. If the width of the counter window is w, we can then obtain the solid angle subtended by the entire window at the source (the transmission factor $T(x)$), when the centre of the window is at x, by integrating the curve in figure 5 between the limits $x + w/2$ and $x - w/2$. Figure 6 shows the variation of $T(x)$ with x, or, in other words, the variation of the counting rate for electrons of momentum P as the counter slit is moved in the plane of focusing in a constant magnetic field, i.e. the line-shape of a β-ray line of momentum $P = He\rho_0$. Having regard to figure 6 we have chosen as the point fixing the position a of a line, the point A at half the maximum height on the steep right-hand edge of the counting-rate–position curve, since this point can be located with greater accuracy than the position of the peak. The calculated line-shape then enables us to determine the small correction term (less than 0·25%) which must be subtracted from a in order to obtain a_0 from which the value of ρ_0 is calculated.

The resolving power of the spectrograph, defined as $H\rho/\delta(H\rho)$, where $\delta(H\rho)$ is the change in the $H\rho$ value corresponding to the width of a β-ray line at half the maximum height, is obviously $\rho/\delta\rho$ in the case of a constant-field spectrograph. This ratio can be determined from the calculated line-shape. It is found to change with the radius of curvature, from about 33 for the smallest value of ρ to about 60 for the largest ρ employed. For the setting of the F-line in figure 2 the calculated value of 53·8 may be compared with the experimentally determined value of 56·5, in good agreement with the former.

To map out a continuous spectrum the counting rate in counter (1) is determined for a series of positions of the counter, first with the shutter B open, then with it closed. Differences give the counting rates due to β-rays alone. These differences are corrected for counting-rate losses (usually negligible for the continuous spectrum), and for decay of the source. In order to give a true picture of the continuous (momentum) spectrum, the corrected β-particle rate must

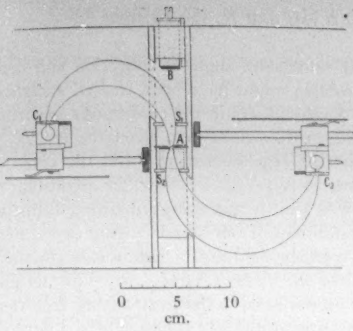

Figure 1. The spectrograph.

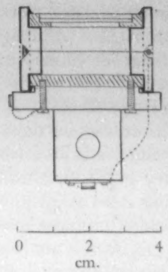

Figure 8.
Section through counter.

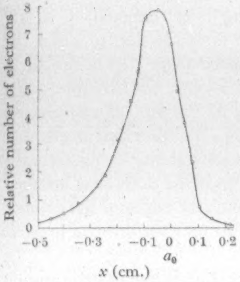

Figure 2.
Observed shape of ThB F line.
$H=237$ gauss. $a_0=11\cdot4$ cm.

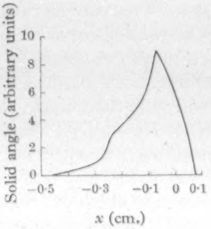

Figure 5.
$b=2$ cm. $s=0\cdot4$ cm.
$2l=1\cdot9$ cm. $a_0=11\cdot4$ cm.

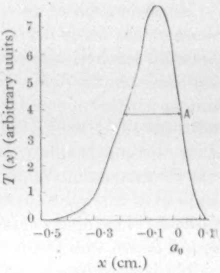

Figure 6.
Variation of $T(x)$ with (x).
$a_0=11\cdot4$ cm. $b=2$ cm.
$\rho_0=5\cdot80$ cm. $s=0\cdot4$ cm.
$w=0\cdot10$ cm. $2l=1\cdot9$ cm.

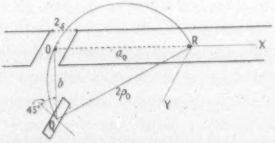

Figure 3.

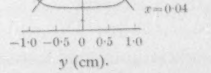

Figure 4.
Source 19 × 2 mm²
inclined at 45°.

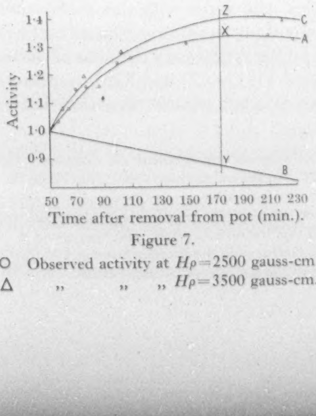

Figure 7.

○ Observed activity at $H\rho=2500$ gauss-cm.
△ ,, ,, ,, $H\rho=3500$ gauss-cm.

further be adjusted to refer to the same solid angle of collection and the same interval of $H\rho$. Although this problem might have been treated analytically it was in fact solved empirically.* A value of $H\rho$ in the continuous spectrum was chosen and observations were made with various field strengths H_1, H_2.... at radii of curvature ρ_1, ρ_2.... such that $H_r\rho_r$=constant. Let the corrected β-particle rates under these conditions be N_1, N_2.... Now, for a constant radius of curvature and a variable field, it is known that the normalizing factor is $1/H$ (Gurney 1925), thus under the conditions of our standardizing experiment the counting rates at ρ_1, ρ_2.... for a constant field and a continuous (momentum) spectrum of uniform height would be as $N_1/H_1 : N_2/H_2$.... This means that H_1/N_1, H_2/N_2.... are respectively proportional to the normalizing factors corresponding to ρ_1, ρ_2.... Plotting these quantities as a function of ρ, a normalizing curve is obtained for the particular counter used. This curve could be checked by the method described in §6.

Normalization of the continuous spectrum having been effected, it is still necessary for many purposes to know the solid angle for collection to which the spectrum has been normalized. This may be calculated from curves similar to that shown in figure 5. For a radius of curvature of 5·8 cm., for example, and a counter window of area $1{\cdot}9 \times 0{\cdot}10\,\mathrm{cm}^2$, we obtain $3{\cdot}4 \times 10^{-3}$ of 4π. To be precise, this fraction represents, in the conditions specified, the probability that an electron of the continuous spectrum will enter the counter, the probability being averaged over the momentum range $H\rho$ to $H\rho + \Delta(H\rho)$, where $\Delta\rho$ is the difference between the radii of curvature corresponding to entry by the extreme edges of the counter window. During the experiments described below entrance windows of breadth from 0·10 cm. to 0·15 cm. were used at various times.

The last problem in dealing with the continuous spectrum is that of determining the "representative" ρ value for any setting of the counter. This was solved by a method similar to that used by Lawson and Tyler (1940) for the same purpose.

§ 3. THE SOURCE

Sources of thorium active deposit were obtained by the exposure of aluminium foils of 0·28 mg/cm² thickness to the thoron given off by a "dry" emanating preparation of radiothorium, of strength approximately 40 millicuries. For activation a foil is bent over a suitably formed brass block in an arrangement which allows an area of $19 \times 2\,\mathrm{mm}^2$ of foil only to be exposed. Both short- and long-exposure sources were prepared in this way. With long-exposure sources, transient equilibrium having already been attained, the ratio of the absolute activities of ThC and ThB remains constant at $\lambda_C/(\lambda_C - \lambda_B)$ during the subsequent decay; with short-exposure sources this ratio varies with time. The numerical value of the constant ratio is 1·11. Important for our experiment is the fact that with a source in transient equilibrium 1·11 is very closely the ratio of the numbers of electrons in the continuous spectra of Th(C + C″) and ThB, respectively, the disintegration constant of ThC″ being so much greater than the disintegration constants (λ_B, λ_C) of ThB and ThC.

---

* Attempts to calculate the normalizing factor in our arrangement are necessarily difficult on account of the form of the counter window (§ 4). In general the electrons do not strike the plane of focusing normally, but arrive at angles to the normal spread over a wider range, and more inclined, the smaller the value of ρ. Thus a fraction of the electrons entering the counter slit (which has finite depth) strikes the far wall of the slit and this fraction increases with decreasing ρ. Some of these electrons, after scattering, may produce a discharge in the counter but many of them will not. Obviously the effect is not susceptible of exact evaluation except by experiment.

With short-exposure sources information concerning the relative contributions of the β-particles of ThB and Th(C + C″) to any given interval of the experimental continuous spectrum can be obtained by the observation of the growth (or decay) of the β-particle counting rate when a source is used which has just been removed from the exposure pot and the Geiger counter is adjusted to accept the appropriate momentum range in the spectrograph. If we consider a source which has been exposed for one hour only, then, whilst the activity due to ThB should decay as shown by curve B, figure 7, the activity due to Th(C + C″) should follow curve C (calculated using standard equations). If an observed activity curve, such as A, lies between the curves C and B then the fraction of the activity due to ThB is given by the ratio XZ/YZ. Clearly, for a particular setting of the counter, this ratio should be constant within the limits of experimental error for any vertical secant to the curves. In order to achieve this result in practice it has been found necessary to wait for about half an hour after the end of an exposure before starting activity measurements of this type. It would appear that during activation atoms of ThC″, given off by recoil from the active deposit which invariably accumulates on the walls of the pot, are collected together with ThB on the foil. If this additional ThC″ activity is not allowed to die out before measurements are begun, the ratio XZ/YZ will be found to vary along the curves.

In general, in order to prevent the escape of recoil atoms from a source in the spectrograph, the activated foil is covered with a similar aluminium foil (0·28 mg/cm^2 thickness) before being clamped in the source holder. In position, the active deposit, sandwiched between the two thicknesses of foil, is inclined at an angle of 45° to the plane containing the central axes of the two defining slits and is symmetrically placed with respect to this plane. In this connection, the shape of the F-line of ThB was determined first with a bare source and then with a "sandwich" source, but no detectable difference was observed either in the height or shape of the line. It therefore appears that the effect of absorption and straggling produced by the 0·28 mg/cm^2 covering of the source is negligible—at least for β-particles of energy as great as 147 kev.

§ 4. COUNTERS

The Geiger counters are necessarily of small dimensions since they have to be capable of movement in the restricted space between the magnet pole pieces. While this means that the advantages of a relatively low background counting rate (5–10 min^{-1}) and a short recovery time (30 μsec.) are enjoyed (Muehlhause and Friedman 1946), at the same time it implies that at high counting rates the life of a counter is short (counting rates as high as 60 000 min^{-1} had to be sustained for several hours when a counter was registering a strong photoelectron line, or was placed close to the source to count α-particles).

In figures 1 and 8 are shown the details of counter construction. The cathode is made of brass suitably finished to provide a slit 1·0–1·5 mm. broad for the entrance of the β-particles. End pieces are of perspex and are threaded with a central wire of platinum of 0·1 mm. diameter as anode. The thin mica film ($\sim$1 mg/cm^2) which is used to cover the slit is mounted on a concave surface in order to withstand better the atmospheric pressure to which it is subject during the filling process. A small amount of lead screening, 1 cm. thick, is mounted together with the counter on a carriage of ebonite.

A mixture of 10% ethyl alcohol and 90% argon at a pressure of 10 cm. Hg was used to fill the counter after the cathode surface had been washed in alcohol and polished with silk. The filling line was simply constructed, use being made of rubber connections and vacuum stop-cocks, but the counters were evacuated to 10^{-4} mm. Hg with a diffusion pump. Otherwise the technique employed was similar to that described recently by Regener (1947). Satisfactory "plateaux", 200–300 v. long, were obtained with threshold potentials ranging from 900–1100 v. and positive plateau slopes of about 0·10–0·15% per volt, though this latter quantity was found to increase somewhat when the counting rate was high. Another troublesome effect observed during periods of rapid counting was a gradual increase of threshold voltage (up to 20 or 30 v.) which occasionally made it necessary to use a radium standard to check the counter sensitivity throughout the course of an experiment.

The importance of obtaining an accurate correction for absorption and scattering in the mica window cannot be over-estimated since it becomes very large for energies below 70 kev. ($H\rho \sim 900$ gauss-cm.). Additional thin sheets of mica covering the counter slit were therefore used to plot absorption curves for electrons of a number of energies in the thorium spectrum and, in this way, by extrapolation of the results to zero thickness, the correction curve given in figure 9 was obtained. This curve shows reasonable agreement with that of Martin and Townsend (1939), though it should be emphasized that the magnitude of the correction factor for electrons of any energy depends on the precise arrangement of the counter slit and of the mica covering the slit.

§ 5. ELECTRICAL CIRCUITS

In any coincidence experiment it is necessary that provision should be made both for determining the individual rates of entry of particles into the two counters and for counting the coincident pulses which may occur as a consequence of the association in time of these particles.

Figure 10 illustrates the basic circuit used for single channel counting. All H.T. voltage supplies are stabilized. It will be noted that a load resistance of 1 MΩ is used in the counter circuit, but even so, with the small output pulse obtained with a counter of small volume, it is necessary to use a conventional cathode-follower unit mounted close to the counter. The cathode-follower operates through a screened cable into an amplifier designed for the equalization of the pulses (the higher the counting rate the larger the proportion of pulses which are smaller than normal). The particular equalizing circuit used is a modification of the cathode-coupled multivibrator (West 1944). This has proved to be exceedingly stable and reliable in operation.

The 50 kΩ rheostat in the screen grid lead of valve V_2 is used to obtain suitable conditions for operation from triggering pulses, and can in fact be varied over a large range. The output pulses, of 5 μsec. duration, from the screen grid of V_3 are used to operate a scaling circuit having a factor either of 100 or, for individual rates greater than 50 000 min^{-1}, of 3200. The Dynatron Model X200 "Scaler", with its decimal counting system, has proved in every way satisfactory and extremely convenient in use. The input resolving-time of this scaler is 5 μsec., thus it is evident that the 30 μsec. recovery time of the Geiger counter alone determines the resolving-time of the counting system as a whole.

It was found that, even at the highest counting rates used (100 000 min^{-1}), both the size and shape of the output pulses from the amplifier remained constant. Thus it can be taken as established that the resolving-time for coincidence counting was independent of the single counting rates throughout the entire investigation.

The output to the coincidence mixing set is taken from the anode of V_3 in each amplifier. A conventional Rossi coincidence circuit is used, with a fixed grid bias on the output valve but with a choice of grid leaks (2000 Ω and 20 000 Ω) for the Rossi valve. In this way two values of the resolving-time, $2{\cdot}5 \times 10^{-7}$ sec. and $1{\cdot}8 \times 10^{-6}$ sec., are available. The requirement of the highest possible resolving power (smallest τ) has already been stressed (Dunworth 1940). However, attempts to reduce τ much below 2×10^{-7} sec. do not succeed, because of the statistical time-lag between the entry of the ionizing particle and the appearance of the voltage pulse across the counter (Dunworth 1940, Bradt and Scherrer 1943 a); instead genuine coincidences are lost. The larger of the two resolving-times available is used for purposes of checking that there is no loss at the smaller τ and also when delayed coincidences are in question—as when the β-particle of ThC is followed by the α-particle of ThC′ after a mean time interval of $(3{\cdot}7 \pm 0{\cdot}6) \times 10^{-7}$ sec. —the average life of ThC′ (Bradt and Scherrer 1943 b).

A separate recorder was not provided for determining the coincidence rate, although this was only of the order of a few counts per minute; instead, registration on the same scaler as was used for the single counting rates was arranged without inconvenience.

§ 6. EXPERIMENTS WITH THE ACTIVE DEPOSIT OF THORIUM

Thorium active deposit sources were chosen for the initial tests of the new method, and of our spectrograph generally, for two reasons: first because there is present in the complete β-particle spectrum an intense photoelectron line (F-line) eminently suitable for coincidence studies, and secondly because so much information is already available * regarding the radiations in general. In the course of our tests we have, however, been able to add to this information in certain particulars, details of which will be apparent from the descriptions which follow.

(i) *Investigations using a single counter*

A study was first made of the complete continuous β-ray spectrum of the thorium deposit in transient equilibrium. Because this spectrum extends as far as $H\rho = 9000$ gauss-cm., it was necessary to make measurements at four different values of the magnetic field (250, 500, 1000 and 2000 gauss). From these the distribution curve shown in figure 11 was obtained after the appropriate normalizations (see § 2), corrections for decay and absorption corrections (see § 4) had been made. The fact that a smooth curve resulted from such a series of overlapping junctions provides a good test of the accuracy of the method of normalization.

A further test is provided by a comparison of the areas of the ThB and Th(C + C″) spectra deduced from the curve (the justification for using the dotted projection of the (C + C″) curve to separate the two spectra is given below). These areas, which should be proportional to the numbers of ThB and Th(C + C″) atoms disintegrating per second, were found to be in the ratio 1 : 1·12 in good agreement with the ratio 1 : 1·11 quoted in § 3.

The continuous β-spectrum of the ThB having been obtained, the absolute intensity of the strong F-line of ThB may be calculated. The area under the F-line profile (§ 2, figure 2) represents the number of photoelectrons emitted per second through a known solid angle, hence, adjusting the solid angle for collection to be equal to that assumed in normalizing the continuous spectrum, we have

---

* Gurney 1926, Ellis 1932, Sargent 1932, Sze Shin Yuan 1933, Henderson 1934, Wang 1934 Surugue 1937, Arnoult 1939, Flammersfeld 1939, Siegbahn 1944, Siegbahn and Johansson 1946.

$$\text{number of F-electrons per disintegration} = \frac{\text{area under F-line profile}}{\text{area of } \beta\text{-spectrum}} = 0{\cdot}288.$$

This result agrees more closely with that of Flammersfeld (0·284) * than with the results of Arnoult (0·222) or Gurney (0·250).

For the end-point of the ThC spectrum a Fermi plot of the single counting rates for $H\rho > 7500$ is given in figure 12, where $(N/F)^{\frac{1}{2}}$ is plotted with F calculated for $Z = 83$. From the point of intersection with the energy axis we obtain $E_{\max} = 2{\cdot}256$ MeV. ($H\rho = 9070$ gauss-cm.), in good agreement with the result of Henderson (1934), $H\rho = 9040$.

The end-point of the ThB spectrum cannot similarly be determined by simple extrapolation. It will be shown in (ii) below how the main component of this spectrum (associated with the γ_F transition) can be separated out. However, it appeared from figure 11 that a component of higher energy might also be present, and experiments with a single counter were made to test this assumption. A series of measurements was performed of the growth and decay of the β-activity at different points of the spectrum, using sources exposed for one hour only. We have already discussed (§ 3) the way in which the activity of such a "non-equilibrium" source should vary after a "short" exposure (see figure 7).

With the counter at a setting corresponding to $H\rho = 3500$ gauss-cm., experimental points were obtained showing the presence of a pure Th(C + C″) activity (figure 7, C). At $H\rho = 2500$ gauss-cm., on the other hand, the growth of activity was less marked (figure 7, A), indicating the presence after 50 minutes of an effect due to ThB amounting to $12 \pm 3\%$ of the total. It can be shown that this effect would correspond to $7 \pm 2\%$ of ThB activity once transient equilibrium had been reached (after 50 minutes the ThC in the source is still growing, while the ThB is of course decaying in amount). Thus in figure 11 we can identify the point X with certainty as belonging to the (C + C″) spectrum. To complete the low energy end of this spectrum ($H\rho < 3000$ gauss-cm.) the distribution given by Flammersfeld (1939) has been used.

We have just seen that the ThB spectrum must have a component extending beyond $H\rho = 2300$ gauss-cm., the currently accepted end-point. It is not difficult to imagine that this weak high energy component, with apparent end-point about 589 kev., corresponds to a ground state–ground state transition between ThB and ThC. The maximum energy of the partial component associated with the γ_F transition is shown in (ii) to be 355 kev., and the energy of the F γ-ray (emission of which is believed to lead to complete de-excitation of the nucleus) is 238·2 kev. The numerical check ($355 + 238 \sim 589$) is fairly convincing.†

---

* Flammersfeld's value 0·284 was deduced on the assumption that the areas of the continuous spectra of ThB and Th(C + C″) should be equal. He apparently did not regard the difference of 3·5% in area which he found as significant. If his source was in transient equilibrium there should have been a difference in area of 11% as stated above, and in that caes values of 0·289 and 0·310 would have been obtained if he had referred his F-line intensity to the observed areas which he assigned to ThB and Th(C + C″) respectively.

† We have to thank Dr. H. O. W. Richardson of this department for drawing our attention to his work on the ThB spectrum. His results, as yet unpublished, and those of Flammersfeld (1939) both clearly show the existence of the high-energy component, though it is remarkable that Flammersfeld does not comment upon this feature of his curve.

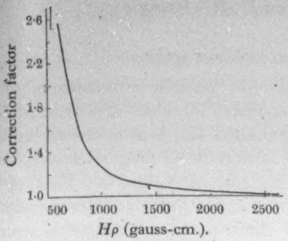

Figure 9. Correction curve for mica window absorption (1·3 mg/cm²).

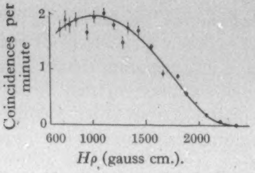

Figure 13. Spectrum of coincidences of disintegration electrons with electrons of the F-line. The vertical lines represent probable errors.

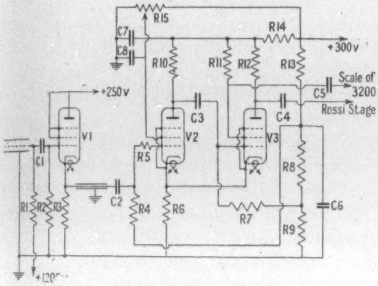

Figure 10. Single channel circuit.

COMPONENTS

Resistances

R1 $1\times10^6\Omega$	R6 $7\cdot5\times10^3\Omega$	R11 $10\times10^3\Omega$
R2 $0\cdot25\times10^6$	R7 100×10^3	R12 2×10^3
R3 10×10^3	R8 320×10^3	R13 220×10^3
R4 50×10^3	R9 100×10^3	R14 5×10^3
R5 100	R10 10×10^3	R15 50×10^3

Condensors		Valves
C1 100 μμF	C5 1000 μμF	V1 }
C2 150 μμF	C6 8 μF	V2 } EF 50
C3 25 μμF	C7 8 μF	V3 }
C4 50 μμF	C8 8 μF	

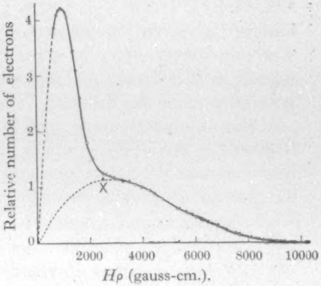

Figure 11. The momentum distribution of the disintegration electrons of the active deposit of thorium in transient equilibrium. Ordinates normalized to equal momentum intervals and corrected for counter window absorption.

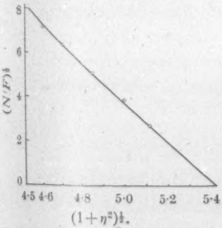

Figure 12. Fermi plot giving ThC end point.

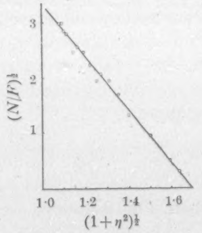

Figure 14. Fermi plot of points given in figure 13. F calculated for $Z=82$.

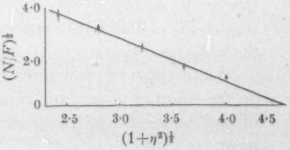

Figure 15. Fermi plot of β-γ coincidences (ThC″ spectrum). Probable errors are shown.

(ii) *Investigations using the coincidence technique*

β-photoelectron coincidences. The number of genuine coincidences to be expected between photoelectrons entering counter (1), when it is centred on a β-line, and disintegration electrons entering counter (2), as it is moved through the continuous spectrum, may be calculated as to order of magnitude as follows.

Let photoelectrons enter counter (1) at the rate of $N_p\,\text{min}^{-1}$. Then of the corresponding disintegration electrons a fraction $\omega_2 F(P)\Delta P$ will enter counter (2) where $4\pi\omega_2$ is the solid angle subtended by the counter window at the source, $F(P)$ is the momentum distribution function describing the partial spectrum for the disintegration mode with which the β-line is associated, and ΔP is the range in momentum, about the mean momentum P, of the particles which enter the counter. The value of ω_2, as we have seen in § 2, may be assumed to be of the order of 4×10^{-3}, and since $F(P)$ must be normalized so that $\int_0^{P_m} F(P)\,dP = 1$, P_m being the upper limit of the (partial) momentum spectrum, $F(P)\Delta P$ may be of the order of 1/50. The coincidence rate to be expected is then $N_G = N_p\omega_2 F(P)\Delta P \sim 4\,\text{min}^{-1}$, if we take N_p as $50\,000\,\text{min}^{-1}$. This value of N_p could conveniently be attained in our arrangement for the F-line of ThB.

When counter (1) was fixed on this line, coincidences were observed with counter (2) at various positions in the continuous spectrum. A coincidence resolving-time of $2{\cdot}5\times10^{-7}$ sec. was used, and a typical set of results obtained near the momentum peak of the main ThB spectrum reads:

N_2 (continuous spectrum $+\gamma$ background) $= 7000\,\text{min}^{-1}$
N_1 (F-line + continuous spectrum $+\gamma$ background) $= 40000\,\text{min}^{-1}$
N_{12} (coincidences observed) $= 5{\cdot}1\,\text{min}^{-1}$
N_A (accidental coincidences $= 2N_1N_2\tau$) $= 2{\cdot}3\,\text{min}^{-1}$
N_G (genuine coincidences) $= 2{\cdot}8\,\text{min}^{-1}$

It may be noted that with a counting period of one hour the accuracy of determination of N_G is only about 8 % in this case.

An extended series of observations was carried out with the object of deducing the complete momentum spectrum of coincidences. The usual corrections were made—for decay, for absorption in the counter window, and for the variation of the effective solid angle of collection with the position of the counter (see § 2)—as also corrections for (γ–γ) and (β–γ) coincidences (< 5 % of the total even in the most unfavourable case). There was no necessity to correct for cosmic-ray coincidences, which were negligible throughout. After all corrections had been made, the final spectrum of coincidences was as shown in figure 13. Two field strengths ($H = 280$ and 440 gauss) were used to obtain this spectrum.

No genuine coincidences with the F-line were detected beyond $H\rho = 2350$ gauss-cm., and the observed points were found to fit a Fermi plot ($Z = 82$) very well (figure 14). The Fermi end-point appears at $(1+\eta^2)^{\frac{1}{2}} = 1{\cdot}695$ or $E_{\text{max}} = 355$ kev., the value used above.

An increase of resolving-time to $1{\cdot}8\times10^{-6}$ sec. was found to be without effect on the number of genuine concidences observed, thus we may conclude that the lifetime of the 238 kev. excited state of ThC cannot be greater than 10^{-7} sec. at the most.

While these results are to be regarded as satisfactory, the method obviously allows of much improvement in the direction of shortening the periods of counting which are required under conditions of great stability of operation of counters and circuits. A limiting factor at present is undoubtedly in the Geiger counter itself, the essential characteristics of which determine the smallest resolving-time which can profitably be employed. If the electron multiplier could be used in place of the counter, the scope of the method would clearly be greatly extended; this change would probably enable τ to be reduced by a factor of 10^2 and the loss of accuracy involved in the background of accidental coincidences to be largely avoided.

β–γ coincidences. In an experiment similar to that of Bothe and Maier-Leibnitz (1937) one of the counters, shielded so as to record only γ-rays, was placed as near as possible to the source (dotted position in figure 1) and another counter used to traverse the continuous spectrum as before. Coincidences were observed for electron energies above 650 kev. ($H\rho > 3500$ gauss-cm.).

Since the disintegration electrons of ThC are followed by only a small amount of medium-energy γ-radiation, the spectrum of coincidences which is obtained in this arrangement will follow very closely the β-spectrum of ThC″ (which emits a 2·62 MeV. γ-ray in every disintegration). The Fermi plot (figure 15) of the experimentally determined coincidence spectrum is a straight line cutting the axis at $E_{\max} = 1{\cdot}805 \pm 0{\cdot}02$ MeV.* Henderson (1934) obtained the value 1·795 MeV. using a pure ThC″ source by a single counting method in a magnetic spectrograph; the only other published determination with such a source is that of Chalmers (1929) who obtained 1·75 MeV. by an absorption method.† The coincidence resolving-time used in our experiments was $2{\cdot}5 \times 10^{-7}$ sec.

α–β coincidences. The α-particles from ThC′ (8·6 cm. range) follow the disintegration electrons from ThC at a mean interval of $(3{\cdot}7 \pm 0{\cdot}6) \times 10^{-7}$ sec. (see above). Thus if an α-particle counter is set up near the source, with an 8 mg/cm^2 sheet of mica (to cut out the unwanted α-particles from ThC of 4·7 cm. range) replacing the lead screen used in the last arrangement, it will register coincidences with the disintegration electrons of ThC if the longer resolving-time ($1{\cdot}8 \times 10^{-6}$ sec.) is used. In this way the total β-spectrum of ThC may be mapped out once the contribution of the β–β ‡ and γ–β coincidences has been assessed ($<10\%$ of the total). Because of the increased resolving time the results obtained with the present arrangement were not good enough to reproduce accurately the shape of this spectrum, but they established the fact that genuine α–β coincidences could be recorded up to the known end-point (9070 gauss-cm.).

Photoelectron–photoelectron coincidences. The β-spectrum of the thorium deposit contains no suitable pair of lines for the study of a cascade process, but the work is being continued with the active deposit of radium in the β-spectrum of which there are a number of β-lines (e.g. A, B, F, G and H) all of sufficient intensity to allow of such an investigation. This work will be reported on in a later communication.

ACKNOWLEDGMENTS

The permanent magnet and associated equipment used in this research was originally purchased by means of grants from the Caird Fund and the Government

---

* Quite recently Siegbahn and Johansson (1946) have reported measurements by the method described in this section and have given a value of 1·72 MeV. for the ThC″ end-point.

† The quoted value has been deduced from Chalmers' measured range using the currently accepted range–energy relation.

‡ The use of a slit system to separate α- and β-particles magnetically proved to be a disadvantage because of the deterioration in the solid angle for collection.

Grants Committee of the Royal Society, and was used in the Cavendish Laboratory, first by Professor C. D. Ellis, F.R.S., and his associates, and later in work directed by one of us (N.F.). We have to thank the Royal Society and Sir Charles Ellis, as also the Director of the Cavendish Laboratory, for their agreement that the equipment should be moved to Edinburgh and used in this investigation. One of us (R.W.P.) has been in receipt of a Senior Research Award from the Department of Scientific and Industrial Research during the later stages of this research and wishes to express his appreciation of the opportunities so afforded.

REFERENCES

ARNOULT, R., 1939, *Ann. Phys., Paris*, **12,** 241.
BOTHE, W., and MAIER-LEIBNITZ, H., 1937, *Z. Phys.*, **104,** 604.
BRADT, H., and SCHERRER, P., 1943 a, *Helv. Phys. Acta*, **16,** 251 ; 1943 b, *Ibid.*, **16,** 259.
CHALMERS, J. A., 1929, *Proc. Camb. Phil. Soc.*, **25,** 331.
COCKCROFT, J. D., ELLIS, C. D., and KERSHAW, H., 1932, *Proc. Roy. Soc.* A, **135,** 628.
DUNWORTH, J. V., 1940, *Rev. Sci. Instrum.*, **11,** 167 (containing a list of the earlier papers).
ELLIS, C. D., 1932, *Proc. Roy. Soc.* A, **138,** 318.
FEATHER, N., 1940 a, *Rep. Prog. Phys.*, **7,** 66 ; 1940 b, *Proc. Camb. Phil. Soc.*, **36,** 224.
FLAMMERSFELD, A., 1939, *Z. Phys.*, **114,** 227.
GURNEY, R. W., 1925, *Proc. Roy. Soc.* A, **109,** 540 ; 1926, *Ibid.*, **112,** 380.
HENDERSON, W. J., 1934, *Proc. Roy. Soc.* A, **147,** 572.
LAWSON, J. L., and TYLER, A. W., 1940, *Rev. Sci. Instrum.*, **11,** 6.
LI, K. T., 1937, *Proc. Camb. Phil. Soc.*, **33,** 164.
MARTIN, L. H., and TOWNSEND, A. A., 1939, *Proc. Roy. Soc.* A, **170,** 190.
MUEHLHAUSE, C. O., and FRIEDMAN, H., 1946, *Rev. Sci. Instrum.*, **17,** 506.
REGENER, V. H., 1947, *Rev. Sci. Instrum.*, **18,** 267.
ROBERTS, A., ELLIOTT, L. G., and DEUTSCH, M., 1944, *Rev. Sci. Instrum.*, **15,** 178.
SARGENT, B. W., 1932, *Proc. Roy. Soc.* A, **139,** 659.
SIEGBAHN, K., 1944, *Ark. Math. Astr. Fys.*, **30 A,** 20.
SIEGBAHN, K., and JOHANSSON, A., 1946, *Ark. Mat. Astr. Fys.*, **34 A,** 10.
SURUGUE, J., 1937, *Ann. Phys., Paris*, **8,** 484.
SZE SHIN YUAN, 1933, *Ann. Phys., Paris*, **19,** 59.
WANG, K. C., 1934, *Z. Phys.*, **87,** 633.
WEST, S. S., 1944, *Electronic Engng.*, **17,** 118.

Note on the Impedance Variations of an Electro-Acoustic Transducer in a Reflecting Field

BY S. BYARD
Royal Naval Scientific Service, Department of Physical Research, Admiralty

Communicated by A. B. Wood ; MS. received 2 *March* 1948

WHEN a reflecting surface is introduced into the field of an electro-acoustic transducer so that a certain proportion of the radiated energy is returned to the source, the measured electrical impedance of the transducer will vary according to the relative phasing of the returned energy. Consequently if the reflecting surface be moved towards or away from the transducer, or alternatively, if the frequency of the electrical input be varied, periodic fluctuations may be observed in the input voltage or current. The Pierce interferometer uses this effect in determining acoustic wavelength in a liquid or gas. The purpose of this note is to relate the impedance changes responsible for the voltage and current fluctuations to the efficiency of the electro-acoustic device by making use of the reciprocity principle. It is also indicated how, in theory at least, the absolute calibration of a projector or a receiver may be obtained by impedance measurements on a single instrument, and how this is related to Carstensen's more practical "self-reciprocity" method of determining transducer constants.

Let E_0 be the open-circuit voltage response of an electro-acoustic transducer when placed in a sound field of pressure $Pe^{-i\omega t}$. If M is the receiver sensitivity expressed in open-circuit volts/dyne/cm², then

$$E_0 = MP. \qquad \ldots\ldots(1)$$

Let Z_0 be the nominal electrical impedance of the transducer. Suppose now that a voltage E, of the same frequency as E_0, be applied to the transducer terminals; the equivalent circuit is shown in figure 1, and the resulting current I is given by the expression

$$E = IZ_0 + E_0. \qquad \ldots\ldots(2)$$

The measured impedance Z under these conditions would be

$$Z = E/I = Z_0 + E_0/I, \qquad \ldots\ldots(3)$$

or from (1), expressing E_0 in terms of P,

$$Z = Z_0 + MP/I. \qquad \ldots\ldots(4)$$

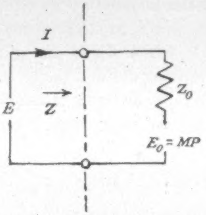

Figure 1.

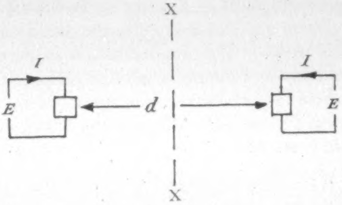

Figure 2.

The field P may be assumed to be produced by an identical transducer excited by a current I at the same frequency, and situated at a distance d from the first transducer as in figure 2. If S_d is the pressure produced at this distance d per ampere excitation, then

$$P = S_d I, \qquad \ldots\ldots(5)$$

and substituting this value for P in (4),

$$Z = Z_0 + MS_d. \qquad \ldots\ldots(6)$$

The factor MS_d in (6) above is the change in impedance due to the sound field of the second transducer and is added vectorially to Z_0 in order to obtain Z. Z will have a maximum whenever MS_d is in phase with Z_0, and a minimum when MS_d is 180° out of phase, and the impedance will show periodic fluctuations of diminishing amplitude as the transducers are moved away from one another.

Let two impedance measurements Z_1 and Z_2 be made at an adjacent maximum and minimum when the transducers are at distances d_1 and d_2 apart respectively ($d_2 = d_1 + \lambda/2$, where λ is the wavelength). Then if S_1 and S_2 be the appropriate transmitting constants obtaining at the two positions,

$$|Z_1| = |Z_0| + |MS_1|; \qquad |Z_2| = |Z_0| - |MS_2|, \qquad \ldots\ldots(7)$$

and the difference between these two moduli is

$$|\Delta Z| = |Z_1| - |Z_2| = |M(S_1 + S_2)|. \qquad \ldots\ldots(8)$$

The reciprocity parameter J which relates the transmitting and receiving responses of a transducer is given (Schottky 1926, Maclean 1940) by

$$J = |M/S_d| = (2\lambda d/R) \times 10^{-7}, \qquad \ldots\ldots(9)$$

where λ is the wavelength of the sound and R the characteristic acoustic impedance of the medium in c.g.s. units. If this is assumed to be valid for the system, it follows that

$$|\Delta Z| = \left|\frac{M^2R}{2\lambda}\left(\frac{1}{d_1} + \frac{1}{d_2}\right)\right| \times 10^7. \qquad \ldots\ldots(10)$$

Now suppose the second transducer replaced by a perfect reflector, XX in figure 2, which can be moved to satisfy the required impedance conditions. If d' and d'' are the two distances of the reflector from the source, satisfying the two impedance conditions, then equation (10) becomes

$$|\Delta Z| = \left|\frac{M^2R}{2\lambda}\left(\frac{1}{2d'} + \frac{1}{2d''}\right)\right| \times 10^7 \simeq \left|\frac{M^2R}{2\lambda d}\right| \times 10^7, \qquad \ldots\ldots(11)$$

where d is the mean of d' and d''. In this equation the distances between source and reflector are doubled to give the total lengths (d_1 and d_2 in (10)), of the transmission paths. The approximation is permissible when $d \gg \lambda$, and this will obtain at those distances where the reciprocity parameter defined in (9) is valid, and where the inverse relationship between pressure and distance is established.

From (9) and (11), the transducer constants may be expressed in terms of ΔZ, R, λ and d:

$$|M| = [(2\lambda d/R)|\Delta Z| \times 10^{-7}]^{\frac{1}{2}}; \qquad |S_d| = [(R/2\lambda d)|\Delta Z| \times 10^7]^{\frac{1}{2}}. \qquad \ldots\ldots(12)$$

An examination of these expressions with reference to the performance of practical transducers shows that their application to the absolute calibration of a transducer would be limited to efficient projectors functioning at resonance, and that in any case the accuracy will be low since the result depends upon the measurement of a small change in impedance. Carstensen (1947) has, however, recently described a pulse technique in which the transmitter current I and the received voltage E_0 are measured separately. A train of waves is used short enough to ensure that the transmission does not overlap the reception of the echo. Reference should be made to the original paper for practical details and for a discussion of the limitations. The expressions for the transducer constants $|M|$ and $|S_d|$ are, in terms of E_0 and I,

$$|M| = [(4\lambda d/R)(E_0/I) \times 10^{-7}]^{\frac{1}{2}}; \qquad |S_d| = [(R/\lambda d)(E_0/I) \times 10^7]^{\frac{1}{2}} \qquad \ldots\ldots(13)$$

and it will be observed that the ratio E_0/I in these expressions is the added impedance of equation (3) and is equal to half the differential impedance ΔZ.

Thanks are due to the Admiralty for permission to publish this note.

REFERENCES

Carstensen, E. L., 1947, *J. Acoust. Soc. Amer.*, **19**, 961.
Maclean, W. A., 1940, *J. Acoust. Soc. Amer.*, **12**, 140.
Schottky, W., 1926, *Z. Phys.*, **36**, 689.

LETTERS TO THE EDITOR

Dependence of β-Decay on the Sign of the Change in Nuclear Spin

The calculation of the probability of β-decay for given values of the magnitudes of the initial and final angular momenta of the nucleus may be abbreviated, as has been done by Marshak (1942), by application of a sum rule and of conservation of angular momentum. Professor Feather and Dr. Richardson have pointed out to me a discrepancy between Marshak's results and a statement of Greuling (1942). Here Marshak's argument is amplified and Greuling's statement shown to be wrong.

Under certain approximations the interaction between the nucleons and the electron-neutrino field contains terms of the type V_N, V_F, where V_N, V_F are respectively functions of the nuclear variables only, and of the field variables only. Let $P(j, m : j', m')$ denote the probability of transition of the system from a state where the angular momentum of the nucleus corresponds to the usual designation j, m to the state labelled by j', m', the probability being summed for all consistent values of energy, linear momenta, angular momenta and spin momenta of the electron-neutrino field. Total angular momentum is conserved to the usual approximation. Since V_N is Hermitian, and since the part of the transition probability arising from V_F is independent of the sense of the change of angular momentum,

$$P(j, m : j', m') = P(j', m' : j, m). \qquad \ldots\ldots (1)$$

Define $Q(j, j')$ to be the probability of the transition from a single m belonging to j to any of the $2j'+1$ values of m' belonging to j' : thus

$$Q(j,j') = \sum_{m'=-j'}^{j'} P(j, m : j', m'). \qquad \ldots\ldots (2)$$

That $Q(j, j')$ is, as the notation suggests, independent of m, may be seen as follows. The usual expansion of the light particle wave functions (evaluated at the position of a nucleon) in ascending powers of the radius (see for example Konopinski and Uhlenbeck 1941) means that eventually the operator V_N contains, among other things, coordinate vectors of the nucleons : if ψ_e, ψ_n are wave functions of electron, neutrino the term $\psi_e^* V_F \psi_n$ contains operators (in V_F) not involving spatial coordinates, together with spherical harmonics, etc. When an integration over the azimuth ϕ is performed, the integrand contains the azimuth in a factor of the form $\exp(iM\phi)$ and in terms involving coordinate vectors of the nucleons. This is now entirely similar to the theory of light emission, and a similar sum rule (see for example Condon and Shortley 1935) is valid.

Summation of (2) for all values of m belonging to j gives, on account of (1), the usual result :

$$(2j+1)Q(j,j') = (2j'+1)Q(j',j). \qquad \ldots\ldots (3)$$

Marshak's simplification. Let k, μ specify the angular momentum of the electron-neutrino field so that, using suffixes i, f to denote initial, final values,

$$|j_i - j_f| = k, \qquad \ldots\ldots (4)$$

$$m_i - m_f = \mu. \qquad \ldots\ldots (5)$$

Suppose first that $j_i - j_f > 0$. We may choose $m_i = j_i$ in evaluating (2). Thus

$$j_i - j_f = k \geqslant \mu = m_i - m_f = j_i - m_f.$$

Hence $j_f \leqslant m_f$ and, since also $j_f \geqslant m_f$, we must have $j_f = m_f$. Thus only one term occurs in the summation (2), viz.

$$Q(j_i, j_f) = P(j_i, j_i : j_f, j_f). \qquad \ldots\ldots (6)$$

Then, for $j_i < j_f$, (3), (6) give $Q(j_i, j_f) = [(2j_f+1)/(2j_i+1)]P(j_f, j_f : j_i, j_i)$.

The discrepancy. Greuling's equations (1), (3) contain a summation over m which corresponds to our summation over μ or m_f. He does not explain in detail his derivation of his equations (11), but the general implication of his statement in the second paragraph of p. 575 of his paper seems to be wrong. For $j_i > j_f$ Greuling's summation over m should be equivalent to Marshak's result. Marshak's summation reduces to one term when $m_i = j_i$, but the result would be the same whatever value of m_i were chosen and however many were the terms in the summation. Thus there is no need to multiply half-lives by $2(j_i - j_f) + 1$ if Greuling's equations (1), (3) are correctly applied.

The number of terms in the summation may be easily calculated. By equation (5), for given m_i, j_i, j_f, μ may take the values $m_i - j_f$, $m_i - j_f + 1$, ... , $m_i + j_f$, and, in order that $|\mu| \leqslant k$, we have by (4) $-|j_i - j_f| \leqslant m_i - j_f + \lambda \leqslant |j_i - j_f|$, where λ is any integer satisfying $0 \leqslant \lambda \leqslant 2j_f$.

Thus there are $2|j_i - j_f| + 1$ or $|j_i - j_f| - m_i + j_f + 1$ terms according respectively as $-|j_i - j_f| - m_i + j_f \geqslant 0$ or < 0. Thus, if $j_i < j_f$, there are $2(j_f - j_i) + 1$ terms, while if $j_i > j_f$ there are $2(j_i - j_f) + 1$ or $j_i - m_i + 1$ terms according as $2j_f \geqslant$ or $< j_i + m_i$. Thus, if $j_i > j_f$ and $m_i = j_i$, there is just one term.

Department of Natural Philosophy,
University of Aberdeen.
1st September 1948.

C. STRACHAN.

CONDON, E. U., and SHORTLEY, G. H., 1935, *The Theory of Atomic Spectra* (Cambridge : University Press).
GREULING, E., 1942, *Phys. Rev.*, **61**, 568.
KONOPINSKI, E. J., and UHLENBECK, G. E., 1941, *Phys. Rev.*, **60**, 308.
MARSHAK, R. E., 1942, *Phys. Rev.*, **61**, 431.

The Attenuation of Ultra-High Frequency Electromagnetic Radiation by Rocks

We were interested by Mr. Cooper's paper (1948) on the attenuation of very short radio waves in rocks, and would like to draw attention to some very similar work which we carried out at the National Physical Laboratory in 1942, the results of which were published later (McPetrie and Saxton 1945).

We made measurements on wavelengths of 2 and 5 metres of the field strength produced in two specially excavated tunnels by a horizontal aerial fed from a small power transmitter which was erected over each tunnel in turn. The two tunnels were made as nearly identical in structure as possible, except that one was at a depth of 1·15 metres and the other at 1·85 metres. It was hoped that any disturbing " tunnel effect " could be eliminated by making comparative measurements in the two tunnels when subsidiary tests made above ground showed that the same field existed at the surface of the earth immediately above the tunnels. This seems to us a more reliable procedure than that followed by Mr. Cooper, in which an attempt is made to evaluate this tunnel effect theoretically. Any such attempt must necessarily be uncertain. In Mr. Cooper's experiments, fortunately, the transmission path through the earth is sufficiently long for the absorption in the earth to be very much greater than such losses as may be expected, on any reasonable hypothesis, to arise from the effects of the tunnel.

Our two tunnels were close together on the same site, which was of sandy loam overlying gravel, and the observations thus gave directly the attenuation in a path of 0·7 metres through this medium. We also made measurements of the reflection coefficient of the earth's surface on the same site, and these, together with the absorption measurements, enabled us to determine both the dielectric constant and the conductivity of the ground, assuming uniform properties with depth for the latter. Since this assumption is not strictly true, the values so obtained must be regarded only as reasonable mean values. Our results indicated that the attenuation of both 2-metre and 5-metre waves was about 12 db/m., which is not very different from the value of 10·5 db/m. for Pennant sandstone quoted by Mr. Cooper.

The actual figure for the attenuation obtained, as the author states, depends largely upon the amount of water present. We should like to point out, however, that Mr. Cooper's statement that at a frequency of 200 Mc/s. the dielectric losses in water are still negligible in comparison with the conductivity loss is not strictly accurate. In fact, at this frequency for the usual amount of dissolved salts occurring in fresh water, which leads to an ionic conductivity of about 10^8 E.S.U. ($\sim 10^{-13}$ E.M.U.), the dielectric and conductivity losses are just about equal.

Signals Research and Development Establishment,
Somerford, Christchurch, Hants.,
and
Radio Division, National Physical Laboratory,
Teddington, Middlesex.
21st July, 1948.

J. S. McPetrie.
J. A. Saxton.

Cooper, R. I. B., 1948, *Proc. Phys. Soc.*, **61,** 40.
McPetrie, J. S., and Saxton, J. A., 1945, *J. Instn. Elect. Engrs.*, **92,** Part III, 256.

I was very grateful to Drs. McPetrie and Saxton, with whose work I am, of course, familiar, for their comments on my paper. I must apologize for not having referred to them in it, but I should like to point out that my work was concerned with the electrical properties of large thicknesses of rock *in situ*, and not with the properties of the surface soil-layer. I had hoped that the consolidated Pennant Sandstone which I used would have held less water and therefore show a smaller attenuation than the sandy loam mentioned in their work. I agree that their procedure was more reliable, but the experimental difficulties with which I had to contend prevented any more satisfactory arrangements from being made. In fact I find some consolation in the agreement obtained with their results.

As a matter of interest I also observed a rainfall effect similar to that mentioned in their paper during my work ; on the last day of the experiments in Pontypridd tunnel rain fell, but it was not until the following day that any diminution was observed in the echo-strength inside the tunnel. This effect was not investigated sufficiently well for inclusion in the paper, however.

Finally, I am indebted to Drs. McPetrie and Saxton for pointing out the error mentioned in the last paragraph of their letter.

Department of Geodesy and Geophysics,
Downing Place, Cambridge.
3rd August 1948.

R. I. B. Cooper.

The Performance of a New Radio-Frequency Ion Source

The observations of Hertzberg (1927) on the low intensity of the molecular spectrum of an electrodeless ring discharge in hydrogen suggested that this method of excitation should prove very effective in achieving a high proton percentage in an ion source. This mode of excitation has been used in a recently described ion source (Bayley and Ward 1948). The characteristics of such an ion source are of great interest to users of accelerated ion beams. The radio-frequency ion source which has been developed in this laboratory is reliable and gives high ion currents, a high atomic content and ions of uniform energy.

A high concentration of atomic hydrogen is maintained in a pyrex discharge tube by reducing the exposed metal surfaces to a minimum and producing a high degree of ionization by a coil round the tube excited by a 20 Mc/s. 150 watt oscillator. The discharge is self-starting provided the probe voltage is off. A tungsten wire anode is isolated from the main discharge by a constriction. This reduces the flow into the discharge space of molecular hydrogen formed by recombination on the anode. The duralumin probe electrode enclosed in a glass cylinder projects into the discharge space as it has been found (Hertzberg 1927) that the concentration of atomic gas and hence the proton percentage diminishes towards the walls. Because of the high concentration of positive ions the exposed probe surface can be reduced to small dimensions and recombination reduced to a minimum.

The form of the electric field resulting from the presence of the glass cylinder around the probe focuses the ions into the canal. This mode of focusing has been demonstrated before (Thonemann 1946).

Figure 1 shows the mechanical details of the source used for making measurements. Approximately 50 watts of high-frequency energy are dissipated in the tube. A small air-blower is used to keep the wax joint cool.

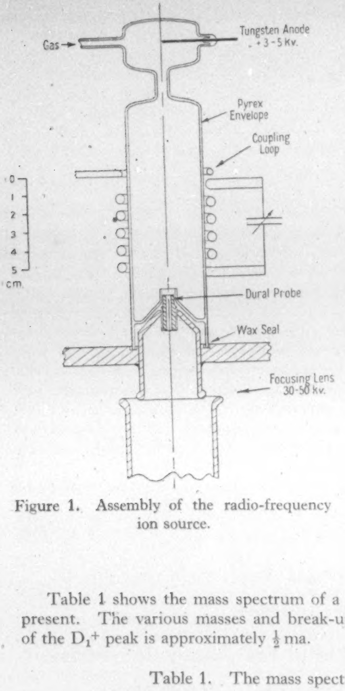

Figure 1. Assembly of the radio-frequency ion source.

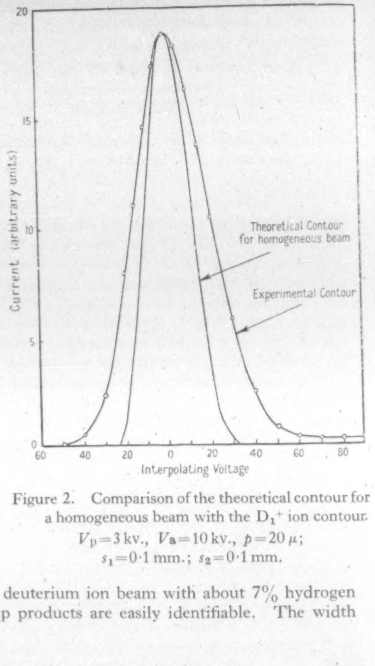

Figure 2. Comparison of the theoretical contour for a homogeneous beam with the D_1^+ ion contour. $V_p=3$ kv., $V_a=10$ kv., $p=20\ \mu$; $s_1=0{\cdot}1$ mm.; $s_2=0{\cdot}1$ mm.

Table 1 shows the mass spectrum of a deuterium ion beam with about 7% hydrogen present. The various masses and break-up products are easily identifiable. The width of the D_1^+ peak is approximately ½ ma.

Table 1. The mass spectrum of a deuterium ion beam

Magnet current (ma.)	Species	Percentage abundance
29	D_1^+ from dissociation of D_3^+	0·9
32	H_1^+; D_1^+ from dissociation of D_2^+	6·0
54	D_1^+ and H_2^+	79·0
60	D_2^+ from dissociation of D_3^+	1·0
62	HD^+ and H_3^+	0·9
80	D_2^+ and H_2D^+	8·8
90	HD_2^+	1·4
99	D_3^+	2·1

The variation of proton and deuteron percentage with pressure in the source is shown in tables 2 and 3. The discharge extinguishes at the low pressure limit. Hydrogen was supplied through a heated palladium tube. The differences in atomic percentage between deuterium and hydrogen may be due to the difference between the radio-frequency powers absorbed in deuterium and in hydrogen.

When a new source is first operated the discharge may change suddenly from its normal brilliant red to a dull white and the proton current may fall by a factor of 10. This is probably due to the evolution of hydrocarbons and other gases from electrodes under positive ion bombardment in the accelerator. After the system has been outgassed the proton current remains stable and shows no deterioration after months of intermittent use.

The homogeneity of the deuterons after a 10 kv. acceleration was measured on a mass spectrometer. A Faraday screen was introduced to eliminate any possible modulation of the ion energy by the electrostatic R.F. field. The discharge had then to be initiated by bringing a Tesla coil close to the upper section of the source. Figure 2 shows the contour for the D_1^+ ion. The theoretical contour from a homogeneous source, taking into account the aberrations in the spectrometer, is given for comparison. It is concluded that 90% of the ions have an energy spread of less than ±20 electron volts. The magnitude of the tail on the low energy side of the experimental curve increases with pressure in the accelerator and spectrometer and is attributed to scattering and energy loss by collision in the high vacuum side of the apparatus.

Table 2

Pressure (microns)		14	16	18	20	23	25	26	28
Percentage Abundance	H_1^+	84	85	88	89	90	90	92	91
	H_2^+	14	11	10	8	7	8	5	6
	H_3^+	2	4	2	3	3	2	3	3

Table 3

Pressure (microns)		13	15	17	20	22	25	28	30
Percentage Abundance	D_1^+	72	73	85	85	84	89	87	87
	D_2^+	23	20	13	11	12	8	8	8
	D_3^+	5	7	2	4	4	3	5	5

In adapting this ion source for use on our high voltage accelerators we have found it more convenient to connect the gas leak and Pirani gauge through the base of the ion source. To increase the focusing efficiency the outside diameter of the probe has been reduced from 1/4 in. to 3/16 in. The same high atomic percentage has been measured with this arrangement. With 3 kv. extraction volts and 10 ma. probe current no difficulty has been found in focusing a ½ ma. beam of ions in a 6 mm. diameter spot after passing through 3 metres of the accelerating tube.

P. C. THONEMANN.
J. MOFFATT.
D. ROAF.
J. H. SANDERS.

The Clarendon Laboratory,
Oxford.
31st August 1948.

BAYLEY, A. J., and WARD, A. G., 1948, *Canad. J. Res.*, **26**, 69.
HERTZBERG, G., 1927, *Ann. Phys., Lpz.*, (4), **84**, 565.
THONEMANN, P. C., 1946, *Nature, Lond.*, **158**, 61.

The Absorption Coefficient of the β Rays from $^{35}_{16}$S in Aluminium

During the course of some measurements using radio sulphur $^{35}_{16}$S it became necessary to make an estimate of the correction due to self absorption of the β rays. The end point of the β-ray spectrum is known (Libby and Lee) but as this lies outside the range of Feather's empirical formula it is hoped that the following experimental determination of the absorption coefficient in aluminium may be of use to other workers using counters with cylindrical symmetry.

The measurements were made with a demountable counter ; it differs only in details from that used by Collie and Morgan in 1939. The active barium sulphate was distributed as evenly as possible as a film whose mean weight was less than 1/10 mg/cm² on the inside of a movable glass cylinder. The counter was filled with a carefully controlled air alcohol mixture using a bellows manometer of the type described by East and Kuhn (1946). A long series of measurements showed that variations in the observed activity of a single specimen due to refilling the counter and replacing the specimen did not amount to more than 3% (including the statistical error). The aluminium foil used as an absorber was wrapped round the perforated cathode of the counter and unwrapped layer by layer. On examining the pulses with a cathode-ray tube it was observed that the aluminium foil caused the production of a small proportion of double counts. These were insufficient to interfere with the stability of the counter at the highest rate of counting used.

The absorption curve was calculated on the assumption that the number of double counts was a constant proportion of the true activity. The correctness of this assumption was verified experimentally by varying the resolving time of the counting circuit and comparing the results with those obtained with a counter free from doubles. The absorption was found to be exponential with an absorption coefficient $\mu=780\pm25$ cm^{-1}. The greatest uncertainty of the determination is due to the difficulty of measuring the exact weight of foil through which the β particles have passed. Using this figure for μ, the activity of a bare source will be halved by 2·4 mg/cm^2 of aluminium. This result may be compared with the observation of Hendricks and his collaborators (1943) that the halving mass in mica is 3 mg/cm^2. The small difference between these results is not more than would be expected when the very different geometrical arrangements are taken into account.

We have to thank Professor Peters for putting the radio sulphur at our disposal, the Board of Education for a maintenance grant and Lord Cherwell for extending to us the facilities of his laboratory.

The Clarendon Laboratory, Oxford.
7th September 1948.
(First communicated 3rd August 1946).

C. H. Collie.
M. A. Grace.

Collie, C. H., and Morgan, F., 1939, *J. Sci. Instrum.*, **16**, 369.
Feather, N., 1938, *Proc. Camb. Phil. Soc.*, **34**, 599.
East, H. G., and Kuhn, H., 1946, *J. Sci. Instrum.*, **23**, 185.
Hendricks, R. H., Bryner, L. C., Thomas, M. D., and Ivie, T. O., 1943, *J. Phys. Chem.*, **47**, 469.
Libby, W. F., and Lee, D. D., 1939, *Phys. Rev.*, **55**, 245.

The Effect of Room Temperature Radiation on the Infra-Red Response of Lead Telluride Photoconductors

One of the principal objects in studying the photoconductivity of semiconductors is to search for substances which show photosensitivity to radiation as far into the infra-red as possible. The practical importance of these substances is in their ready application to infra-red detection, and in particular to detection for the purposes of infra-red spectroscopy. It has been generally recognized that as the long wavelength limit of photoconductivity is extended, the temperature at which a detector may profitably be used must be decreased in order to cut down thermal excitation in the material. However, if the thermal radiation from the surroundings of a photoconductor contains appreciable energy at wavelengths to which the detector is photosensitive, there will be an effective background of illumination which will increase the conductivity even when no source of illumination is deliberately applied. This will be true at whatever temperature the photoconductor is maintained, unless it is surrounded by an enclosure at the same, or lower, temperature.

Lead telluride, in the form of thin films, has been found to show photoconductivity at least as far into the infra-red as 5·5 μ, and it has been shown that at −190° c. its performance as an infra-red detector surpasses that of a good Hilger-Schwartz thermocouple for wavelengths shorter than 4·7μ (Simpson, Sutherland and Blackwell 1948). It has recently been discovered that the conductivities of all photoconductive lead telluride films are much less when they are cooled to −190° c. and surrounded by an enclosure at that temperature than when they are cooled to −190° c. but surrounded by an enclosure at room temperature. That this effect is due to the thermal radiation which in the latter case is emitted by the enclosure at 15° c. is demonstrated in the figure where the logarithm of the conductivity of a film is plotted against the reciprocal of the temperature. Curve A shows the conductivity that is observed when the film is allowed to warm up from $-190°$ c. to room temperature, the photoconductor being exposed all the time to an enclosure at 15° c. It will be observed that below $-170°$ c. ($1/T>9{\cdot}7\times10^{-3}$), the conductivity decreases with increasing temperature; this in itself is anomalous for a semiconductor. The anomaly is removed in curve B where the conductivity of the same film is shown under conditions in which the thermal radiation was excluded by surrounding the film by an enclosure at $-190°$ c. The conductivity at $-190°$ c. was more than six times greater when the film was exposed to the room temperature radiation; this effect decreased rapidly as the temperature was increased, and was negligible at temperatures above $-140°$ c.

The effect of the thermal radiation on the photoconductive response may best be illustrated by considering the following equation which is found experimentally:

$$(\sigma_i/\sigma_d)^2=1+bI,$$

where σ_d is the conductivity at $-190°$ c. with the thermal radiation excluded, and σ_i the conductivity under an intensity of illumination I watts/cm². The constant b depends upon the wavelength of the incident light and was $2{\cdot}2\times10^6$ watt^{-1} cm^2 at $2{\cdot}2\,\mu$ for the film shown in the figure. Using this equation, the voltage change across a film caused by the absorption of radiation while the film is passing a fixed current may be readily calculated. It is found that for an exciting current of 1μa. the voltage output is $9{\cdot}2$ v/μw/cm², $\lambda=2{\cdot}2\,\mu$, when the film is entirely shielded from thermal radiation. The output for the same exciting current when the thermal radiation is not excluded is only $0{\cdot}053$ v/μw/cm².

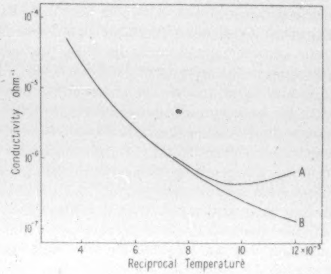

In order to assess the effect of the thermal radiation on the ultimate limit of sensitivity of lead telluride further data are required concerning the noise characteristics of the films. Clark Jones (1947) has shown that fluctuations in the radiation field set the ultimate limit for any detector operating under prescribed conditions. It has been shown here that by excluding the background of thermal radiation the signal output may be increased; the signal-to-noise ratio will be further increased by this means if the noise output of the film is predominantly due to statistical fluctuations in the background radiation. There is at present insufficient evidence for it to be certain that this is in fact the case.

The spectral response curve for lead telluride (Simpson, Sutherland and Blackwell 1948) has so far only been obtained with films exposed to room temperature radiation; there is a possibility that under these conditions the photosensitivity at long wavelengths is at least partly saturated. If this were so the photoconductive response would be increased even more at long wavelengths than at the wavelength $2{\cdot}2\,\mu$ which has been used as standard in this discussion. It seems possible that the changes in the spectral response of PbS, PbSe and PbTe obtained by Moss (1948) by operating at very low temperatures are not unconnected with the above results.

I am indebted to Dr. G. B. B. M. Sutherland and Dr. E. F. Daly for helpful discussions.

O. Simpson.

Cavendish Laboratory, Cambridge.
12th August 1948.

Jones, R. C., 1947, *J. Opt. Soc. Amer.*, **37**, 879.
Moss, T. S., 1948, *Nature, Lond.*, **161**, 766.
Simpson, O., Sutherland, G. B. B. M., and Blackwell, D. E., 1948, *Nature, Lond.*, **161**, 281.

REVIEWS OF BOOKS

Radar Beacons, edited by ARTHUR ROBERTS. Pp. xx+489 with 246 figures. (New York: McGraw-Hill Book Co. Inc., 1947.) $6.

After world war II the Radiation Laboratory of the Massachusetts Institute of Technology undertook the heavy task of preparing for publication in book form the war-time developments of Radar and Radar Techniques. Several volumes of this series have already appeared and are proving of real value to the specialist and student alike. The present volume is Volume III of the series and deals with the important subject of Radar Beacons.

A radar beacon is a small receiver transmitter apparatus which is used at the target to be located. It is actuated (or triggered, to use the correct technical term) by the pulsed signals sent out by the radar set, and in turn the beacon sends out pulsed signals which may be received at the radar set. The time delays in the beacon system can usually be made very small and constant so that range finding by timing the interval between the radar transmitted pulse and the pulse echo received back from the beacon is possible as for " primary radar ". This latter depends on the target itself reflecting back some of the incident energy. The beacon system (called by Watson-Watt " a secondary radar system ") has, however, several advantages when circumstances allow its use. Thus it allows target location in circumstances where ground clutter would prevent the operation of a primary radar system, greater range and, if the beacon transmissions are coded, positive identification of the target echoes. For these, and for other reasons, the beacon system was much used during the last war for general navigation of aircraft and surface vessels, for approach systems at airfields, for paratroop dropping, for bombing aids and for other purposes, and it is now finding application in civil aviation and in maritime service. The present book attempts to give a survey of these developments and, it can be said at once, that the 24 authors who have collaborated in this work have succeeded in providing a very valuable treatise which should be of special interest to all those who want to obtain a thorough understanding of the present state of the beacon art.

The book is divided into four parts: Basic Considerations, Beacon Design, Interrogator and System Design, and Beacons in the Field. The first part is especially valuable and gives a thorough treatment of the principles of the subject. After a brief introductory section dealing with the types and functions of beacons it gives a detailed discussion of the requirements of systems using beacons, considering in turn range requirements, propagation and coverage, choice of frequency, use of coding and communications, and questions of traffic and capacity. All this is explained in a very lucid manner and should be easily assimilated by the would-be beacon designer.

Part II deals with beacon design and includes sections on the design of all the component parts of the beacon. There are chapters on the design of the R.F. components, beacon receivers, interrogation coding, response coding, beacons as pulse communication systems, the design of modulators and transmitters and the associated problems of power supplies and performance testing. This is all very well explained, particularly so far as the components of microwave systems are concerned, but, in some cases, the treatment of the component parts of the longer wave systems is dealt with far too briefly.

Part III gives details of the Interrogator and system design and includes chapters on radar design for beacon operation, the design of interrogator-responsors and the design of typical beacon systems. This latter chapter is well worth careful study as an outline is given of the application of the principles discussed in Part I to meet requirements of different types of beacons and will therefore be of particular value to the designer.

Part IV discusses beacons in the field and includes chapters on installation, operation and maintenance. Questions of this sort tend to be forgotten in many books and it is pleasing to a reviewer to find these subjects so well presented.

The book can be recommended with every confidence.

DENIS TAYLOR.